Institut de Physique
Université de Neuchâtel

Model study of anomalous properties of short coherence length superconductors

THÈSE

PRÉSENTÉE À LA FACULTÉ DES SCIENCES

DE L'UNIVERSITÉ DE NEUCHÂTEL

POUR L'OBTENTION DU GRADE DE DOCTEUR ÈS SCIENCES

PAR

Alain SEWER

Physicien diplômé ETH

originaire de Leuk-Stadt (VS)

Neuchâtel, mai 2002

IMPRIMATUR POUR LA THESE

Model study of anomalous properties of short coherence length superconductors

de M. Alain Sewer

UNIVERSITE DE NEUCHATEL

FACULTE DES SCIENCES

La Faculté des sciences de l'Université de Neuchâtel sur le rapport des membres du jury,

MM. H. Beck (directeur de thèse), P. Martinoli, X. Zotos (Fribourg) et F. Gebhard (Marburg D)

autorise l'impression de la présente thèse.

Neuchâtel, le 25 mars 2002

Le doyen:

F. Zwahlen

Résumé

Ce travail de thèse contient une étude de divers aspects d'un type particulier de supraconducteurs, dits à courte longueur de cohérence ξ. Cette quantité fondamentale correspond à la distance séparant les deux électrons qui forment une paire de Cooper, un des ingrédients principaux de l'approche microscopique de la supraconductivité, établie en 1957 par Bardeen, Cooper et Schrieffer (BCS). Dans le cas "conventionnel" décrit par la théorie BCS originale, ξ est très grand devant la constante du réseau cristallin sous-jacent a, alors que dans la situation considérée ici ξ est du même ordre de grandeur que a. Cette différence a pour conséquence que certaines propriétés importantes des supraconducteurs à courte longueur de cohérence présentent des déviations (ou anomalies) par rapport au comportement BCS conventionnel. L'étude de ces dernières nécessite l'utilisation de méthodes analytiques et numériques remplaçant le schéma d'approximation "champ moyen" applicable dans le cas BCS mais invalide lorsque $\xi \sim a$. Une attention particulière est portée à l'analyse des manifestations précurseuses de la supraconductivité apparaissant au-dessus de la température de transition dans l'état supraconducteur. La motivation de ces considérations théoriques réside entre autres dans l'observation de phénomènes semblables dans certains types de matériaux récemment synthétisés, dans le contexte de la problématique actuellement très discutée du "pseudogap" dans les oxydes de cuivre supraconducteurs sous-dopés.

Une première partie présente une nouvelle approche théorique destinée à expliquer certaines anomalies observées dans le réponse diamagnétique orbitale de composés sous-dopés. Basée sur un modèle phénoménologique, elle permet en particulier de comprendre la dépendance en température de la susceptibilité magnétique mesurée expérimentalement dans des composés du type YBCO. La deuxième partie contient une analyse des propriétés thermodynamiques du régime "pseudogap" du modèle microscopique de supraconducteurs à courte longueur de cohérence le plus utilisé, le modèle de Hubbard attractif. Il y est montré par un calcul analytique comment le système peut être dans une situation proche d'une condensation de Bose-Einstein (BEC), alors que cette dernière est a priori attendue pour des régimes de couplage bien plus forts. Dans la troisième partie sont présentés les résultats des simulations Monte Carlo quantique du modèle de Hubbard attractif tridimensionnel. Ils montrent comment se fait la transition entre les régimes BCS et BEC en trois dimensions avec, en particulier, la séparation entre les échelles de températures de condensation et de formation des paires de Cooper.

Abstract

This thesis contains a study of various aspects of a special type of superconductors characterized by a short coherence length ξ. This quantity corresponds to the distance separating the two electrons constituting a Cooper pair, one of the principal features of the microscopic approach of superconductivity, which was established in 1957 by Bardeen, Cooper and Schrieffer (BCS). In the "conventional" case described by the original BCS theory, ξ is very large compared to the underlying crystal lattice constant a, whereas ξ and a have the same order of magnitude in the case considered here. This difference implies that certain important properties of short coherence length superconductors exhibit deviations (or anomalies) from the conventional BCS behavior. Studying the latter requires both analytical and numerical methods going beyond the usual "mean-field" approximation scheme, which works in the BCS case but not when $\xi \sim a$. Particular attention is devoted to the analysis of precursor manifestations of superconductivity which appear above the transition temperature into the superconducting phase. These theoretical considerations are motivated by the observations of similar phenomena in some types of recently synthetized materials, in the context of the widely discussed problematics of the pseudogap in underdoped high-T_c superconducting copper oxides.

The first part presents a new theoretical approach intended to explain some anomalies which have been observed in the orbital diamagnetic response of underdoped compounds. Based on a phenomenological model, it allows in particular to understand the temperature dependence of the magnetic susceptibility which has been experimentally measured in the YBCO compounds. The second part contains an analysis of the thermodynamic properties of the pseudogap regime of the widely used microscopic model for short coherence length superconductors, the attractive Hubbard model. It is shown by means of an analytical calculation how the physics of this system can be close to a Bose-Einstein condensation (BEC), whereas the latter is a priori expected for the strong coupling regime only. In the third part the results of the Quantum Monte Carlo simulations to the tridimensional attractive Hubbard model are presented. They show explicitly the crossover between the BCS and BEC regimes and, in particular, the separation between the temperature scales for Cooper pair formation and Cooper pair condensation.

Contents

Chapter 1

Introduction

In this first chapter the phenomenon of superconductivity is presented with a special emphasis on the microscopic aspect of electronic pairing. The latter is characterized by a length scale called the coherence length which turns out to be much smaller in the high-T_c copper oxide compounds than in the conventional low-T_c superconductors. In this thesis a simple model is used to study several properties of short-coherence length superconductors that deviate from the predictions of the traditional BCS theory. These considerations may help to understand better some aspects of high-temperature superconductivity.

1.1 Superconductivity and electronic pairing

As suggested by its name, the first signature of superconductivity is the *perfect conductivity* and was discovered in 1911 by Kamerlingh Onnes. He observed that, below a very low temperature $T_c \sim 5$ K, the electrical resistance of simple metals like mercury and lead drops abruptly to zero. The second fundamental property of a superconductor is the *perfect diamagnetism*, discovered in 1933 by Meisnner and Ochsenfeld. They remarked that, when lowering the temperature in presence of a (small) applied magnetic field B, the latter is expelled from inside the material as soon as T becomes lower than T_c. These two complementary properties show that a superconductor in equilibrium at a temperature T and under a magnetic field B constitutes a thermodynamic state, i.e. a state whose properties are independent from how it was produced. Thus superconductivity characterizes a well-defined state of condensed matter.

After these discoveries, several approaches were developed to understand theoretically the observations. However they were all at a phenomenological level and a satisfying explanation of the phenomenon using the principles of quantum mechanics was missing during a long time. In 1957 Bardeen, Cooper and Schrieffer proposed what

is called today the BCS theory which turned out to be the correct way to understand superconductivity at the microscopic level [1]. The key ingredients were an effective *attractive* interaction between the electrons due to the coupling with the lattice vibrations (phonons) and new ground state for the electronic system. The latter replaces the Fermi sea as soon as the electronic interaction becomes attractive and is characterized by a coherent superposition of *electronic pairs*, called Cooper pairs. One of the first predictions of the BCS theory concerned the existence of gap Δ situated around the Fermi level in the electronic density of states and closing at the transition temperature T_c. Its observation in 1960 using tunneling experiments between a superconductor and a normal metal was an important confirmation of the correctness of the BCS approach. The pairing of the electrons, a priori not directly deductible from one-particle spectral properties, was also verified explicitly in 1961 by measurements of the magnetic flux appearing in a hollow cylinder in the walls of which a supercurrent was circulating. The flux turned out always to be an integer multiple of the constant $\Phi_0 = hc/2e$, called the quantum flux and whose denominator accounts explicitly for the fact that the current is produced by "particles" of charge $2e$. The latter were naturally identified as the Cooper pairs.

Quite generally, a Cooper pair can be characterized by a length scale ξ_0 called the coherence length and corresponding roughly to the distance between the two electrons it contains.[1] For the case of the BCS superconductor discussed above, the pairing is found to take place in the reciprocal space, that is the two involved electrons have opposite spins ($\uparrow$ and $\downarrow$) and momenta ($\mathbf{k}$ and $-\mathbf{k}$). Since the (phononic) coupling between the latter is *weak*, it is not surprising that the BCS theory predicts a very large coherence length, much larger that the lattice constant. Another length scale exists in the problem, given simply by the interparticle distance or, equivalently, by the inverse of the Fermi wave vector k_F^{-1}. It is fixed by the electronic density per lattice site $0 < n < 2$. For the traditional superconductors well described by the BCS theory it turns out that the ratio $k_F\xi_0$ of the two length scales is always very large. In other words a Cooper pair overlaps with many others and this feature plays a fundamental role in determining the physical properties of the superconductor. It is usually referred to as *mean-field* behavior.

In this context one could imagine reducing the coherence length to the order of the interparticle distance, i.e. $k_F\xi_0 \sim 1$. Then the overlap between the pairs becomes much smaller and one expects some properties to deviate from the (BCS) mean-field behavior. This thesis is exactly concerned with the study of the problems which follow from a pairing with a more pronounced local character. It turns out that such a feature is realized in a category of materials that were discovered in 1986: the copper oxide high-temperature superconductors (HTSC) where the size of a Cooper pair is found to be of the order of the lattice constant. They are presented in the next section.

[1] For simplicity these considerations are restricted to the zero temperature.

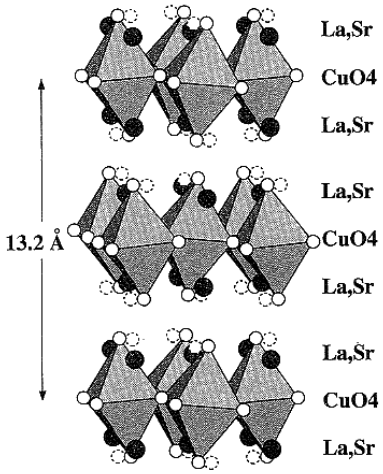

Figure 1.1: Crystal structure of $La_{2-x}Sr_xCuO_4$, one of the simplest copper oxide high-temperature superconductors.

1.2 High-temperature superconductivity

The first high-temperature superconductor was discovered by Bednorz and Müller [2] after which several other compounds were synthesized, all presenting maximal transition temperatures in a range from 40 K up to 130 K, values which were never observed before. Although its nature may be different from the one of the BCS theory, the pairing of the electrons in the superconducting state was found to be also present in these materials [3]. The corresponding coherence length was found to be of order of 10 Å, a value very similar to the ab-lattice constant which is of order of 5 Å[4]. Before discussing in more details the electronic properties of these short-coherence length superconductors, it is important to recall some basic material characteristics which play an important role.

- The *crystal structure* of these materials is complicated, with several different types of atoms in the lattice unit cell, as illustrated in Figure 1.1 for the case of $La_{2-x}Sr_xCuO_4$ (LSCO). A common feature between the various compounds is the presence of CuO_2 layers, perpendicular to the crystallographic c axis. They are separated by what is commonly called "charge reservoirs" which contain atoms of oxygen and several other elements which are specific for each compound (lanthanum and strontium in the case of LSCO).

- Superconductivity is produced by *hole doping*: some atoms in the charge reservoirs are substituted by elements with a lower oxidation number. In the case of LSCO for instance, a fraction x of the trivalent La is replaced by the divalent Sr. The resulting vacancies are compensated by absorbing electrons from the CuO_2 layers which contain thereby a finite density x of holes. It turns out that these

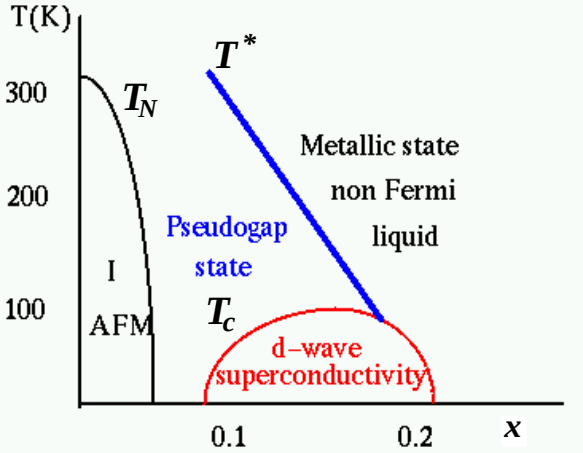

Figure 1.2: The generic phase diagram doping versus temperature of the copper oxide high-temperature superconductors. Differences can appear from one compound to the other and according to the definition of the crossover temperature T^*.

holes are forming the Cooper pairs responsible for superconductivity. Therefore the latter is characterized by a pronounced *anisotropy* due to the particular material structure.

The electronic properties of the high-temperature superconductors depend crucially upon the doping x and are summarized in the generic $x - T$ phase diagram shown in Figure 1.2. It is constituted of several distinct regions:

- At zero doping all HTSC are *Mott insulators*. The conduction electrons of the Cu atoms are immobile because any hopping to another Cu site is blocked by the strong Coulomb repulsion occurring in case of a double occupancy. Below a Néel temperature T_N of a few hundred K, an antiferromagnetic order is present. As the doping x increases, T_N tends rapidly to zero and the antiferromagnetic state disappears above $x \simeq 0.04$, the precise value depending on the compound.

- Between the doping values $x_u \simeq 0.05$ and $x_o \simeq 0.3$ (for LSCO to be concrete), a *superconducting* phase appears with a critical temperature $T_c(x)$ reaching its maximal value around $x_m = 0.17$, called the optimum doping. The region $x \in [x_u,\ x_m]$ ($x \in [x_m,\ x_o]$) is referred to as the underdoped (overdoped) regime. Due to the layered structure, the effective mass of the charge carriers is much larger in the direction perpendicular to the CuO_2 layers and can be characterized by an anisotropy ratio γ. It has been found experimentally that γ is also depending on x: it is minimal at $x = x_o$, increases slowly up to $x \simeq x_m$ and suddenly grows much faster in the underdoped regime [5]. Therefore in the latter case a (quasi-) two-dimensional behavior is expected. An important property

of the superconducting state of HTSC is the symmetry of the gap parameter Δ. While the original BCS theory predicts isotropic s-symmetry, the experiments have shown that Δ is predominantly of d-symmetry, vanishing in four nodes along the diagonals of the 2D Brillouin zone [6].

- The deviations from the BCS theory in the superconducting state are already numerous but the situation becomes even more surprising in the *normal* state above T_c, especially when moving on underdoped side of the phase diagram ($x \lesssim x_m$) [7]. In this case the low carrier density makes the product $k_F\xi_0$ still smaller and thus differing further from the mean-field regime suited to the BCS theory. The predictions of the latter is that superconductivity totally disappears at the transition temperature so that the physics above T_c is the one of a normal metal, described by Fermi liquid theory. Experimentally this behavior is indeed observed in the overdoped regime ($x \gtrsim 0.2$) but deviations become more and more pronounced when reducing x. In the underdoped region they have been attributed to a new feature called the *pseudogap*, which consists in an anomalously low value of the one-electron density of states at the Fermi level, a kind of "partial" version of the superconducting gap existing below T_c.[2] A new temperature scale T^* has been introduced to measure the extension of this particular regime above the superconducting transition temperature. T^* is very close to T_c at optimal doping $x \simeq x_m$ but becomes rapidly much larger for lower values of x.

Because of the unusual physical properties it presents, the pseudogap regime has attracted a lot of attention in recent years and the present thesis will be also concerned (partly) by this particular region of the phase diagram of the HTSC. From the experimental point of view its appearance in the one-particle density of states of underdoped compounds is now well established [8]. Direct evidences for this peculiarity were provided by techniques measuring the spectral density of available electronic states, the angle-resolved photoemission spectroscopy (ARPES) and the tunneling spectroscopy. A lower spectral weight at the Fermi level also affects numerous others properties, so that the pseudogap was indirectly detected in the magnetic response (using nuclear magnetic resonance), in transport properties (DC electrical resistivity and optical conductivity) and in thermodynamic quantities (specific heat and thermal expansion).

The interpretation of all the above mentioned experimental observations is presently still controversial, even the exact form of the phase diagram from Figure 1.2 may be different from one author to the other. In fact an agreement about the most important ingredient, the mechanism leading to electronic paring in the superconducting state, does not yet exist. Consequently the explanation of the pseudogap phase remains open as well, but it acquires a considerable importance since it constitutes a crucial test for

[2] However the relations between the two "gaps" are still not clearly established, see later.

any microscopic theory of high-temperature superconductivity.

In this context it is clear the choice of one of the possible interpretations of the experimental facts will not be unanimously accepted. It is nevertheless interesting to explore the consequences of the short coherence length that are observed in these materials. Such a phenomenological approach has the advantage of being a priori independent of the pairing mechanism. It can be moreover integrated in the framework of a more general theoretical issue: the crossover between BCS superconductivity and Bose-Einstein condensation (BEC). The latter is presented in the next section.

1.3 The BCS-BEC crossover problem

Consider the limit of electronic pairs with a extremely small coherence length ξ_0 in three dimensions, i.e. $k_F\xi_0 \ll 1$. The fermions are tightly bound and form a spin singlet which have thus clear *bosonic* properties. In this case the phase transition at T_c is expected to resemble to a Bose-Einstein condensation of these pairs which thus remain present in the system at temperatures $T > T_c$ and "dissociate" only at a much higher value T^* corresponding to their binding energy $E_b \gg T_c$. As a consequence, a *gap* appears in the single-particle excitation spectrum, because an energy of order E_b has to be provided to "break" a fermionic pair. One can now easily imagine what happens when the size ξ_0 of these pairs becomes larger: T_c and T^* move closer to another and meet when reaching the BCS limit of very large ξ_0. In the intermediate region, the situation presents some similarities with the case of underdoped high-temperature superconductors: a short coherence length ($\xi_0 \sim$ lattice constant), two still distinct temperature scales T_c and T^* and a (pseudo-) gap in the single-particle spectrum above T_c. These similarities demonstrate the interest of BCS-BEC crossover issue in the context of high-temperature superconductivity: it constitutes the simplest way to understand the presence of a pseudogap in the one-particle density of states above T_c [16].

This explanation suggests that the pseudogap may be the consequence of some local "precursor" pairing below T^*, the long-range superconducting order appearing only at T_c. But in order to apply these considerations to the underdoped HTCS, it is necessary to include as well the additional effects of both the strong anisotropy γ and the small charge carriers density n on the order parameter characterizing the superconducting state below T_c. The importance of the latter two ingredients follows from the fact that in (quasi-) 2D systems the thermal fluctuations of the phase of the (complex) superconducting order parameter are strongly enhanced. [3] The small value of n favors even further the development of this regime by reducing the cost in energy of the phase fluctuations [17]. As a consequence, these order parameter thermal fluctuations are expected to play an important role in the appearance of precursor superconducting

[3] In a strictly 2D system this corresponds to the Berezinskii-Kosterlitz-Thouless (BKT) physics [30].

effects, for instance in helping to make T_c (further) different from T^* by lowering the appearance of phase coherence and thereby the onset of the long-range superconducting order [18].

The question of determining the relative importance of the two approaches discussed above in explaining a pseudogap of superconducting origin is still open. In principle their manifestations above T_c are quite different: the first possibility based on a short coherence length only implies the existence of "pre-formed" local Cooper pairs. The second predicts the presence of enhanced thermal superconducting (phase) fluctuations with vortex-like features. In a regime interpolating between the BCS and BEC limits in a strongly anisotropic system, it is however not clear that such an unambiguous distinction still exists between the two approaches.

In this thesis a theoretical study of certain aspects of precursor pairing is presented (see next section). It is based on a simple model for short-coherence length superconductors that includes as well the effects of the strong anisotropy γ and the small charge carriers density n discussed above. This model is defined on the microscopic level by the attractive (or negative-U) Hubbard Hamiltonian [25] and will be presented in more details in Chapter 2. It is particularly well suited for the study of the BCS-BEC crossover problem since the control quantity $k_F\xi_0$ can be "tuned" at will by simply varying the attraction strength U. Although it is certainly too simplistic to describe all the complex physics that takes place in the copper oxide high-temperature superconductors (see Section 2.3), it allows nevertheless to understand some aspects of the pseudogap issue, as long as one assumes that the latter has something to do with superconductivity!

It is therefore worth mentioning briefly some (strong) experimental support that exists for this assumption, coming principally from spectroscopic studies (ARPES and tunneling) [19, 20]. They have shown that the pseudogap displays both the same amplitude and nontrivial d-wave symmetry as the superconducting gap and goes over smoothly into the latter as the phase transition is approached. Other techniques have been used to detect the presence of precursor superconductivity in the high-frequency conductivity [21], through the presence of vortex-like excitations [22] and in the local diamagnetic response [23]. Some experiments also lead to the conclusion that the pseudogap is not related to superconductivity [24], so that the a combination of more two or more mechanisms (see below) cannot be excluded neither.

This scenario of a superconducting origin for the pseudogap observed in the "normal" state of underdoped high-temperature superconductors is by far is not unique and other mechanisms have been have been proposed as well. Briefly, they are based on enhanced antiferromagnetic spin fluctuations in the proximity of the Mott insulating state at zero-doping [10], on the existence of a quantum critical point at doping $x = 0.19$

[11], on the fractionalization of the charge carriers (spin-charge [12] or even more exotic [13]) or finally on the presence of a microscopic phase separation in the form of stripes [14]. The validity of these different approaches is still debated, essentially because the large amount of experimental facts does not allow to favor clearly one or the other of the competing interpretations.[4] It is also not excluded that the solution may lie in a *combination* of two or more of these scenarios, as it has been recently considered for the example of enhanced spin fluctuations and precursor d-wave pairing [15].

1.4 Main contributions of this thesis

This thesis is concerned with three different aspects of superconductivity which cannot be described by the traditional BCS mean-field approach valid for long-coherence length superconductors. They concern principally the precursor pairing issue that may be of some importance in the understanding of the pseudogap phenomenon observed in copper oxide high-temperature superconductors.

- The first problem to be treated is related to the fluctuation-induced diamagnetism above the transition temperature, a remanent effect of the perfect diamagnetism present in the superconducting state below T_c. Recent experiments on $YBa_2Cu_3O_{6+x}$ (YBCO) [26] have shown that the available approaches based on Gaussian fluctuations of the order parameter can account for the observations in optimally doped samples but not in underdoped ones. In Chapter 3 a new treatment is proposed, based on the assumption that the relevant fluctuations for the diamagnetic response concern the phase of the order parameter. The latter is described by a layered XY model for which the introduction of the vortex degrees of freedom allows to treat on an equal footing the dependences on both the temperature T and the applied magnetic field B. The results of the calculations of the orbital magnetic susceptibility χ and the magnetization M are compared with the experimental data and show a good agreement. They also provide a clear physical interpretation of the diamagnetic response in term of an interplay between thermally excited vortex loops and field-induced vortex lines.

- In Chapter 4 a study of the thermodynamic properties of short-coherence length superconductors is performed. It is motivated by recent measurements of the specific heat of strongly anisotropic underdoped high-temperature superconductors which show clear features of a Bose-Einstein condensation (BEC) [27]. These observations were interpreted in a "strong coupling" approach [28]: *all* the electrons already form local (singlet) Cooper pairs above T_c, which undergo a BEC at the phase transition. Contrasting with this point of view, the results of the analysis of Chapter 4 show that BEC-like properties can already appear in

[4] Or, inversely, the various theoretical approaches are not accurate enough to allow for a quantitative analysis of the experiments in order to test rigorously their predictions.

the case of short-coherence length superconductors, which corresponds to an intermediate coupling regime, and that they concern only one part of the electrons. More precisely, the calculations show the propagator of the pairing fluctuations above T_c describes long-lived noninteracting bosonic quasiparticles as soon as a well-developed pseudogap is present in the density of states. As the phase transition is approached, the chemical potential of these bosons tends to zero, like in a BEC. These properties are strongly dependent upon the magnitude of the anisotropy γ and disappear when γ is too small. Since underdoped compound like $Bi_2Sr_2CaCu_2O_{8+x}$ (BSCCO) and YBCO are also characterized by a short coherence length, these considerations may help to understand better the different shapes of their specific heat curves.

- The third part of this thesis contains the results of the application of the Determinant Quantum Monte Carlo (DQMC) technique to the study of the 3D attractive Hubbard model. This numerical method is of great interest, since it is in principle free of systematic errors (i.e errors resulting from an approximation scheme). It is thus the ideal tool for treating the intermediate coupling regime between BCS and BEC because most other approaches are affected by uncontrolled errors in this typically non-perturbative parameter range. An inevitable drawback is the restriction to small systems: the largest size considered in this work is a cubic lattice of 1000 sites. However, by performing a finite-size scaling, the value of quantities like the transition temperature T_c can be evaluated in the limit of an infinite system. This could not be done before because of too weak computational facilities. The physical results concern essentially the BCS-BEC crossover: the two temperatures T_c and T^* are calculated and their dependence in the coupling U and in the density n is analyzed. A comparison between 2D and 3D realizations of the model points out to significant differences in the precursor pairing effects in the intermediate coupling regime, confirming the importance of the dimensionality in pseudogap phenomena, as mentioned previously.

1.5 Plan of this manuscript

The next chapter contains an introduction to the attractive Hubbard model, which is the basic theoretical tool used in this thesis, as well as a discussion of the methods which are used to treat the various problems. Chapter 3 is devoted to the study of the fluctuation-induced diamagnetism and its application to underdoped YBCO. The analysis of the thermodynamic properties of anisotropic superconductors in the pseudogap regime is presented in Chapter 4. An introduction to the DQMC technique as well as the results of its application to the 3D attractive Hubbard model are shown in Chapter 5. The last chapter contains some general concluding remarks.

Chapter 2

The attractive Hubbard model

The theoretical framework of this work is presented. It is based on the attractive Hubbard Hamiltonian which describes lattice fermions with a local isotropic pairing interaction. After having discussed the physics associated with this model, the mathematical methods used to study specific aspects are introduced and their formal aspects compared.

2.1 Basic definitions

The attractive Hubbard Hamiltonian is given by the following expression, written in the formalism of the second quantization:

$$\mathcal{H} = \mathcal{H}_0 + \mathcal{H}_I \tag{2.1}$$

where

$$\mathcal{H}_0 = -t \sum_{\langle i,j\rangle,\, \sigma=\uparrow,\downarrow} (c^\dagger_{i\sigma} c_{j\sigma} + c^\dagger_{j\sigma} c_{i\sigma}) - \mu \sum_i (n_{i\uparrow} + n_{i\downarrow}) \tag{2.2a}$$

$$\mathcal{H}_I = -U \sum_i n_{i\uparrow} n_{i\downarrow}. \tag{2.2b}$$

The operator $c^\dagger_{i\sigma}$ ($c_{i\sigma}$) creates (annihilates) a fermion of spin σ on site i of a regular (square or cubic) lattice of N points and $n_{i\sigma} = c^\dagger_{i\sigma} c_{i\sigma}$ gives the corresponding particle density. As suggested by Eq.(2.1), $\mathcal{H}$ implies a competition between the two distinct tendencies illustrated in Figure 2.1:

- the kinetic energy $\mathcal{H}_0$ which is characterized by the hopping amplitude $t > 0$ and allows for the particles to delocalize by moving between different points of the lattice. In Eq.(2.2a) only the motion between two neighboring sites $\langle ij\rangle$ is retained for simplicity, but more complicated cases can be considered as well.

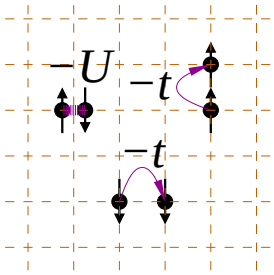

Figure 2.1: Schematic representation of some of the processes allowed by the attractive Hubbard Hamiltonian in 2D: hoppings onto one of the four nearest neighboring sites (energy gain t) and the double occupancy of one site (energy gain U).

The second sum in $\mathcal{H}_0$ is the consequence of the grand canonical treatment of the problem and will be discussed at the end of this section.

- the pairing energy $\mathcal{H}_I$ which is quantified by the prefactor $-U < 0$ and favors the presence of two fermions of opposite spins on each site i. [1] The appearance of a superconducting phase with singlet s-wave pairs at low temperatures is a direct consequence of this two-body interaction term.

In order to study the physical properties of the attractive Hubbard model, it is in principle necessary to diagonalize $\mathcal{H}$, which is unfeasible in practice for an arbitrary value of $U > 0$. But for the noninteracting case $U = 0$, $\mathcal{H}$ is equal to $\mathcal{H}_0$ and thus becomes a one-body operator (i.e. quadratic in the c's) whose spectrum can be found by Fourier transformation due to the translational symmetry of the lattice. One defines

$$c_{\mathbf{k}\sigma} = \frac{1}{\sqrt{N}} \sum_j c_{j\sigma} \exp(i\,\mathbf{k}\cdot\mathbf{r}_j) \tag{2.3}$$

where $\mathbf{r}_j \in \mathbb{Z}^D$ is the position vector for site j, $D = 2$ or 3 being the dimension of the lattice, and $\mathbf{k}$ is a (wave) vector situated in the Brillouin zone $[-\pi, \pi]^D$.[2] Unless specified (as in Chapter 3), all the distances are given in units of the constant of the underlying square or cubic lattice. $\mathcal{H}_0$ is tranformed into the diagonal expression

$$\mathcal{H}_0 = \sum_{\mathbf{k},\sigma=\uparrow,\downarrow} (\varepsilon_{\mathbf{k}} - \mu)\, c^\dagger_{\mathbf{k}\sigma} c_{\mathbf{k}\sigma} \tag{2.4}$$

[1] In fact the original (repulsive) Hubbard model [29] differs only by the sign of the prefactor of the interaction but describes a totally different physics.

[2] To be precise, $\mathbf{k}$ must be of the form $\frac{2\pi}{\sqrt[D]{N}}(i,j,k)$ for the integers $-\frac{\sqrt[D]{N}}{2} < i,j,k \leq \frac{\sqrt[D]{N}}{2}$ when periodic boundary conditions are used.

and the function $\varepsilon_{\mathbf{k}}$ is the tight-binding dispersion which reads

$$\varepsilon_{\mathbf{k}} = -2t \sum_{i=1,\ldots,D} \cos(k_i). \tag{2.5}$$

It allows to define the noninteracting bandwidth $W = 4Dt$ which gives the extension of the spectrum of $\mathcal{H}_0$.
In Eq.(2.5), the zero point of the energy scale is fixed at the middle of the tight-binding band $\varepsilon_{\mathbf{k}} = 0$. This also concerns the chemical potential μ present in Eqs.(2.2a) and (2.4) which plays an important role in the grand canonical treatment of the finite-temperature properties of the system described by the Hamiltonian (2.1). Indeed, in order to guarantee a constant density n when varying the temperature T, it is necessary to consider first the equation [3]

$$n = n(T, \mu, U) \equiv \frac{1}{N} \langle \mathcal{N} \rangle \equiv \frac{1}{N} \sum_i \langle n_{i\uparrow} + n_{i\downarrow} \rangle. \tag{2.6}$$

This relation is called "number equation" and has to be inverted to find the function $\mu = \mu(T, n, U)$ allowing to work at constant filling $0 < n < 2$ for all values of T and U.

2.2 Basic properties

The fundamental properties of the attractive Hubbard model (2.1) are briefly recalled in order to introduce the theoretical context underlying this work. The maybe most important feature is the fact that the Hamiltonian $\mathcal{H}$ presents a superconducting phase for all parameters values $U > 0$ and $0 < n < 2$. It is characterized by a "normal" low-temperature state of broken U(1) gauge symmetry for $D > 2$ and by a Berezinskii-Kosterlitz-Thouless (BKT) regime [30] for $D = 2$.[4] In what follows the realizations of this superconducting phase in some particular regions of the $U - n$ parameter space are discussed in more details (in $D = 3$ for simplicity).

Weak coupling limit $U \ll W$

In this case the theory of Bardeen, Cooper and Schrieffer (BCS) applies to understand the appearance of superconductivity. At low temperatures the Fermi sea, which is the many-particle eigenstate of the noninteracting Hamiltonian $\mathcal{H}_0$, becomes unstable as soon as $U > 0$ (Cooper instability) and the system adopts a ground state which is given by the BCS wave function. The latter describes a *coherent* superposition of

[3] The definition of the expectation value of an operator is given in Eq.(5.1).

[4] Although this statement is a consequence of the general theory of phase transitions for the universality class $D = d = 2$, it has been confirmed only numerically for the moment [31, 32].

states with a variable number of fermionic pairs with opposite momenta and spins, i.e. corresponding to the product $c^\dagger_{\mathbf{k}\uparrow}c^\dagger_{-\mathbf{k}\downarrow}$. The spectrum of the Hamiltonian $\mathcal{H}$ is characterized by an energy gap Δ around the Fermi energy $\mu + W/2$ given by the implicit equation (for $T = 0$)

$$\frac{1}{U} = \frac{1}{N}\sum_{\mathbf{k}} \frac{1}{2\sqrt{\Delta^2 + (\varepsilon_{\mathbf{k}} - \mu)^2}}. \tag{2.7}$$

The derivation of Eq.(2.7) assumes that the spatial extension ξ_0 of the Cooper pairs is much larger than the lattice constant so that they strongly overlap on another. This corresponds to the mean-field regime already discussed in Section 1.1. Now it can be justified by calculating the coherence length of the BCS superconductor. The result reads (see Appendix D of Ref.[1])

$$\xi_0 = \frac{v_F}{\Delta} \sim \frac{\sqrt[D]{n}}{\Delta/t} \tag{2.8}$$

where $v_F = 2k_F t$ is the Fermi velocity. Taking for instance $U = 0.75t$ and $n = 0.5$ gives $\Delta \simeq 0.001t$ so that the relation $\xi_0 \sim 800 \gg 1$ is indeed satisfied. The finite-temperature properties of the BCS superconductor are governed by the Bogolubov excitations, which consists in occupying the states above the gap by "breaking" the fermionic pairs. Thus at the critical temperature $T_c = e^\gamma/\pi\,\Delta \approx 0.56\,\Delta$ all the pairs have disappeared and the gap at the Fermi level definitely closes, so that the physics of the Fermi sea is entirely restored above T_c.

Strong coupling limit $U \gg W$

When the interaction strength U is large, the fermions arrange themselves in tightly bound singlet pairs localized at each lattice site i. The latter have a clear bosonic character so that it makes sense to define operators like $b^\dagger_i \equiv c^\dagger_{i\uparrow}c^\dagger_{i\downarrow}$ describing "local pairs" and calculate their commutation rules. They read

$$b_i^2 = b_i^{\dagger\,2} = 0 \tag{2.9a}$$

$$[b_i, b_j^\dagger] = \delta_{ij}(1 - 2\,b_i^\dagger b_i). \tag{2.9b}$$

These results imply that the system is equivalent to hard-core bosons for which the double occupancy of one site i in Eq.(2.9a) is forbidden by the Pauli principle still valid for the underlying fermions. The original Hamiltonian (2.1) can be re-expressed in terms of these (quasi-) bosonic operators and expanded in powers of the small parameter t^2/U using perturbation theory [25]. To lowest order, it describes lattice bosons with a hopping amplitude $t_B = 2t^2/U$ and a density-density interaction between nearest neighbors $\langle i, j\rangle$ given by $V_B = t^2/U$. For simplicity this bosonic interaction $V_B \ll W_B \equiv 8Dt^2/U$ as well as the hard-core constraint (2.9a) are neglected in the following, an approximation which becomes better when considering low densities n.

As a consequence, $\mathcal{H}$ describes a gas of free lattice bosons for which the original superconducting phase transition can be re-interpreted as a Bose-Einstein condensation (BEC).[5] In this case, at $T = 0$, all the (composite) particles are in the same quantum state with zero momentum represented by $b_{\mathbf{k}=0}$. The excitations of the BE condensate for $T > 0$ consist in particles "dropping out" the condensate and occupying a finite-momentum state $b^{\dagger}_{\mathbf{k}}$ available in the (tight-binding) bosonic band $W_B = 4Dt_B$. At $T = T_c$ the condensate disappears and the system is then constituted by independent bosonic pairs moving around. At a temperature scale $T^* \sim U$ pair-breaking processes start to become important so that for $T \gg U$ all pairs have "dissociated" and the free fermion physics is finally restored. As an extension of the BCS point of view, the behavior described above can be summarized by admitting the existence of a gap $\Delta \sim U$ between a lower band of bosonic excitations and an upper band of fermionic single-particle states which start to be occupied for $T \gtrsim T^* \gg T_c$ only.
The coherence length for the strong coupling can be obtained from Eq.(2.8) and reads

$$\xi_0 \sim \frac{\sqrt[D]{n}}{\Delta/t} \sim \frac{\sqrt[D]{n}}{U/t} \ll 1 \tag{2.10}$$

which means that the pairs become smaller and smaller when U increases, as expected intuitively.[6]

Intermediate coupling $U \sim W$

As suggested by the two cases considered above, this regime corresponds to the intermediate region of the BCS-BEC crossover, a concept which was already mentioned in the Introduction. Since the pioneering works by Legett [35] at $T = 0$ and by Nozières and Schmitt-Rink [36] for $T \geq 0$, it has been established and confirmed by many authors [16] that the crossover between the BCS superconductivity and the BEC of "preformed" fermionic pairs is a *smooth* process. An important property of the attractive Hubbard Hamiltonian (2.1) is the fact that it allows to cover the latter entirely by simply varying the interaction strength $U > 0$.
The physical properties appearing for $U \sim W$ are expected to interpolate between the two limiting regimes BCS and BEC. For instance, the well-defined bosonic states present above the BEC phase transition become progressively damped when U decreases and their dispersion changes as well. In this way they represent short-lived sound-like collective excitation modes in the weak coupling regime and play a minor role in determining the physical properties of the system. An exhaustive understanding of this coupling regime is however not yet achieved and many efforts, including the present thesis, are devoted to improve the latter. A particular attention is given

[5] The presence of a lattice does not modify fundamentally the BEC but some unexpected effects can be observed at finite temperatures, for instance in the specific heat c_V [33].

[6] Although expression (2.8) was initially calculated in the BCS weak coupling limit, it gives a satisfactory estimate of the coherence length in the other cases as well. A rigourous definition of the pair size ξ_0 at zero temperature and valid for any U is given in Ref.[34].

to the "normal" state where the two temperature scales T_c and T^* are close but still distinct, due to its possible relevance in understanding the pseudogap phase of underdoped high-temperature superconductors (see Sections 1.3 and 2.3).
By comparing the results for the BCS and the BEC cases in Eqs.(2.8) and (2.10), it is easy to find an estimate for the coherence length in the intermediate coupling regime. It satisfies:

$$\xi_0 \sim 1 \tag{2.11}$$

which constitutes the middle point between the real-space BEC pairing $c^\dagger_{i\uparrow}c^\dagger_{i\downarrow}$ and the reciprocal-space BCS pairing $c^\dagger_{\mathbf{k}\uparrow}c^\dagger_{-\mathbf{k}\downarrow}$.

Half-filling $n = 1$ and $U > 0$

For an average density of exactly one particle per site, the tight-binding band given by the dispersion (2.5) displays particle-hole symmetry. By choosing the chemical potential as

$$\mu(T, n = 1, U) = -\frac{U}{2}, \tag{2.12}$$

the whole Hamiltonian (2.1) is made invariant under the particle-hole transformation $c^\dagger_{\mathbf{k}\sigma} \rightarrow h_{-\mathbf{k}-\sigma}$ for all values of T and U. Thus the solution of the number equation (2.6) for $n = 1$ is already found through Eq.(2.12).
Another consequence of this additional symmetry is the fact that the phase transition described by the model changes its universality class at half-filling. This concept is defined by two quantities: the spatial dimension D of the system (here $D = 2,\ 3$) and the dimension d of the order parameter characterizing the phase below T_c.

- For $n \neq 1$, the Hubbard Hamiltonian (2.1) contains the gauge symmetry U(1), i.e. $\mathcal{H}$ is invariant under global gauge transformations $c^\dagger_{j\sigma} \rightarrow c^\dagger_{j\sigma}e^{i\alpha}$ for any real number α. [7] The U(1) symmetry is associated with the conservation of the total particle number, as indicated by the commutator $[\mathcal{H}, \mathcal{N}] = 0$. Below T_c the system is in a state which is no more an eigenvector of $\mathcal{N}$ and thus "breaks" the gauge symmetry U(1). In this case the order parameter dimension d is equal to 2.

- For $n = 1$, one uses the canonical transformation defined by $c^\dagger_{j\uparrow} \rightarrow d^\dagger_{j\uparrow}$ and $c^\dagger_{j\downarrow} \rightarrow d_{j\downarrow}\, e^{i\mathbf{Q}\cdot\mathbf{r}_j}$ where $\mathbf{Q} = (\pi, ..., \pi)$ to map the attractive Hubbard Hamiltonian onto the *repulsive* Hubbard Hamiltonian at half-filling as well. At low energies, the latter is equivalent to an isotropic Heisenberg Hamiltonian which is used to describe quantum magnets. In addition to establishing a relation between

[7] $\mathcal{H}$ satisfies also a SU(2) symmetry due to its invariance under rotations in spin space, but the latter is not relevant here.

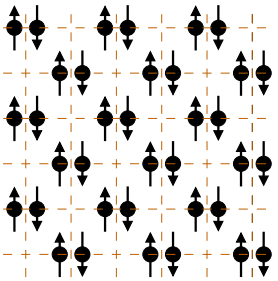

Figure 2.2: Charge-density wave (CDW) order (in 2D): one sublattice has charge 2 on each site whereas the other one has charge 0 everywhere.

superconductivity and magnetism, the above transformation shows also clearly that the symmetry of $\mathcal{H}$ for $n = 1$ is the SO(3) group which leaves invariant the Heisenberg Hamiltonian. Therefore the order parameter dimension d is equal to 3 is this case.

A consequence of the above properties is the fact that the superconducting order represents only a partial aspect of the ordered state below T_c at half-filling, i.e. 2 components of a tridimensional vector. The remaining component describes the charge-density wave (CDW) order illustrated in Figure 2.2, which appears in the half-filled system as soon as U is different from zero. Thus the attractive Hubbard model allows to consider the case where superconductivity represents only one part of the order parameter. This is interesting in regard of the SO(5) approach to high-temperature superconductivity where the 1D CDW is replaced by the 3D antiferromagnetic order [37].

2.3 Physical content of the model

After presenting the main physical properties of the attractive Hubbard model, it is useful to discuss shortly its philosophy and its relevance in the description of real materials.

Unlike high-energy physics, there exists no “standard” model that describes the solid state in a unified way because of its intrinsic complexity. Instead, the theoreticians proceed by studying simplified models which contain only the ingredients assumed to be essential to the understanding of the considered problem and allow for an accessible mathematical treatment. In what concerns the particular cases of “strongly correlated” electronic systems, an approximation-free solution to even the simplest models (Hubbard for instance) is still missing for some parameters values of interest. This is due to the nonperturbative nature of these problems for which the effects of the electronic interactions lead however to probably the most intriguing phenomena of condensed

matter physics. The attractive Hubbard model introduced above belongs to the latter category: it is indeed the simplest tool to study superconductivity, because involving only the three free parameters U/t, n and T/t beside the lattice dimension D. Yet, as discussed in Section 2.4, there still exists no rigorous solution for its intermediate coupling regime. It may look surprising to consider an *attraction* between equally charged electrons and some explanations about this feature are given in the following.

The attractive Hubbard model is in fact the lattice generalization of the BCS effective Hamiltonian for which the energy cut-off at the Debeye frequency has been replaced by the finite bandwidth W. This substitution has suppressed the long-range character of the phononic interaction, the Hubbard interparticle coupling acting only locally when two fermions occupy the same site.[8] Historically, the difficulty in finding a microscopic theory for (conventional) superconductivity can be partially explained by the fact that it was hard to guess that the electronic interaction may become attractive. As Fröhlich first showed for this case [39], it was the consequence of a subtle many-body effect due to the electron-phonon coupling. Over the years other mechanisms that lead to an effective electronic attraction have been found and are summarized in Ref.[25]. As suggested by the Cooper instability [40] and later by the Thouless criterion [41], the fact that the electronic interaction becomes attractive in a wave-length and frequency window constitutes a sufficient condition to enforce the system to become superconductor (whether it is also a necessary condition is still an open question). Thus the attractive Hubbard model (2.1) can be considered as a "short-cut" for the study of superconductivity, avoiding the complications of determining the microscopic mechanism responsible for the attraction. This pragmatic approach allows in particular to use the Hamiltonian (2.1) for the study of certain properties of the high-temperature superconductors. Indeed a microscopic theory overall accepted is still missing for the latter materials and they present several fundamental features that can be easily taken into account by the attractive Hubbard model.

It was already mentioned in Section 1.3 that HTSC were characterized (among other things) by a strong anisotropy and a short coherence length. It was also suggested that certain properties of these materials could be understood in the framework of a crossover between BCS theory (in the overdoped region) and BE condensation (in the underdoped phase). As shown in Section 2.2, the attractive Hubbard model is a convenient theoretical tool to study these problems, which explains why it became so popular in the last years. In particular, as anticipated above, the intermediate coupling regime ($U \sim W$) is the most interesting since it allows to examine the appearence of a pseudogap above T_c, which results from precursor electronic pairing. This idea of a pseudogap related to superconductivity has been already discussed in Section 1.3 and

[8] This distinction is not important for small U, unlike the strong coupling regime where the phononic case described by the Eliashberg theory [38] is quite different from what has been presented in the previous section for $U \gg W$.

turned out to be one of the possible explanations of the non-Fermi-liquid properties observed in the "normal" state above T_c of underdoped high-temperature superconductors. These reasons are sufficient to justify the choice of the attractive Hubbard model as the fundamental theoretical ingredient of this thesis.

However its defects and limitations must not be disregarded: besides the attraction of unspecified origin, this model yields s-wave pairing instead of the d-wave observed experimentally. There exists similar Hamiltonians [43] which can take this feature into account. They allow furthermore to include the presence of antiferromagnetism at zero doping, an aspect which is totally absent in the model (2.1). A corrollary of this absence is the fact that the particles described by the attractive Hubbard Hamiltonian (2.1) correspond in reality to the *holes* appearing in the CuO_2 planes when the doping x in nonzero. It is therefore important to keep in mind the above considerations when applying this (simple) model to real materials.

But it is useful to recall that studies of the BCS-BEC crossover based on the attractive Hubbard model appeared well before the high-temperature superconductors were discovered. This shows that this problem is already interesting by itself. In particular a pre-BCS attempt to explain (conventional) superconductivity was based on a BEC scenario [44]. Thus this property of a smooth crossover between the two limiting cases allows to reconcile these two aspects of quantum superfluidity.

2.4 Discussion of the theoretical methods

Since three rather different approaches to the attractive Hubbard model are used in this thesis, it is useful to recall first some general considerations about the various ways of dealing with the Hamiltonian (2.1). Then a synopsis of the methods used in Chapters 3, 4 and 5 is presented.

An exact solution to the attractive Hubbard model, which consists in finding the eigenvalues and eigenstates of the operator $\mathcal{H}$ from Eq.(2.1), is unfortunately not known. It is therefore necessary to rely on various approximations to perform the calculations allowing the answer the questions raised in Section 1.4. Ideally, these approximations should be based on assumptions about some physical properties. For instance in the BCS approach mentioned above, the mean-field approach assumes that a Cooper pair overlaps with many others so that it "feels" the latter globally as if they were constituting a constant external potential Δ, called the pairing field. [9] But on the other hand,

[9] The validity of this assumption was confirmed a posteriori by the fact that the spatial extension of a pair ξ_0 was much larger that the interparticle distance $\sqrt[D]{n}$. Indeed for $U = 0.75t$, the combination of Eqs.(2.7) and (2.8) gives $\xi_o/\sqrt[3]{n} = \Delta^{-1} \sim 1000 \gg 1$.

approximations are often necessary in order to overcome the mathematical and numerical difficulties represented by treating an interacting quantum many-body problem.

Generally, two a priori distinct points of view can be taken in approaching theoretically the phenomenon of superconductivity. As first done successfully by BCS, superconductivity can be investigated on the electronic (microscopic) level and the attractive Hubbard Hamiltonian $\mathcal{H}$ is an ideal tool in this context. But it can be studied as well by focusing on the *collective* behavior of the electrons, by developing a classical field theory for a space-time dependent version of the above mentioned pairing field Δ. One finds then exactly the Ginzburg-Landau (GL) functional that describes the low-energy long-wavelength properties of the superconductors. As first shown by Gorkov, the latter can be derived from a microscopic Hamiltonian like $\mathcal{H}$. The relations between the individual and collective aspects of the electrons have been intensively studied recently, mainly in the context of the pseudogap issue. Indeed going beyond BCS mean-field treatment is necessary in order to describe correctly the consequences on one-particle properties (like the density of states) of the strong thermal fluctuations of the order parameter Δ which are present in (quasi) two-dimensional systems.

The above distinction is very useful in allowing to classify schematically the main approaches that have been developed to study the attractive Hubbard model. This discussion is however restricted to the formal aspects since the physics will be treated in the corresponding chapters.

- A first category uses the formalism of functional integration to replace the electronic interaction by a coupling to the classical field Δ using the Hubbard-Stratonovich transformation. These methods allow to treat nonperturbatively the whole BCS-BEC crossover [45, 46, 47] and are quite appropriate for the study of the interplay between the collective behavior and the individual aspects of the electrons [18]. For problems restricted to low-energy and long-wavelength regimes, the electronic degrees of freedom can be integrated out to finally retrieve the Ginzburg-Landau theory. This approach was the most successful in the description of both the critical regime around T_c [5, 48] and the orbital magnetic properties of the HTSC compounds [49].

- Another category is constituted by the many-body approaches based on the calculation of Green's functions which thus give the proper information about the one- or two-body quantities. They consist in ressummation schemes of Feynman diagrams for the case of the T-matrix [36, 50, 51, 52] and fluctuations exchange (FLEX) methods [32]. They present in principle a self-consistent character, due to the fact that the pairing aspect is considered from a purely electronic point of view without referring to Δ. The sum rule approach [42] also belongs to this category and turns out to give very accurate results for weak to intermediate couplings U. The dynamical mean-field theory (DMFT) has been applied very

recently to the attractive Hubbard model [53, 54] and constitutes a nontrivial improvement of the mean-field approximation mentioned above by treating exactly the local fluctuations of the microscopic degrees of freedom.

- The quantum Monte Carlo (QMC) numerical techniques form the third category. They allow to evaluate expectation values of electronic quantities and are in principle free of any systematic errors. Algorithms exist for both ground state and finite-temperature properties [55, 56]. Their application to the attractive Hubbard model does not generate the fermion minus-sign problem which makes them inapplicable otherwise. Due to technical limitations, finite-size effects are present in the results and an extrapolation to the thermodynamic (TD) limit has to be performed in order to draw meaningful conclusions.

In this thesis a method from each category will be used to treat the problems mentioned in Section 1.4 of the Introduction. Their choice is briefly discussed in the context of the above considerations and further details will be given in the respective chapters.

- The discussion of the orbital diamagnetism above the critical temperature T_c in Chapter 3 will be based on a GL-type approach, emphasizing thereby the collective aspect of the electrons. The latter is contained in the response currents to the applied magnetic field B for which the typical length scales are *mesoscopic* (~ 0.1 μm), given typically by the Abrikosov vortex lattice constant $\sqrt{\Phi_0/B}$ where Φ_0 is the flux quantum and $B < 10$ T. Since they dictate the choice of the model (3D layered XY), the microscopic details remain important. The central part of the calculation consists then in evaluating a current-current correlation function for which the duality between the XY model and the (classical) Coulomb gas will be used [57].

- In Chapter 4, the study of the relations between the electronic structure and the thermodynamic properties in the pseudogap regime requires naturally an approach from the second of the above categories. For the considered case of a short-coherence length superconductor (intermediate coupling $U = 4t$), the self-consistent T-matrix approximation scheme is used. But in order to perform a tractable analytical calculation, the full self-consistency is replaced by an approximate iterative strategy where some numerical results are used to construct the solution. This allows to treat the pairing field Δ in a "renormalized" Gaussian approximation, taking into account the feed-back effects on Δ of the nontrivial electronic structure.[10]

- The Determinant Quantum Monte Carlo (DQMC) technique is used to study the finite-temperature properties of the 3D attractive Hubbard model in Chapter 5. In this thesis only thermodynamic quantities and time-independent two-point correlation functions are calculated. In particular the evaluation of $\langle \mathcal{N} \rangle$ allows to

[10] The non-self-consistent version considers the fluctuations of Δ on the Gaussian level.

solve numerically the number equation (2.6) and consider a density n different from half-filling ($n = 1$). The detailed study of the correlation functions gives all necessary information about the presence of long-range order (LRO) and allows to construct the functions $T_c(U, n)$ and $T^*(U, n)$.

2.5 Comparison of the basic formalisms

To be more concrete about the different approaches discussed above, the basic equations defining each method are presented. This allows to compare how the various aspects of the basic Hamiltonian (2.1) are treated in each case.
At the microscopic level the basic object for describing the finite-temperature properties of the electrons is the imaginary-time Green's function defined as

$$G(1|2) = -i\,\frac{\mathrm{Tr}\,\exp(-\beta\mathcal{H})\,\mathcal{T}_\tau(c_2\,c_1^\dagger)}{\mathrm{Tr}\,\exp(-\beta\mathcal{H})} \tag{2.13}$$

where the trace means $\mathrm{Tr}\,\mathcal{A} = \sum_n \langle\psi_n|\mathcal{A}|\psi_n\rangle$ for the eigenstates $|\psi_n\rangle$ of $\mathcal{H}$, the labels 1 and 2 stand for (i, τ, σ) where $0 \leq \tau < \beta$ is the imaginary time and $\mathcal{T}_\tau$ represents the time-ordering operator. The concept of imaginary time is defined by making the substitution

$$t \to i\tau \tag{2.14}$$

in the Heisenberg equations of motion for the operators $c_1^\dagger$ and c_2. Then the (formal) solution of the latter is introduced in Eq.(2.13) and implies the fundamental property that G is *antiperiodic* in its time arguments:

$$G(\tau_1 + \beta|\tau_2) = G(\tau_1|\tau_2 + \beta) = -G(\tau_1|\tau_2) \tag{2.15}$$

This allows to define the corresponding Fourier series by defining the (fermionic) Matsubara frequencies as

$$z_\nu = (2\nu + 1)\,\frac{\pi i}{\beta} \tag{2.16}$$

where the label ν is an integer. A bosonic counterpart can be defined as well, but in this case the Green's function is periodic in β so that the corresponding frequencies are $z_\alpha = \alpha\, 2\pi i/\beta,\ \alpha \in \mathbb{Z}$. In addition to enabling the advantageous use of Fourier series, this formalism makes the summation of infinite quantities of Feynman diagrams well-defined because of the convergence generated by the exponentials with negative (real) arguments. At the end of the calculation, an analytical continuation $z_\nu \to \omega + i\delta,\ \delta \to 0$, has to be performed in order to restore the real-time dynamics. Although this step is trivial in an analytical calculation, it is very delicate numerically

[58, 59] and will not be attempted in this work.[11]
All the information about *one-particle* properties is contained in G. The description of superconductivity, which is a *collective* effect, requires the introduction of a two-particle Green's function $G_2(1,2|1',2')$ defined analogously to Eq.(2.13). The T-matrix consists then in selecting a particular type of Feynman diagrams (the "ladder" diagrams) in order to construct an approximation of G_2 in terms of G.
In Determinant QMC, the Hirsch transformation is used to map the (quantum) problem of 3D lattice fermions into a classical problem of an Ising magnet in $D = 3 + 1$, the additional dimension being the imaginary time τ. The partition function of the system reads therefore

$$Z = \sum_{\{x\}} p[x] \tag{2.17}$$

where x is a configuration of $L \times N$ Ising spins ($x(i,\ell) = \pm 1$), L being the number of steps used to discretize the time interval $\beta = L\Delta\tau$. The expectation values of time-independent operators $\mathcal{A}$ are calculated as

$$\langle \mathcal{A} \rangle = \sum_{\{x\}} p[x]\ A[x] \tag{2.18}$$

This sum is calculated numerically using a standard Monte Carlo method.
For the Ginzburg-Landau approach, it is first necessary to apply a Hubbard-Stratonovitch transformation to replace the interacting electrons by the classical pairing field Δ. This procedure is performed conveniently using the formalism of functional integration. Only the final result is presented here, more details about this standard calculation can be found in Refs.[46, 60]. The partition function reads then

$$Z = \int \mathcal{D}\Delta\, \mathcal{D}\Delta^*\ \exp\big(-\beta \mathcal{S}_{\rm GL}[\Delta, \Delta^*]\big). \tag{2.19}$$

where the explicit expression of the GL functional $\mathcal{S}_{GL}$ is given in Eq.(3.1). The coupling to an external magnetic field represented by the vector potential $\mathbf{A}(\mathbf{r})$ is fixed by the requirement of invariance under the gauge transformations

$$\begin{cases} \mathbf{A}(\mathbf{r}) & \rightarrow & \mathbf{A}(\mathbf{r}) + \boldsymbol{\nabla}\chi(\mathbf{r}) \\ \Delta(\mathbf{r}) & \rightarrow & \Delta(\mathbf{r})\ \exp\big(-\dfrac{2\pi i}{\Phi_0}\,\chi(\mathbf{r})\big) \end{cases} \tag{2.20}$$

where $\chi(\mathbf{r})$ is a regular real function. This leads to the usual canonical momentum expression $\boldsymbol{\nabla} - \dfrac{2\pi}{\Phi_0}\,\mathbf{A}(\mathbf{r})$ which takes into account the fact the magnetic field couples to pairs of charge $2e$. In this way the linear response to a variation of the vector potential can be calculated by functional derivative to obtain finally the magnetic susceptibility.

[11] This is one reason for the restriction to time-independent correlations in the QMC calculations.

Chapter 3

Fluctuation-induced diamagnetism in underdoped high-temperature superconductors

The fluctuation-induced diamagnetism appearing above the transition temperature is studied for the case of underdoped high-temperature superconductors. The orbital susceptibility χ and the magnetization M are calculated in the framework of a Lawrence-Doniach model. These results allow to understand recent measurements on underdoped YBCO where anomalous behaviors were observed in both the temperature and the magnetic field dependences of the diamagnetic response.

3.1 Introduction

The perfect diamagnetism observed in the Meissner effect is, beside the zero electrical resistance, the most spectacular property of superconducting materials. In the context of underdoped high-temperature superconductors where strong pairing fluctuations are present above the critical temperature T_c, one may expect that the orbital diamagnetic response displays some reminiscences of the Meissner effect. This phenomenon is called the fluctuation-induced diamagnetism and constitutes the subject of the present chapter.

The diamagnetism above T_c was already studied in the 1970s for the traditional low-T_c superconductors, although the thermal fluctuations are considerably weaker in the latter than in the high-T_c compounds. The original suggestion by Schmid [61] that it should manifests itself as a divergence of the zero-field susceptibility at $T \searrow T_c$ (i.e. $\chi \propto (T - T_c)^{-1/2}$ in a 3D isotropic sample) was confirmed experimentally by Gollub *et al.* [62]. The effects of a finite external magnetic field B were considered

as well [63]. The early developments in this domain are summarized in Tinkham's textbook [64].

More recently the intense studies of the $B-T$ phase diagram of anisotropic layered copper oxide superconductors has revealed a very rich physics [49]. Concerning the fluctuation-induced diamagnetism above T_c, it turned out that most compounds could be satisfactorily well understood by improving existing theories [65] whereas others, essentially underdoped, require a new approach. In particular the experiments by Carretta *et al.*[26] show that underdoped $YBa_2Cu_3O_{6+x}$ presents intriguing anomalies that find no evident theoretical interpretation. More precisely, the fluctuation contribution to the zero-field orbital susceptibility χ shows appreciable values extending over a wide temperature range ($\sim$ 15 K) above T_c, in strong contrast to the corresponding optimally doped sample where χ is nonzero only over a few K above the transition, in agreement with Schmid's prediction. In addition the finite-field magnetization M also displays an unexpected behavior, incompatible with theoretical predictions [65]. It consists in an extremely sharp crossover between a low-field regime where $M \approx \chi B$ is very steep (since χ is large) and a high-field region where the slope of M is much smaller, the crossover field being around 0.05 T. The work presented in this chapter constitutes an attempt to understand theoretically these experimental facts.

In the two previous chapters the attractive Hubbard Hamiltonian was presented as a suitable model for short-coherence length superconductors. It turns out that it might describe some aspects of real materials such as underdoped high-T_c compounds like YBCO which is considered here. However the study of orbital magnetic properties on the microscopic level becomes rapidly complicated [66] and it is preferable to choose a mesoscopic description based on a Ginzburg-Landau type of action for the pairing field Δ. As mentioned in Section 2.5, both approaches are in fact related by the Hubbard-Stratonovich transformation. It replaces the interacting electronic problem by a classical field theory for Δ which describes the *collective* aspects of the underlying electrons. The latter intervene then only in the coefficients of the corresponding GL functional. But two microscopic quantities are still important: the coherence length ξ_0 and the charge carriers density n.[1] To avoid any confusion, the temperature dependent length scale $\xi(T)$ associated with the spatial variations of the order parameter Δ is called the *correlation length*, as it is usually done in the context of a second-order phase transition. It has been shown that both quantities $\xi(T=0)$ and ξ_0 are practically equal as long as the pair size ξ_0 is of the order of the lattice constant or larger [67]. Thus a short correlation length $\xi(T=0)$ and a small charge carriers density n (implying a large London penetration depth) indicate that one deals with an *extreme-type II* superconductor (the Ginzburg-Landau parameter κ is very large). This property will be important when choosing an appropriate model in Section 3.2.1.

[1] n corresponds to the electronic density in the Hubbard model and to the doping (x $\sim$0.1) in real materials.

As a starting point for the forthcoming theoretical approach, it is useful to recall some of the major trends in the description of fluctuation-induced diamagnetism. They can be divided in two groups. In the first one, as initiated by Schmid for $B = 0$ [61] and extended by Prange for $B \neq 0$ [63], Δ is treated in a regime of Gaussian fluctuations. An anisotropy or a layered structure can be taken into account as well [64, 68] but the main difficulty consists in treating properly the divergent Landau-level sums appearing for $B \neq 0$ [63, 65]. The other group considers directly the critical regime of the complex order parameter Δ which is governed by XY-like models [5, 48] or, eventually, more complicated physics [69].

The calculation of the fluctuation-induced orbital diamagnetic response for the specific case of an extreme-type II superconductor is presented in Section 3.2. In order to take into account to thermal fluctuations above T_c of the (complex) pairing field Δ that have been observed in some underdoped high-T_c compounds (LSCO or YBCO) [21, 22], a model of the XY type is chosen. This corresponds to the assumption that the precursor regime above T_c is dominated by the fluctuations of the phase of Δ whereas its amplitude takes a nonzero weakly temperature-dependent expectation value [17]. The thermal properties of such a system are expressed in terms of the phase field singularities: the vortex-antivortex pairs in 2D [30] and the vortex loops and lines in (anisotropic) 3D [69, 70]. This picture allows to include easily the presence of an external field $\mathbf{B}$ which manifests itself in the same way as in a "normal" type II superconductor in the mixed phase. The orbital diamagnetic susceptibility is calculated in the framework of the linear response theory and requires thereby the evaluation of a current-current correlation function. The latter is given by the structure factor of the corresponding Coulomb gas for which a low-energy expansion is known. It contains an important parameter, the areal vortex-line element density n_V whose temperature dependence will be important in characterizing the considered fluctuation regime.

In Section 3.3 the above approach is used to analyze the experimental data by Carretta *et al.* [26] for (moderately) underdoped YBCO. This allows to fix several yet unspecified material parameters, in particular the areal vortex line element density n_V which is found to follow a thermally activated behavior, unlike in a pure critical regime where it is proportional to the inverse square of the (diverging) correlation length [71]. This regime is called "pre-critical" and turns out to be suitably described by the 3D (anisotropic) vortex loops and lines picture developed above. The agreement of the theory with the experiments is very good for the temperature dependence of the zero-field susceptibility and somewhat less spectacular for the B-dependent magnetization where the observed sharp crossover mentioned previously cannot be faithfully reproduced. However it can be interpreted as the result of a subtle interplay between thermally excited vortex loops and field-induced lines. A more quantitative study of such a problem is unfortunately beyond the present approach.

3.2 Calculation of the diamagnetic response

3.2.1 Choice of the model

Any tractable approach to the properties of such complicated materials as high-temperature superconductors requires first the choice of a model which concentrates on the essential physics for the forthcoming analysis. It must therefore describe the consequences of thermal fluctuations of the superconducting order parameter $\Delta(\mathbf{r})$ and include an external (constant) magnetic field $\mathbf{B}$. The latter is represented by the vector potential $\mathbf{A}(\mathbf{r})$ coupling in a gauge-invariant way to $\Delta(\mathbf{r})$. The "standard" model that describes this situation is based on the Ginzburg-Landau (GL) functional:

$$\mathcal{S}_{\mathrm{GL}}[\Delta,\mathbf{A}] = \int d^3r \left(a\,|\Delta(\mathbf{r})|^2 + \frac{b}{2}\,|\Delta(\mathbf{r})|^4 + c\,|(\boldsymbol{\nabla} - \frac{2\pi}{\Phi_0}\mathbf{A}(\mathbf{r}))\Delta(\mathbf{r})|^2 \right). \tag{3.1}$$

a, b and c are GL coefficients, a vanishes at the critical temperature T_c and Φ_0 is the quantum of magnetic flux. This model has been very successful in describing the B-T phase diagram of both low and high-temperature superconductors. In the present case it will be modified by implementing an important assumption concerning the relevant degrees of freedom of the field Δ. Writing

$$\Delta(\mathbf{r}) = \rho_0\, e^{i\theta(\mathbf{r})}, \tag{3.2}$$

where the amplitude ρ_0 is a temperature-independent constant, corresponds to the assumption that the relevant physics lies essentially in the fluctuations of the phase θ [17]. Eq.(3.1) then becomes the action of the XY model:

$$\mathcal{S}_{XY}[\theta,\mathbf{A}] = \frac{J}{2}\int d^3r \left(\boldsymbol{\nabla}\theta(\mathbf{r}) - \frac{2\pi}{\Phi_0}\mathbf{A}(\mathbf{r}) \right)^2. \tag{3.3}$$

Here $J = 2c\rho_0^2$ is the Josephson coupling constant. The above step is called the London approximation and has been widely used to describe extreme-type II superconductors below $T_c(B)$. In the present context ($T > T_c$), it expresses the idea that some aspects of the precursor phenomena observed in underdoped cuprates may be explained by strongly enhanced phase fluctuations. Consequently the forthcoming theory is an attempt to understand the anomalous fluctuating diamagnetism reported in Ref.[26] by the same mechanism. It is well known from the theory of critical phenomena that the superconducting transition itself belongs to the 3D XY universality class [5], but here it is moreover assumed that the same kind of fluctuations are still dominating outside the critical region itself, in what will be called a "pre-critical" regime.
Since the present theory will be applied to a YBCO, it is important to take into account a further important feature: the anisotropic structure along the direction perpendicular to the CuO_2 planes (or the z axis). This is done by introducing two distinct Josephson coupling constants $J_{\parallel}$ and $J_{\perp}$. Their ratio

$$\gamma^2 = \frac{J_{\parallel}}{J_{\perp}} > 1 \tag{3.4}$$

is a material-dependent parameter quantifying the anisotropy of the system. It will turn out that the continuous description along the z axis is not appropriate and that a discrete parameterization is more compatible with the layered structure of the considered material. This property is specifically taken into account by the Lawrence-Doniach (LD) model in which the interlayer coupling is assumed to be of the Josephson type, i.e. proportional to the cosine of the phase difference between two points in consecutive layers [68]. The final action reads therefore

$$\mathcal{S}_{\mathrm{LD}}[\theta,\mathbf{A}] = \frac{d}{2\Omega_0}\sum_n \int d^2\rho \left(J_\parallel a^2 \left[\boldsymbol{\nabla}_{\boldsymbol{\rho}}\theta_n(\boldsymbol{\rho}) - \frac{2\pi}{\Phi_0}\mathbf{A}_{\boldsymbol{\rho}}(\mathbf{r})\right]^2 + 2J_\perp\left[1-\cos\big(\theta_n(\boldsymbol{\rho})-\theta_{n+1}(\boldsymbol{\rho})\big)\right]\right). \tag{3.5}$$

The lattice parameters are a (in-plane lattice constant) and d (interlayer distance), the unit cell volume is $\Omega_0 = a^2 d$ whereas the coordinate $\mathbf{r}$ means $(\boldsymbol{\rho}, nd)$, $0 \leq n \leq N$, N being the number of layers. The z component of the vector potential $\mathbf{A}$ has been omitted for simplicity. It must be noticed that $\mathcal{S}_{\mathrm{LD}}$ is in fact a partially continuous XY model where the gradient $d^2(\nabla_z\theta)^2$ has been replaced by the Josephson coupling between neighboring layers $2\big(1-\cos(\theta_n-\theta_{n+1})\big) \approx (\theta_n-\theta_{n+1})^2$. It contains the material parameters $J_\parallel$ and $J_\perp$ which will be determined after comparison with experimental data.

3.2.2 Linear response theory

In the present context, due to the absence of Meissner effect above T_c, the magnetic field inside the superconductor can be approximated its value outside the sample. The latter will be restricted to a single nonvanishing component along the z axis with constant value B, i.e. $\mathbf{B} = (0,0,B)$. In the Landau gauge it corresponds to the vector potential

$$\mathbf{A} = (-yB, 0, 0). \tag{3.6}$$

The orbital diamagnetic response is now calculated in the framework of the linear response theory. The equilibrium state of the phase field $\theta_n(\boldsymbol{\rho})$ at temperature T and under an applied magnetic field $\mathbf{B}$ is perturbated by adding a small amount $\delta\mathbf{A}$ to the vector potential (3.6):

$$\mathbf{A} \to \mathbf{A} + \delta\mathbf{A}. \tag{3.7}$$

Then the diamagnetic response function Λ is obtained by taking the second (functional) derivative of the free energy with respect to the variation $\delta\mathbf{A}$. It is useful to consider directly the Fourier transform of this quantity which is given by

$$\Lambda(\mathbf{q}) = \frac{J_\parallel}{d}\left(\frac{2\pi}{\Phi_0}\right)^2 \left(\frac{J_\parallel}{k_B T}\, C(\mathbf{q}) - 1\right). \tag{3.8}$$

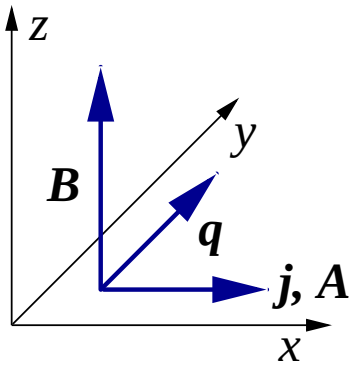

Figure 3.1: Geometry of the problem.

The wave vector reads $\mathbf{q} = (0, q, 0)$ due to the gauge condition $\boldsymbol{\nabla} \cdot \mathbf{A} = 0$, Maxwell's equation $\boldsymbol{\nabla} \cdot \mathbf{B} = 0$ and the choice of the system geometry (see Figure 3.1). The first term in the round brackets in the above expression involves a current-current correlation function, as usual in a linear response scheme:

$$C(\mathbf{q}) = \frac{1}{L^2} \sum_{n,n'} \int d^2p \, d^2p' \, e^{i\mathbf{q}\cdot(\mathbf{r}-\mathbf{r}')} \langle j_x(\mathbf{r}) j_x(\mathbf{r}') \rangle \tag{3.9}$$

$$j_x(\mathbf{r}) = \nabla_x \theta_n(\boldsymbol{\rho}) - \frac{2\pi}{\Phi_0} A_x(\mathbf{r}), \tag{3.10}$$

L being the linear size of a layer. The second term in brackets in Eq.(3.9) is called "diamagnetic term" (because of the minus sign) and is independent of the wave vector $\mathbf{q}$. The orbital susceptibility χ is readily obtained from $\Lambda(\mathbf{q})$ by the relation

$$\chi = \lim_{q \to 0} \frac{\Lambda(\mathbf{q})}{q^2}. \tag{3.11}$$

It follows that this expression leads to a finite result only if $\Lambda(q = 0)$ vanishes, which means that the diamagnetic term in Eq.(3.10) must be compensated by the value at $q = 0$ of the current-current correlation function $C(\mathbf{q})$. This corresponds to the fact that the considered system has no phase stiffness above T_c. As shown below, the present approach satisfies this requirement.

3.2.3 Description of the phase system

The problem is now to develop a satisfactory description of the phase field $\theta_n(\boldsymbol{\rho})$ which allows to evaluate the above quantities, in particular $C(\mathbf{q})$. Given the layered geometry contained in the Lawrence-Doniach model, it seems reasonable to consider the system as a stack of coupled planes, each of them being described by a 2D XY model. It is therefore natural to begin by introducing the essential features of this system. As first

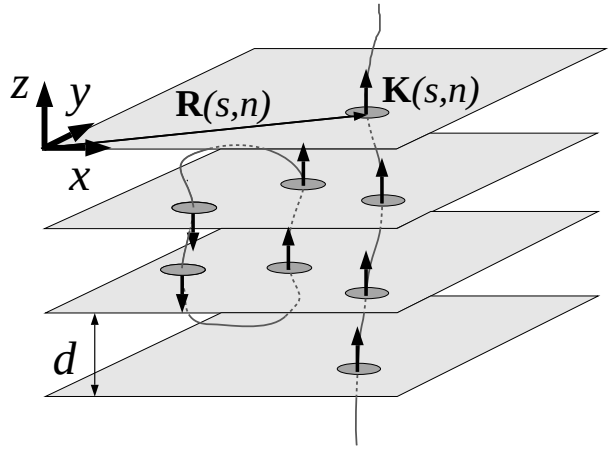

Figure 3.2: Schematic representation of vortex loops (left) and lines (right). In a Lawrence-Doniach approach, the phase field is defined only for discrete values of the z coordinate, giving rise to the image of "vortex pancakes" mentioned in the text.

observed by Berezinskii and independently by Kosterlitz and Thouless (BKT) [30], its finite-temperature properties must be described in terms of vortex and antivortex excitations. The latter are characterized by the vorticity, $t = \pm 1$, and by the position $\mathbf{R}$ of the phase field singularity they are associated with. This description can be extended to the 3D system considered here [48]. It consists then in objects called vortex loops and lines which are constituted by points corresponding to a phase singularity located at a position R in layer n. The loops form closed lines due to topological reasons and represent the thermal excitations of the system[2] whereas the vortex lines run from one end to the other of the sample and are resulting from the presence of an applied magnetic field. These features are schematically sketched in Figure 3.2. In what follows this description is first included in the calculation whereafter the thermal properties of the vortex system are investigated.

As shown in Figure 3.2, the position of a line element s in layer n is given by $\mathbf{R}(n, s)$, s labelling the N_V elements of both vortex loops and lines crossing the plane $z = nd$. The connection between the phase field $\theta_n(\boldsymbol{\rho})$ and the configuration of the vortices described by the set $\{\mathbf{R}(n, s)\}_{n\in\{0,N\},s\in\{0,N_V\}}$ can now be established. It is analogous to a Biot-Savard magnetostatics formula giving the magnetic field induced by a distribution of current loops and lines:

$$\nabla_x \theta_n(\boldsymbol{\rho}) = d \sum_{\alpha,\beta,s,n'} \varepsilon_{x\alpha\beta} \int d^2\rho' \, \frac{(r_\alpha - r'_\alpha)\, K_\beta(s, \mathbf{r}')}{|\mathbf{r} - \mathbf{r}'|^3}. \tag{3.12}$$

Here $\varepsilon_{\alpha\beta\gamma}$ is the fully antisymmetric tensor of rank 3 and the sum over n (s) runs from 0 to N (N_V) where N is the total number of layers (N_V is the total number of vortex-line

[2] Here the spin-wave contributions are neglected because they are not relevant for the critical behavior.

elements in layer n). The vector field $\mathbf{K}(s,\mathbf{r}')$ describes the tangent to line element s in layer n at a point $\mathbf{r}'=(\boldsymbol{\rho}',nd)$:

$$\mathbf{K}(s,\mathbf{r}')=t(s,n')\,\delta\big(\boldsymbol{\rho}'-\mathbf{R}(s,n')\big)\,\hat{\mathbf{z}}. \tag{3.13}$$

Here the choice of a discrete layered structure along the z direction is crucial: the tangential direction of vortex-line elements is restricted to the z direction, i.e. $\hat{\mathbf{z}}=(0,0,1)$ only, in agreement with the usual picture of "vortex pancakes" [49]. This would not have been the case for continuous z variable where all orientations of $\mathbf{K}$ would have been possible. The factor $t(s,n)=\pm1$ accounts for the vorticity of the line elements already mentioned above and allows to represent the considered system as a stack of XY planes where the line elements with $t=1$ ($t=-1$) correspond to 2D vortices (antivortices).
Introducing the above expression (3.12) and (3.13) into Eqs.(3.9) and (3.10) allows to rewrite the fundamental correlation function $C(\mathbf{q})$ in terms of the vortex variables $\{\mathbf{R}(s,n)\}$. It reads

$$C(\mathbf{q})=\frac{4\pi^2}{L^2Nq^2}\left(S(\mathbf{q})-\left(\frac{L^2NB}{\Phi_0}\right)^2\delta_{\mathbf{q},0}\right). \tag{3.14}$$

The first term, stemming from the phase gradient in the current density (3.10), represents the structure factor of the vortex-line elements associated to the "pancakes":

$$S(\mathbf{q})=\sum_{s,n,s',n'}t(s,n)\,t(s',n')\,\langle e^{i\mathbf{q}\cdot(\mathbf{R}(s,n)-\mathbf{R}(s',n'))}\rangle. \tag{3.15}$$

The second term of Eq.(3.14) comes from the diamagnetic part of the current (3.10). It has the important property of being equal to the singular part at $q=0$ of the structure factor $S(\mathbf{q})$, as shown in Appendix A. This property uses the neutrality of the phase system, i.e. the fact that the global "charge" in every layer is exactly equal to the applied flux B/Φ_0. This makes the limit of expression (3.14) well defined for $q\to0$ so that only the nontrivial "correlation" part $S_{\text{reg}}(\mathbf{q})$ of $S(\mathbf{q})$ is relevant. It must be noticed that in the derivation of expression (3.14), the expectation values of cross-terms involving $\boldsymbol{\nabla}\theta$ have been set to zero due to the fact that a constant magnetic field does not generate a global current through the sample (but only current loops which annihilate one another).

3.2.4 Thermal properties of the phase system

Before evaluating $S_{\text{reg}}(\mathbf{q})$, it is useful to develop a qualitative picture of the phase system which must be considered. In the B-T phase diagram of anisotropic layered type II superconductors, the fluctuation-induced diamagnetism manifests itself in a region lying beyond the different transition lines, i.e. the Abrikosov vortex-lattice melting line and the vortex-decoupling line [49, 69]. This region is usually referred

to as the vortex-liquid phase, characterized by a disordered structure where strongly wrinkled and thermally fluctuating vortex loops and lines go through the sample [69, 70]. In order to describe faithfully these properties, it is worth considering first the case of totally uncorrelated layers (i.e. independent XY planes) and then introducing a coupling between neighboring layers to restore the original situation.

1. In the extreme case of independent layers, each plane is described by a 2D XY model which is frustrated when a magnetic field is applied. Above the critical temperature, its vortex structure corresponds to the one of a neutral Coulomb gas, i.e. of an ensemble of classical charged particles with total charge zero interacting via the 2D Coulomb potential [57]. Although this mapping is not rigorously exact[3], it allows to borrow results from the theory of 2D Coulomb gas. Equation (3.15) can be written as ($n = n' = 0$)

$$\begin{aligned} S_{\text{reg},2D}(\mathbf{q}) &= N \sum_{s,s'} t(s,0)\, t(s',0)\, \langle e^{i\mathbf{q}\cdot(\mathbf{R}(s,0)-\mathbf{R}(s',0))} \rangle \\ &= N L^2 n_V S_C(\mathbf{q}) \end{aligned} \tag{3.16}$$

   where $n_V = N_V/L^2$ is the areal density of vortices and antivortices. The sum over all the vortex positions is now included in the Coulomb gas structure factor $S_C(\mathbf{q})$ which is given by the approximate form [72]

$$S_C(\mathbf{q}) = \frac{q^2}{q^2 + b^2(n_V)} \tag{3.17}$$

   where $b^2(n_V) = 2\pi n_V q_V^2/k_B T$ and the "charge" q_V^2 of each vortex is related to the in-plane Josephson coupling constant by [73]

$$q_V^2 = 2\pi J_\parallel. \tag{3.18}$$

   Expression (3.17) describes correctly the long-wavelength behavior of the Coulomb gas and is valid for temperatures not too close to T_c. An expression valid for the case $T \to T_c$ is given later. It turns out that Eq.(3.17) yields a vanishing value for $\Lambda(q = 0)$ from Eq.(3.8), which makes the present approach well defined.

2. It is clear that, due to the strong anisotropy of the material of interest and to the irregular shape of the vortex loops and lines, the effective interlayer coupling will be very weak. This can be taken into account by separating explicitly intralayer and interlayer contributions to the structure factor (3.15), i.e. by splitting the sum over n and n' according to

$$\sum_{n,n'} = \sum_{n=n'} + \sum_{n\neq n'}. \tag{3.19}$$

[3] The exact mapping involves a mixture of a neutral two-component Coulomb gas (corresponding to the equal number of vortices and antivortices) and of a one-component gas (the field-induced vortices) in a neutralizing background given by the applied flux.

The case $n = n'$ corresponds to the situation treated in case 1, i.e. to uncorrelated layers. The intralayer contribution to $S_{\text{reg}}(\mathbf{q})$ is therefore directly given by

$$S_1(\mathbf{q}) = NL^2 n_V S_C(\mathbf{q}). \tag{3.20}$$

It must be noticed that both n_V and S_C do not refer anymore to "point" vortices and antivortices as in case 1, but to line elements associated with the "pancake vortices" and belonging to extended structure like loops or lines. This 3D structure is taken into account in the interlayer contribution $S_2(\mathbf{q})$, which is now evaluated. This is done in a simple way by introducing a "correlation distance" $\xi_z = n_z d$ over which successive layers are effectively correlated. According to previous studies ξ_z is small, of the order of a few interlayer distances d. A satisfactory estimate of ξ_z is the average extension of the vortex loops along the z direction, as done in Section 3.3.1. Restricting the summation to effectively correlated layers only, the interlayer contribution to the structure factor becomes

$$S_2(\mathbf{q}) = \sum_{s,s',n,n' \neq n} t(s,n)\, t(s',n')\, \langle e^{i\mathbf{q}\cdot(\mathbf{R}(s,n)-\mathbf{R}(s',n'))} \rangle. \tag{3.21}$$

For two correlated layers n and n', the value of the vorticity t of a line element s in layer n is expected to be the same than the one in layer n', i.e. $t(s,n) = t(s,n')$ for $|n - n'| < n_z$. Moreover the positions $\mathbf{R}(s,n)$ and $\mathbf{R}(s,n')$ are expected to be correlated as well, so that it makes sense to write

$$\mathbf{R}(s,n') = \mathbf{R}(s,n) + \mathbf{u}(|n - n'|) \tag{3.22}$$

where $\mathbf{u}$ is the deviation of a given line or loop from a straight line along the z direction. It depends on the difference $|n - n'|$ but not on s for simplicity. Inserting these new features into Eq.(3.21) gives

$$S_2(\mathbf{q}) = \sum_{s,s',n,n' \neq n} t(s,n)\, t(s',n')\, \langle e^{i\mathbf{q}\cdot(\mathbf{R}(s,n)-\mathbf{R}(s',n))}\, e^{-i\mathbf{q}\cdot\mathbf{u}(|n'-n|)} \rangle. \tag{3.23}$$

The average bracket in Eq.(3.23) can be split by factoring out from the sum over n' the first exponential which pertains to layer n. This yields exactly the previous result (3.16) multiplied by a correction factor taking into account the correlations between the positions of a vortex-line element in neighboring layers:

$$S_2(\mathbf{q}) = 2\, S_1(\mathbf{q}) \sum_{n'=1}^{n_z} \langle e^{-i\mathbf{q}\cdot\mathbf{u}(n')} \rangle \equiv 2\, S_1(\mathbf{q})\, X(\mathbf{q}). \tag{3.24}$$

The factor 2 is due to the fact that the sum over $|n - n'| < n_z$ has been reduced to a single sum over n' in Eq.(3.24), in agreement with Eq.(3.22) that assumes the coupling between layers depends only on their relative distance. The quantity $X(\mathbf{q})$ can be approximated by

$$X(\mathbf{q}) \approx \sum_{n=1}^{n_z} \exp\big(-\frac{1}{2}\, q^2 \langle \mathbf{u}^2(n), \rangle\big). \tag{3.25}$$

This expression involves the mean square value of the quantity $\mathbf{u}$ defined above as the short-distance deviation of the shape of the vortex loops and lines from straight lines. If the latter are modeled by elastic strings with a stiffness λ approximately equal to

$$\lambda = \frac{J_\perp}{d} = \frac{1}{\gamma^2}\frac{J_\parallel}{d}, \tag{3.26}$$

then the expectation value of $\mathbf{u}(n)^2$ at temperature T can be evaluated according to the rules of classical statistical mechanics which give the result

$$\langle \mathbf{u}(n)^2 \rangle = \frac{1}{2}\frac{k_B T}{\lambda}\, nd. \tag{3.27}$$

This expression is inserted into Eq.(3.25) and yields a finite geometric series which is easily summed:

$$X(\mathbf{q}) = \frac{1-\exp(-k_B T n_z d\, q^2/4\lambda)}{\exp(-k_B T d\, q^2/4\lambda)-1}. \tag{3.28}$$

Eq.(3.28) completes the calculation of the structure factor (3.15). The current-current correlation function (3.14) containing the diamagnetic response finally reads

$$C(\mathbf{q}) = \frac{4\pi^2}{q^2}\, n_V S_C(\mathbf{q})\,\big(1+2X(\mathbf{q})\big). \tag{3.29}$$

The evaluation of the orbital magnetic susceptibility given by Eq.(3.11) shows that an expansion in powers of q is now necessary to get the final answer. As already mentioned, $C(q=0)$ has to cancel the diamagnetic term in Eq.(3.8) for $\Lambda(q=0)$ to vanish, ensuring thereby a meaningful result for the limit (3.11). This is the case if the charge q_V^2 entering the Coulomb gas structure factor is chosen to be

$$q_V^2 = 2\pi J_\parallel\,(1+2n_z), \tag{3.30}$$

which constitutes a reasonable extension of the 2D expression (3.18), given the fact that the charges are now vortex-line elements correlated over a small distance $n_z d$.

3.2.5 Evaluation of the susceptibility and discussion

Taking the term proportional to q^2 from the expansion of $\Lambda(\mathbf{q})$ gives directly the expression of the orbital magnetic susceptibility:

$$\chi = -\frac{1}{(1+2n_z)d}\,\frac{k_B T}{\Phi_0^2}\,\Big(\frac{1}{n_V} + (\pi\gamma)^2 n_z(1+n_z)d^2\Big). \tag{3.31}$$

The first term describes the response of decoupled XY planes to a weak variation of the magnetic field applied in the z direction. The second one takes into account the coupling between the planes which results from the correlations of the positions of the vortex-line elements in neighboring layers. It turns out that the second contribution to χ is irrelevant in both fixing the temperature dependence of the diamagnetic response and reproducing the crossover to the critical regime (see below). Therefore the discussion of the magnetic susceptibility can be restricted to the first term of expression (3.31).

The most important feature of the latter is its inverse dependence on n_V, the areal density of vortex-line elements. Such a behavior is rather unexpected because one would naively argue that the more vortex-line elements are present in the system, the stronger will be its response to a variation of the applied magnetic field. Indeed, any vortex is associated with planar circular currents which are inducing magnetic dipoles. From this point of view it seems natural to expect a diamagnetic response proportional to the density of dipoles n_V. However more subtle effects are involved - as shown in the following.

First it is interesting to see how the factor n_V^{-1} arises from the formalism leading to expression (3.31). Combination of the definition (3.11) and of the factor q^{-2} in Eq.(3.29) implies that the susceptibility χ depends on the fourth-order coefficient of the q expansion of the structure factor (3.17):

$$\chi = -\frac{k_B T}{(1+2n_z)d\,\Phi_0^2}\,\frac{1}{n_V}\left(-\frac{b^4(n_V)}{24}\,S_C^{(4)}(0)\,\frac{1+2X(0)}{1+2n_z} - \frac{b^2(n_V)}{2}\,S_C^{(2)}(0)\,\frac{b^2(n_V)X^{(2)}(0)}{1+2n_z}\right) \tag{3.32}$$

The second-order coefficient is important in fixing the value of the charge q_V^2 from Eq.(3.30), in order to make the limit (3.11) well defined. The q expansion of the structure factor reads

$$S_C(\mathbf{q}) = \frac{q^2}{b^2(n_V)} - \frac{q^4}{b^4(n_V)} + \mathrm{O}(q^6) \tag{3.33}$$

It shows clearly that the factor n_V appearing in the correlation function (3.29) (and compatible with the above "naive" reasoning) is canceled by a n_V^{-2} factor present in the fourth-order coefficient of the expansion of $S_C(\mathbf{q})$. This yields the n_V^{-1} dependence of χ.

A qualitative interpretation of this feature can be developed as well by coming back to the Coulomb gas picture from which the structure factor $S_C(\mathbf{q})$ is originating [57]. In this context it is worth recalling the fundamental correspondence between the representations:

$$\text{vortex with vorticity } t \longleftrightarrow \text{classical particle with charge } t$$

Thus the diamagnetic response to a small variation of the applied magnetic field given by Eq.(3.7) has to be regarded as the reaction of the Coulomb gas to the addition of a

small amount of identical charges. The latter correspond to the number of flux quanta Φ_0 associated with the perturbation $\delta\mathbf{A}$. The properties of the response are contained in a correlation function which connects the values at different places of the quantity described by the phase gradient $\boldsymbol{\nabla}\theta$ (see Eqs.(3.9) and (3.10)). Recalling that

$$\mathbf{j}(\mathbf{r}) \overset{\text{superfluid}}{\longleftarrow} \boldsymbol{\nabla}\theta(\mathbf{r}) \overset{\text{Coulomb gas}}{\longrightarrow} \hat{\mathbf{z}} \wedge \boldsymbol{\nabla}\phi(\mathbf{r}) \tag{3.34}$$

where ϕ is the electrostatic potential associated with the distribution of the point charges t, it turns out the relevant correlation for the diamagnetic response is the one of the electric field $\mathbf{E} = -\boldsymbol{\nabla}\phi$:

$$\left\langle \mathbf{j}(\boldsymbol{\rho}) \cdot \mathbf{j}(\boldsymbol{\rho}') \right\rangle = \left\langle \left(\hat{\mathbf{z}} \wedge \boldsymbol{\nabla}\Phi(\boldsymbol{\rho})\right) \cdot \left(\hat{\mathbf{z}} \wedge \boldsymbol{\nabla}\Phi(\boldsymbol{\rho}')\right) \right\rangle = \left\langle \mathbf{E}(\boldsymbol{\rho}) \cdot \mathbf{E}(\boldsymbol{\rho}') \right\rangle \tag{3.35}$$

Thus, according to result (3.31), the effect of a variation of the electric field in point $\boldsymbol{\rho}$ is felt in another point $\boldsymbol{\rho}'$ the stronger the smaller is the number of charges present in the system. Such a feature corresponds perfectly to a well-known property of interacting charged systems called the screening. Indeed the two-body Coulomb potential is affected by the presence of all the other charges and becomes short-ranged. It is then characterized by a screening length λ which has the following property:

$$\lambda \sim \frac{1}{\sqrt{n_V}}. \tag{3.36}$$

Therefore a variation of the charge at a point $\boldsymbol{\rho}$ is transmitted to another point $\boldsymbol{\rho}'$ the easier the less charges are present in the system. In other words, the diamagnetic response is becoming weaker when the density n_V of vortices is increasing. This provides a satisfactory qualitative understanding of the result (3.31).

3.2.6 Crossover to the critical regime

The theory presented up to now is supposed to be appropriate for a "pre-critical" regime, i.e. for phase fluctuations which are strong without however being critical in the sense of originating from a diverging correlation length. It is interesting to see how this approach can be extended to describe the complete behavior of the system until $T = T_c$ at $B = 0$. The essential difference appearing when entering the critical regime is the fact that a part of the vortices present in the XY layers starts to be bound into vortex-antivortex pairs (for simplicity uncorrelated layers are considered, i.e. $n_z = 0$). Therefore the vortex density n_V splits into two distinct contributions:

$$n_V(T, B = 0) = n_V^{th,free}(T) + n_V^{th,bound}(T) \tag{3.37}$$

where $n_V^{th,free}$ ($n_V^{th,bound}$) represents the density of free (bound) thermally excited vortices and antivortices. According to the BKT scenario of the 2D XY model [30], more and more pairs form when T approaches T_c so that only bound pairs of a vortex and an

antivortex are present at the critical point. The corollary of this property is the fact that the density of the free vortices is directly proportional to the inverse square of the BKT correlation length, i.e. $n_V^{th,free} \sim \xi_{BKT}^{-2}$. These new ingredients are taken into account by replacing the structure factor $S_C(\mathbf{q})$ from Eq.(3.17) by a more complicated expression involving both $n_V^{th,free}$ and $n_V^{th,bound}$ [74]:

$$S_{C,2}(\mathbf{q}) = \frac{q^2}{b^2(n_V)} \frac{b^2(n_V^{th,free})}{q^2 + b^2(n_V^{th,free})}. \tag{3.38}$$

As observed in Eq.(3.32), only the first two terms of the expansion of $S_C(\mathbf{q})$ in term of q are relevant in determining the orbital magnetic susceptibility χ. It is therefore meaningful to consider the expansion of $S_{C,2}(\mathbf{q})$ which reads

$$S_{C,2}(\mathbf{q}) = \frac{q^2}{b^2(n_V)} - \frac{q^4}{b^2(n_V)\, b^2(n_V^{th,free})} + \mathrm{O}(q^6). \tag{3.39}$$

Comparison with Eq.(3.33) shows that the term proportional to q^2 is the same for both expressions of the structure factor. This ensures that Eq.(3.30) remains valid so that the correlation function $\Lambda(\mathbf{q})$ always vanishes for $q = 0$. The fourth-order terms are different and allow the extension of the theory up to $T = T_c$. Before that it is instructive to check whether the high-temperature behavior is correct. For $T \gg T_c$, all the vortices are free. Thus $n_V = n_V^{th,free}$ and $S_{C,2}(\mathbf{q})$ reduces to expression (3.17) yielding the previous results (3.31) valid in the pre-critical regime. For $T \to T_c$, χ is now readily calculated using Eqs.(3.32) and (3.39). The result is

$$\chi = -\frac{k_B T}{d\, \Phi_0^2} \frac{1}{n_V^{th,free}} \propto \xi_{BKT}^2 \tag{3.40}$$

This expression is similar to the result obtained by Halperin and Nelson using the renormalization group method [71]. They provide in addition the value of the proportionality constant between $n_V^{th,free}$ and ξ_{BKT}^{-2}: $n_V^{th,free} \xi_{BKT}^{-2} = 12\pi$. It describes the critical behavior of the diamagnetic susceptibility at the phase transition. It is clear that Eq.(3.40) is valid for a single XY layer and does not correspond to the experimental situation. Restoring the 3D interlayer coupling is done by replacing d by $(1 + 2n_z)d$. Then the dimensional crossover to 3D occurring in a bulk sample as $T \to T_c$ can be studied in the framework of the Lawrence-Doniach model by taking the limit $n_z \to \infty$.[4] The final result is nothing else than Schmid's expression $\chi \sim \xi$ which is consistent with the 3D XY universality class observed experimentally very close the phase transition [75].

[4] When $n_z \gg 1$, it refers no more to the finite extension of the vortex loops but rather to the diverging length associated with the critical correlations of θ in the direction perpendicular to the layers.

3.3 Application to underdoped YBCO

In order to apply the above theory to the measurements on $YBa_2Cu_3O_{6+x}$ reported in Ref.[26], it is first necessary to recall the main characteristics of the studied samples. They consist in oriented powders[5] with lattice parameters being approximatively given by $a = b = 4$ Å and $d = 12$ Å, yielding a molar volume $\Omega_M = 115$ cm^3. The doping $x = 0.6$ reduces the zero-field critical temperature to $T_c = 63$ K (whereas $T_c(x = 1) = 90$ K). The results given in Ref.[26] allow to study both the temperature and magnetic field dependences of the diamagnetic response. Various background contributions (spin susceptibility and free-electron orbital diamagnetism) have been subtracted in order to display the fluctuation-induced response only.

3.3.1 Temperature dependence of the zero-field susceptibility

The first aspect of fluctuation-induced diamagnetism considered here is the zero-field susceptibility above the superconducting transition temperature. Ref.[26] shows data covering the range from $T = T_c = 63$ K to $T = 110$ K. A nonzero value of χ has been observed up to $T = 80$ K, a value which lies clearly outside the critical region which extends only a few degrees around T_c. This anomalous temperature dependence is not observed in overdoped samples and occurs in a temperature range that is expected to correspond to the fluctuation-dominated pre-critical regime where the above theory is applicable.

Several parameters entering the latter are still undetermined: the anisotropy constant γ, the vortex-line correlation length $\xi_z = n_z d$ and the areal density of vortex lines n_V. The analysis of the magnetization in the next section will show that the second term of the expression (3.31) for χ is irrelevant at low values of B. Therefore γ plays no role for the present considerations and χ is reduced to its first term only. This means that interlayer effects are not involved in this case and allows to assume that ξ_z is temperature independent, at least outside the critical region. Thus the only remaining nontrivial T dependence entering χ lies in the vortex-line density n_V which has not been explicitly discussed up to now. The forthcoming analysis will show that the behavior suggested by the experimental data can be consistently understood within the present theoretical framework.

Figure 3.3 shows the magnetic susceptibility data for underdoped $YBa_2Cu_3O_{6.6}$. It turns out that the measurements are almost perfectly fitted by the expression

$$\chi(T, B = 0) = C \exp(\frac{E_0}{k_B T}) \tag{3.41}$$

[5] These are grains having all the same anisotropy direction (the z axis) whereas the distribution of the in-plane directions is random.

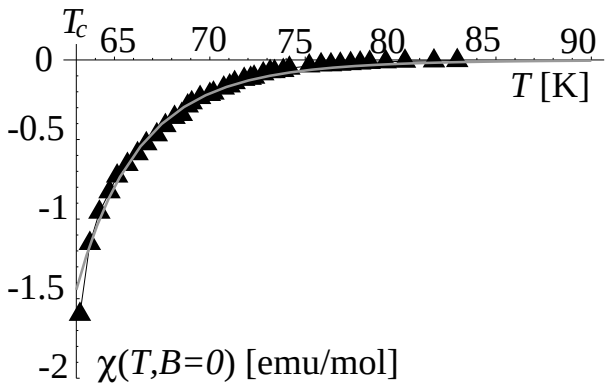

Figure 3.3: Zero-field susceptibility $\chi(T, B = 0)$: the experimental data (▲) are compared to the best fit based on Eq.(3.41), determining thereby the free parameters C and E_0.

where $E_0/k_BT \approx 22$. Including this feature into Eq.(3.31) allows to deduce that the vortex-line density is given by

$$n_V(T) = n_0 \exp(-\frac{E_0}{k_BT}) \tag{3.42}$$

where $n_0 \sim 10^4/a^2$. This temperature dependence corresponds to a thermally activated behavior, characterized by an activation energy E_0 and an asymptotic (saturation) value n_0. Such an equilibrium distribution is indeed commonly admitted for the vortex excitations of the XY model (see below). This agreement between experimental deductions and theoretical expectations constitutes an important justification of the basic assumptions that lead to the choice of the model action (3.5).
A thermally activated behavior concerns classical objects that have a finite formation energy (E_0), in contrast to gapless excitations such as spin waves which are formed for arbitrarily small energies. In the context of the XY model, such a property is mainly deduced from Monte Carlo simulations. In 2D the thermally activated behavior of the number of vortex-antivortex pairs has been confirmed as well as an activation energy approximately given by $E_0 \simeq 10k_BT_c$ [76]. Studies of the 3D case arrive at the same conclusion showing in addition that the value of E_0 depends strongly upon the type of loops [77, 78, 79]. For a 3D anisotropic system such as the one considered here, the activation energy is getting larger the more layers are crossed by the corresponding loops. If the anisotropy is sufficiently strong, the loops present in the low-temperature region ($T < T_c$) are essentially confined in one unique layer. Interlayer segments start to appear at higher temperatures ($T > T_c$) only and allow then 3D loop structures to extend across the layers [48, 79].
In fact, since the diamagnetic response depends only on line elements parallel to the z axis, i.e. belonging to vortex loops extending at least over two layers, the density n_V from Eq.(3.42) can be redefined as the number of loops containing segments perpendicular to the layers. The rather high value of the activation energy found above

($E_0 \simeq 20\, k_B T_c$) confirms this point of view: it corresponds a kind of "average" value of the activation energies of all the loops involved in the diamagnetic response. This value is high since the corresponding loops contain a well-developed 3D structure. It also suggests that the quantity ξ_z measuring the extension of the vortex-structure correlations along the z direction must be of the order of a few multiples of the interlayer distance d (from now on, the value $\xi_z = 2d$ will be taken). This provides an *a posteriori* justification of the truncation of the summation over all the layers in Eq.(3.24). It is also consistent with the picture of the vortex system above the vortex-melting and vortex-decoupling lines [48, 49].
It is now possible to estimate the density of the vortex-line elements in the temperature range of interest. Using the above value for E_0 and n_0 and including a reduction factor $\lambda = 0.15$ (see below) gives $n_V \sim 10^2\ \mu\text{m}^{-2}$ for $T = 65$ K. This value, discussed in the next section, is rather small in comparison to the simulation results. The reason is that it takes into account only the part of the vortex loops that contribute to the diamagnetic response, i.e. those having a well-developed interlayer extension. n_V also satisfies the condition $\sqrt{n_V} \gg a$ in agreement with the continuous approach used in the model action (3.5) inside the layers.

3.3.2 Magnetic-field dependence of the magnetization

Ref.[26] also reports on measurements of the effect of a finite applied magnetic field B on the fluctuation-induced diamagnetic response. The main observed feature is the presence of two distinct regimes in the B dependence of the isothermal magnetization M, related to another by a very sharp crossover taking place at a value of $B \simeq 0.05$ T. In order to describe this situation theoretically, it is necessary to introduce the explicit B dependences in the equations of Section 3.2. In a first step, this is restricted to a redefinition of the quantity n_V that takes into account the fact that vortex-line elements may now belong to field-induced vortex lines as well. Similarly to Eq.(3.37), this is written as

$$n_V(T,B) = n_V^{th}(T) + n_V^f(B). \tag{3.43}$$

The density of thermally excited vortex-line elements n_V^{th} is known from Eq.(3.42) whereas the number of field-induced line elements n_V^f is simply given by the flux number B/Φ_0. It is useful to introduce the quantity

$$z(T,B) = \frac{n_V^f(B)}{n_V^{th}(T)} \tag{3.44}$$

which measures the relative importance of the two types of vortex-line elements. Then the magnetization per unit volume is easily obtained by calculating the primitive of the susceptibility (3.31) with respect to the variable B:

$$M(T,B) = -\frac{1}{(1+2n_z)\,d}\,\frac{k_B T}{\Phi_0^2}\Big(\Phi_0 \log(1+z(T,B)) + (\pi\gamma)^2 n_z(1+n_z)\,d^2 B\Big). \tag{3.45}$$

In order to have a molar quantity for comparison with Ref.[26], M is multiplied by the molar volume Ω_M and by a constant $\lambda < 1$. The latter takes into account the fact that superconductivity occurs in the CuO_2 layers that represent only a fraction of the unit-cell volume. In fact λ was already present in the molar susceptibility plotted in Figure 3.2 but, because it appeared in the combination λ/n_V where n_V was undetermined as well, its value could not be deduced from the data for χ only. It will be shown below how λ can be extracted together with the anisotropy ratio γ from the analysis of the B dependence of the magnetization $M(T, B)$.
Examination of Eq.(3.45) for $M(T, B)$ shows that three different regimes can be distinguished according to the value of z. For constant temperatures, they correspond to different strength of the external magnetic field B.

1. **Weak fields**$(z < 1)$
   In this case, $\log(1 + z) \simeq z$ and the magnetization is essentially given by $\chi(T, B = 0)\, B$. This corresponds to the situation considered in the previous section where all the vortex-line elements present in a given layer belong to thermally excited loops. Due to the persistence of nonzero values of χ over a wide temperature range above T_c, the initial slope of $M(T, B)$ is expected to be anomalously steep.

2. **Strong fields**$(z > 1)$
   This corresponds to the situation where field-induced vortex lines are dominating. While the first term of expression (3.45) only gives a weakly B dependent contribution ($\propto \log(B)$), the second one becomes more important and yields a linear dependence in B. It is interesting to observe that this feature is a proper 3D effect because the slope of $M(T, B)$ is determined by γ and n_z, two quantities describing the interlayer correlations.

3. **Intermediate fields**$(z \simeq 1)$
   The above two (asymptotic) regimes are connected by an intermediate crossover region where both types of vortex-line elements are present in equal quantities. The corresponding value of the magnetic field is directly found by solving the equation $z(T, B_c) = 1$, which gives $B_c = \Phi_0\, n_V^{th}(T)$.

These considerations are now used to interpret the magnetization measurements from Ref.[26] displayed in Figure 3.4. Qualitatively the two asymptotic regions are easily recognized thanks to the steep slope for small B and by the linear dependence for large B. The value of the crossover field B_c depends, by definition, only on n_V^{th}, the density of thermal vortex-line elements. This quantity determined by the analysis of the zero-field susceptibility needs to be corrected by the factor λ, as mentioned above. The latter is extracted from the experimental magnetization data by fitting the theoretical curves to the data (see below). Then the equation $z(T, B_c) = 1$ is solved, providing the result $B_c \simeq 0.025$ T for $T \simeq 65$ K. This estimate has the correct order of magnitude,

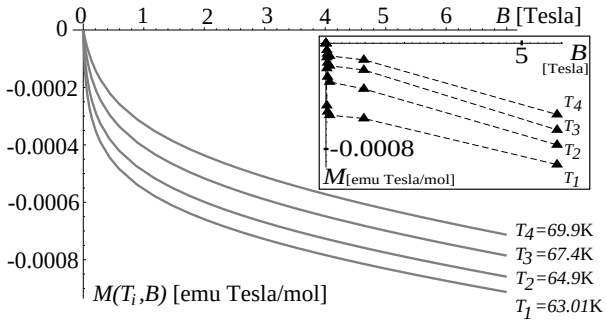

Figure 3.4: Magnetization $M(T = \text{const.}, B)$: the full lines are the best fit based on Eq.(3.45) using the values of λ and γ given in the text and the inset shows the data from Ref.[26].

although it is smaller than 0.05 T, the value deduced empirically from the measurements.
Figure 3.4 shows both the experimental data from Ref.[26] and the corresponding theoretical curves obtained from Eq.(3.45) by choosing appropriate values for the two free parameters λ and γ. The agreement is less spectacular than in the case of the zero-field susceptibility, but it can be improved by introducing other B dependences than the one used in Eq.(3.43) (see Section 3.3.3). The value of the "magnetically active fraction" λ deduced from Figure 3.4 is about 0.15. It is extracted from the small B region and is compatible with all available temperatures values. Such an order of magnitude looks quite reasonable for a layered material such as YBCO where superconductivity takes place in the fraction of the unit-cell volume represented by the CuO_2 planes. The anisotropy γ is found by considering the large B region. The most suitable value is $\gamma \simeq 2$. Multiplied by the lattice anisotropy $d/a = 3$, it gives an estimate for the effective anisotropy $\gamma_{\text{eff}} \simeq 6$.[6] The latter can be determined experimentally by other methods (penetration-depth measurements) providing thereby a check for the consistency of the interpretation. Typical values at $T = T_c$ are $\gamma_{\text{eff}} = 25$ which are substantially higher than the above estimate [5]. This discrepancy may be explained by the fact that γ was introduced in the theory in the context of a crude approximation for the effective vortex line stiffness (see Eq.(3.26)).
Using the above values of λ and γ, it is possible to show that the second term of χ in Eq.(3.31) is irrelevant for small applied magnetic fields ($B < B_c$). This justifies the strategy used in the previous section where this contribution was omitted.

3.3.3 A possible improvement of the theory

The consistent interpretation of both susceptibility and magnetization measurements performed in the two previous sections showed the pertinence of the present theory in

[6] This quantity is exactly the anisotropy of the corresponding GL theory, i.e. $\gamma_{\text{eff}} = \frac{c_\parallel}{c_\perp} = \frac{J_\parallel a^2}{J_\perp d^2}$

describing the pre-critical diamagnetic response. Given the simple way of introducing the magnetic field dependence in Eq.(3.43), it is already gratifying to achieve such a program. It is interesting to try to improve *a posteriori* the theory, in particular by finding a mechanism that is able to give a better account of the experiments. As clearly illustrated in Figure 3.4, this concerns principally the sharpness of the crossover of the magnetization $M(T, B)$ between low-field and high-field regions.
It is in fact possible to understand, in the framework of the present approach, what makes the crossover so sharp. In terms of the susceptibility $\chi(T, B)$ from Eq.(3.31), the sharpness of the crossover suggests that the first term must tend to zero very rapidly as B increases. In this way, only the second (approximately constant) term remains and then yields the linear behavior of the magnetization $M(T, B)$ for $B > B_c$.
Such a behavior can be reproduced by assuming a small magnetic field dependence of the activation energy E_0 and motivated as follows. In Ref.[78] one observes that, below T_c, the effective interaction between vortex loops is screened by the thermal defects of the Abrikosov vortex lattice. For small B, this effect is enhanced when the magnetic field is increased because the density of vortex lines is directly proportional to B. Above a crossover field B^* the screening becomes weaker due to the fact that the stiffness $\propto B^2$ of the field-induced vortex lines inhibits the formation of further defects. In the liquid phase above T_c a similar qualitative behavior may be expected, at least for low fields. A screened interaction between vortex loops then reduces the energetic cost of creating these objects. Thus the total number of thermally excited vortex loops increases with the magnetic field B. Among them a small percentage corresponds to those contributing to the diamagnetic response, as discussed in Section 3.3.1. They also follow the above behavior so that it seems reasonable to assume that their effective activation energy E_0 in Eq.(3.42) decreases slightly when the magnetic field B increases. To lowest order, this is written as

$$E_0 \to E_0(B) = \begin{cases} E_0(1 - \alpha B), & B \ll B_c \\ E_1 < E_0, & B \gg B_c. \end{cases} \tag{3.46}$$

The large B behavior is not important since it affects only the first term of χ when the latter is already very small. This idea is illustrated by taking $\alpha = 1$, such that the value of the activation energy saturates at a value E_1 20% lower than E_0 for $B \gtrsim 0.5$ T. After a numerical integration of $\chi(T, B)$ over B, it gives the curves shown in Figure 3.5. The crossover between the two field regimes is sharper than in the previous case and the corresponding value of the crossover field B_c is higher. Moreover, the fact that the first term of the susceptibility goes to zero faster than in the previous case implies that the corresponding term in $M(T, B)$ becomes "flatter" than $\log(B)$ for high fields. This allows to obtain higher and more correct values for the anisotropy ratio γ, which were indeed found to be a bit small earlier.

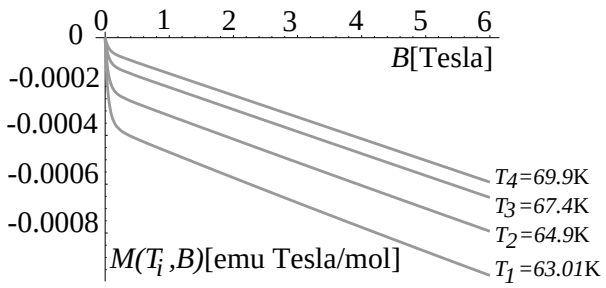

Figure 3.5: Improved version of the magnetization $M(T = \text{const.}, B)$ based on the assumption (3.46) for a B dependent activation energy $E_0(B)$.

3.4 Conclusion

In this chapter the orbital diamagnetic properties of extreme-type II superconductors above the critical temperature have been studied. The calculation was based on London's approximation to the Lawrence-Doniach model in order to take into account the specificities of underdoped high-temperature superconductors in a regime where the fluctuations of the phase of the order parameter are believed to play an important role. This amounts to considering in each layer of the sample a liquid of vortex-line elements which are either thermally excited or result from the application of an external perpendicular magnetic field. The latter form lines crossing the whole sample whereas the former constitute closed three-dimensional loops. Because of both the strong anisotropy and the thermal fluctuations, these 3D structures are not very rigid so that the effective interlayer coupling extends only over a few layers. This property is used in evaluating the structure factor of the phase field (or, to be more precise, of the corresponding Coulomb gas) which enters the current-current correlation function giving the diamagnetic response in the framework of the linear response theory.
The successful analysis of recently reported anomalous features in underdoped YBCO allowed then to complete the theory by fixing several material-dependent parameters. In particular, the number of vortex line elements in a given layer was found to follow a thermally activated behavior, pointing out to a regime in which noncritical phase fluctuations dominate, called "pre-critical" and extending at least over 10-15 K above T_c. The value of the activation energy extracted from the zero-field susceptibility showed that the vortex loops involved in the diamagnetic response are extending over a few layers only, in agreement with the weak effective interlayer coupling deduced above. The density of the latter, together with the estimation of the magnetically active fraction of the unit cell volume as 10-15 percents, allowed to deduce the value $B_c \simeq 0.025$ T for the crossover field observed in the magnetization measurements. Although its experimental value is higher (0.05 T), it appeared as a natural consequence of the above approach, characterizing the transition between two regimes where either thermally activated (low B) or field-induced vortex-line elements (high B) are dominating.

The fact that the extreme sharpness of the observed crossover could not be reproduced without an ad hoc assumption lead to the conclusion that a deeper analysis of a liquid of interacting thermal and magnetic vortices may be useful in this context.
An important conclusion from the above analysis concerns the nature of the thermal fluctuations present above T_c in moderately underdoped YBCO. It turned out that the latter could be suitably described in terms of thermally activated vortex loops associated with the phase field of the superconducting order parameter. This is different from the two approaches mentioned in the Introduction (Section 3.1). First, it does not correspond to a true critical regime with a diverging correlation length and the relation between both cases has been established. Second, the finite activation energy of a vortex loop is to be contrasted with the ungapped wave-like modes of a Gaussian regime which were considered in similar works.
Experimentally it would be instructive to analyze the diamagnetic response above T_c in other underdoped high-T_c compounds in order to test the validity of the assumptions made above. Very recently, it has been shown that the precursor diamagnetism in underdoped LSCO thin films was characterized by a (static) *phase separation* between fully diamagnetic regions (where the Meissner effect takes place) and normal metallic (paramagnetic) regions [23]. These observations reveals the importance of processes characterized by inhomogeneities in space (at the mesoscpic scale $\sim \mu$m), a feature that was not included in the above approach that considered bulk properties only.

Chapter 4

Thermodynamic properties of short-coherence length superconductors in the pseudogap regime

The relations between the electronic structure and the thermodynamic properties are investigated for the case of short-coherence length superconductors in the regime above the critical temperature presenting the pseudogap. When the latter is well-developed, the pairing fluctuations acquire a clear bosonic character and become the dominant degrees of freedom when the phase transition is approached. Application of these considerations to underdoped high-temperature superconductors reveals the important role played by the anisotropy in the direction perpendicular to the CuO_2 planes in this context.

4.1 Introduction

As announced this chapter focuses on the study of the thermodynamics of short-coherence length superconductors in the pseudogap regime above the critical temperature T_c. Although it is restricted to equilibrium properties only, this analysis is of fundamental importance since it allows to determine which are the relevant degrees of freedom in the considered system and characterizes them quantitatively. This study is motivated by intriguing experimental observations which are summarized in the review by Junod *et al.* on specific heat measurements on high-temperature superconductors [27]. The latter quantity is particularly useful since it gives direct information about the nature of the thermal fluctuations that appear close to the superconducting phase transition.

Ref.[27] starts by recalling the situation in low-temperature superconductors where the specific heat c_V displays a jump at T_c, in agreement with the BCS theory [1]. In presence of an external magnetic field $\mathbf{B}$ the transition temperature $T_c(B)$ shifts downward and the shape of $c_V(T)$ becomes less sharp. Such a behavior is also observed in overdoped high-T_c compounds with, additionally, the presence of thermal (phase) fluctuations of the 3D XY-type which smear out a bit the zero-field transition. This effect becomes stronger and stronger when the doping is decreased so that the BCS jump eventually fully disappears under the critical XY divergence of c_V. However, underdoped samples like $Bi_2Sr_2CaCu_2O_{8+x}$, where a pseudogap is clearly observed above T_c, display a rather different behavior. The specific heat curves are quite symmetric around T_c and their shape is perfectly fitted by the one of the a 3D Bose-Einstein condensation (BEC), except maybe for a very small region around T_c where the XY singularity should occur [5]. This similarity is confirmed by measurements under nonzero magnetic field where the maximum of $c_V(T)$ rounds off for $B > 0$, but remains located at the temperature T_c instead of following $T_c(B) < T_c$. These two observations lead to the conclusion that the superconducting phase transition must be very close to a BEC in the case of underdoped materials [28].

From the theoretical point of view these observations demonstrate the relevance of the study of the crossover between BCS superconducitvity and BE condensation. They motivate an analysis of the thermodynamic properties of the attractive Hubbard Hamiltonian (2.1) in the intermediate coupling regime $U \sim W$, since the latter constitutes a simple model for short-coherence length superconductors that may capture some of the physics that appears in underdoped high-T_c compounds (see Section 2.4). This is supported in particular by the fact that this model is able to reproduce a pseudogap due to pairing fluctuations above T_c (in 2D). It allows thereby to investigate the relations between this particular electronic structure and the thermodynamic properties such as the specific heat c_V. An important point to be cleared concerns the following: since the BEC occurs in the strong coupling limit ($U \gg W$) of the model only, are these bosonic degrees of freedom still present for an intermediate coupling and are they relevant in driving the superconductiong phase transition at $T = T_c$? The goal of this part of the thesis is to answer this question and to show under which conditions BEC features can be expected in short-coherence length superconductors.

Although the thermodynamics of the BCS-BEC crossover has been already studied by many authors using the attractive Hubbard model, only a few have focused specifically on the pseudogap phase at intermediate coupling. A possible phenomenological approach for this regime consists in considering a coupled system of fermions and bosons, the latter describing the pairing fluctuations which thus constitute the wanted bosonic degrees of freedom [80, 81]. A partial justification of this ideas starting from the electronic level is proposed in Ref.[82], but it does not apply to the present problem. The considerations exposed in this chapter are very well integrated in this context

and more concrete comparisons with these works are given in Section 4.6.

The structure of this chapter is as follows. In Section 4.2 the self-consistent T-matrix approximation to the attractive Hubbard model is introduced as an adequate approach to study the interplay between free electrons and pairing fluctuations above T_c at the microscopic level. In order to avoid the difficulties represented by the self-consistency, an approximate strategy is developed, based on available numerical results. The main task consists then in calculating four Ginzburg-Landau-like coefficients which give the low-energy expansion of the T-matrix in the intermediate coupling regime. This is done in Section 4.3 where the electronic structure presenting a pseudogap is explicitly taken into account by introducing appropriate spectral functions inspired by numerical calculations. The results are presented in Sections 4.4 and 4.5, first for $D = 2$ and then for $D > 2$ in order to avoid the difficulties of recovering the BKT physics from the electronic level. They allow to deduce a physical picture of a two-fluid system, consisting on one hand in unpaired free electrons and on the other hand on well-defined long-lived bosonic quasiparticles describing the pairing fluctuations. The latter determine the thermodynamics of the system and appear to be close to a BEC regime. This picture, valid as long as the pseudogap is well-developed and when the anisotropy in the third direction is strong enough, is however not equivalent to the one of (quasi) free bosons undergoing a BEC like in the strong coupling limit. Indeed, a nonnegligible part of unpaired electrons also contributes in fixing the superconducting transition temperature T_c, which cannot be given by a usual BEC formula. These considerations are then applied to underdoped high-temperature superconductors in order to try to understand the observations mentioned in the first part of this section. This chapter ends with a discussion of the results and contains some suggestions about possible extensions of this approach.

4.2 Method

4.2.1 The T-matrix to describe pairing fluctuations

As already mentioned in Section 2.4, a description of pairing fluctuations on the electronic level is in principle less evident than a treatment based on the classical Ginzburg-Landau action for the superconducting order parameter field Δ. The goal of this section is then to introduce schematically the T-matrix and its associated approximation scheme as a (minimal) framework to study the coupled system of electrons and pairing fluctuations.
In the context of quantum many-body theory, a pairing fluctuation is a two-body process since it involves two electrons tending to form a Cooper pair. It is then clear that any approach based on a *perturbative* approximation scheme to the *one-particle* self-energy σ is a priori insufficient to treat correctly the considered problem. A more

evolved scheme containing a proper description of the two-electron process is therefore necessary.
A suitable starting point to introduce the chosen approach is the two-electron Green's function $G_2(1,2|1',2')$ describing the evolution of two electrons added to the system at space-time points 1 and 2 and removed later in $1'$ and $2'$.[1] It was defined in Section 2.5 and is schematically represented as follows:

$G_2(1,2|1',2') =$ 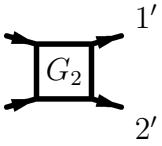

. (4.1)

G_2 can be seen as a "black box" containing all possible Feynman diagrams with four external legs. According to Kadanoff and Baym [83], a sufficient description of the two-body effects induced by a short-ranged interaction V is already achieved by retaining only the ladder diagrams in G_2:

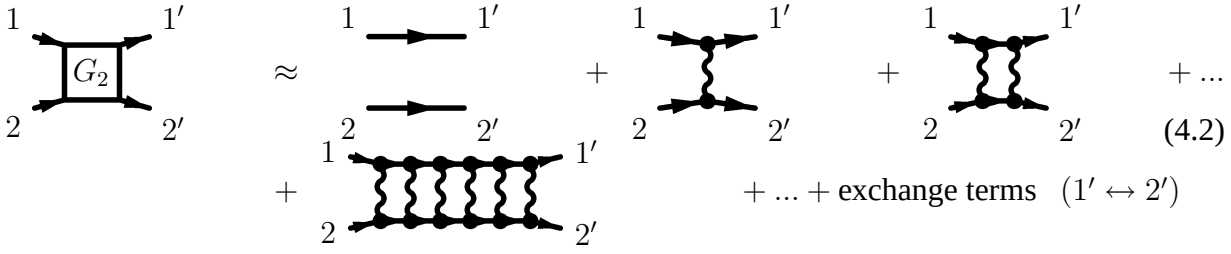

(4.2)

where the one-electron Green's function $G(1|2)$ defined in Eq.(2.13) is represented by

$G(1|2) =$ 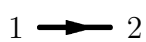

(4.3)

and the *bare* interaction vertex [2] is

$\Gamma_0(1,2,1',2') = \delta(1-1')\,\delta(2-2')\,V(1,2) =$ 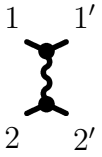

(4.4)

The above infinite sum can be written more compactly by remarking that it is in fact the iteration of a much simpler relation:

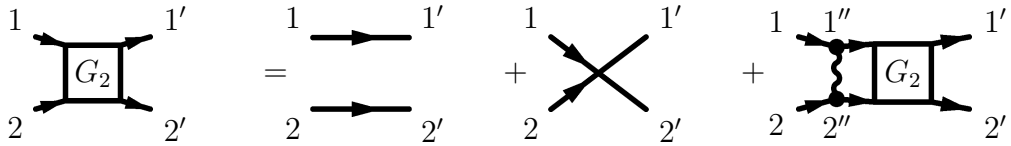

(4.5)

where a summation over the internal vertex positions 1" and 2" is meant.
The interaction V is assumed to be a product of two creation and two annihilation

[1] In this section, the arguments 1, 2 etc. mean $(\mathbf{r}_1, \tau_1)$ where τ_1 is the imaginary time, see Section 2.5.

[2] Not yet specified as the local Hubbard attraction $-U\delta(1-2)$, $U > 0$.

operators. Then the equation of motion for the one-electron Green's function G can be written either by involving G_2 as

$$(\partial_\tau - \mathcal{H}_0)\, G(1|2) - \int d\bar{1}\, G_2(1,\bar{1}|\bar{1},2)\, V(2,\bar{1}) = \delta(1-2) \tag{4.6}$$

or by using the self-energy σ as

$$(\partial_\tau - \mathcal{H}_0)\, G(1|2) - \int d\bar{1}\, \sigma(1,\bar{1})\, G(\bar{1},2) = \delta(1-2). \tag{4.7}$$

where $\mathcal{H}_0$ is the one-body part of the Hamiltonian (see for instance Eq.(2.4)). Eq.(4.6-4.7) allow to derive the expression for σ entering G through Dyson's equation (4.13c) and thus determine completely the approximation scheme.
It is useful to introduce a new quantity which will become of fundamental importance in the following: the T-matrix. Its implicit definition is

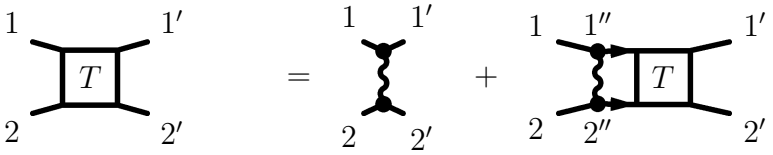

(4.8)

and shows that T consists in an infinite sum of ladder diagrams, similarly to G_2. The relation between both T and G_2 is the following

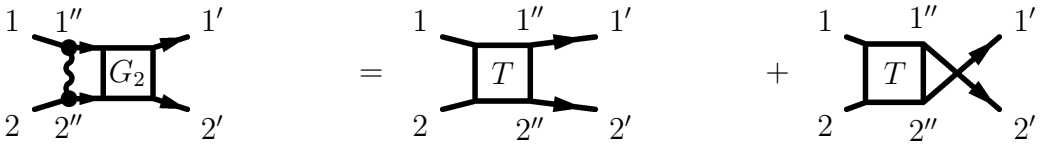

(4.9)

as it is clearly seen by comparing Eqs.(4.5) and (4.8). The T-matrix defined above has several important properties:

- It describes the mutual scattering of two electrons. In the low-density limit ($\beta\mu \to -\infty$), T satisfies

  $$T|\mathbf{k}\rangle = V|\psi\rangle \tag{4.10}$$

  where $|\mathbf{k}\rangle$ is a free two-electron state with relative momentum $\mathbf{k}$ and $|\psi\rangle$ is the full solution of the one-particle scattering problem (Lippman-Schwinger equation) for an interaction potential V and an incoming state $|\mathbf{k}\rangle$.

- If they are well-defined (as in the case considered hereafter), the poles of T are associated with quasiparticles which describe (resonant) bound states of the two electrons, i.e. Cooper pairs if V couples electrons with opposite spins as in the attractive Hubbard model. In other words the T-matrix is the propagator of two-particle states which are the solution of the ladder approximation to the Bethe-Salpeter equation, the latter being originally derived to find the bound states of interacting relativistic particles [84].

- As Kadanoff and Baym pointed out, T may become singular at low temperatures (i.e. have poles for *negative* energies) and the whole approximation scheme is no longer valid. This is directly connected with the occurrence of superconductivity in the system. The characterization of the superconducting phase transition by an instability in the electron-electron scattering channel is called the Thouless criterion [41] and will be used later. Moreover, in the weak-coupling limit ($G \to G_0$), the above condition is exactly equivalent to the BCS gap equation which gives the critical temperature T_c and the T dependence of the order parameter.

- Another important property of the T-matrix is its relation to the one-electron self-energy σ. Inserting Eq.(4.9) into the equation of motion (4.6) and comparing with Eq.(4.7) allows to deduce the simple result

$$\sigma(1,2) = \quad (4.11)$$

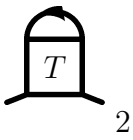

  This equation is particularly transparent and gives T a clear interpretation. σ renormalizes the electronic propagation by including virtual processes. In the present case Eq.(4.11) shows that the latter are associated with the T-matrix which describes two-electron (resonant) bound states or Cooper pairs above T_c. Therefore T is nothing else than the propagator for virtual electronic pairs which appear in the absence of long-range superconducting order above T_c. This gives a precise representation to the concept of "pairing fluctuations" on the electronic level and shows how they couple to the one-electron states.

In the following sections the formalism associated with the T-matrix approximation is introduced in the reciprocal space representation. The Hubbard local interaction is specified as

$$V(1,2) = -U\,\delta(1-2), \quad U > 0. \quad (4.12)$$

This allows to win an explicit definition of the T-matrix since the integral equation (4.8) becomes then a simple algebraic equation from which T is isolated.

4.2.2 The self-consistent T-matrix approximation to the attractive Hubbard model

The considerations of the previous section can be summarized by a closed set of equations defining completely the T-matrix approximation scheme. For a translation-invariant system and a local interaction, it is advantageous to express them directly in

terms of the corresponding Fourier components [85]. [3] Then they read

$$T^{-1}(\mathbf{k}, z_\alpha) = \frac{1}{U} - \mathcal{G}(\mathbf{k}, z_\alpha) \tag{4.13a}$$

$$\mathcal{G}(\mathbf{k}, z_\alpha) = \frac{1}{\beta N} \sum_{\mathbf{q}, z_\nu} G(\mathbf{k}-\mathbf{q}, z_\alpha - z_\nu)\, G(\mathbf{q}, z_\nu) \tag{4.13b}$$

$$G^{-1}(\mathbf{k}, z_\nu) = G_0^{-1}(\mathbf{k}, z_\nu) - \sigma(\mathbf{k}, z_\nu) \tag{4.13c}$$

$$\sigma(\mathbf{k}, z_\nu) = -\frac{1}{\beta N} \sum_{\mathbf{q}, z_\alpha} G(\mathbf{k}-\mathbf{q}, z_\alpha - z_\nu)\, T(\mathbf{q}, z_\alpha). \tag{4.13d}$$

Here β is the inverse temperature T^{-1} (k_B as well as $\hbar$ are taken equal to 1 from now on), N is the number of lattice sites, the wave vector sums run over a 2D Brillouin zone $[-\pi, \pi]^2$ and z_α and z_ν are bosonic and fermionic Matsubara frequencies, respectively (see Eq.(2.16)). Eqs.(4.13a) and (4.13b) defining the T-matrix result from the combination of Eqs.(4.8) and (4.12). Relation (4.13c) is Dyson's equation for the one-electron Green's function G, strictly equivalent to the equation of motion (4.7), and involves its noninteracting version G_0 given by

$$G_0(\mathbf{k}, z_\nu) = \frac{1}{z_\nu - \xi_\mathbf{k}} \tag{4.14}$$

where $\xi_\mathbf{k} = \varepsilon_\mathbf{k} - \mu$ contains the free electronic dispersion (2.5) and the chemical potential μ. Finally Eq.(4.13d) defining the self-energy corresponds to diagram (4.11) and closes the equation set (4.13).

The validity of the above approximation scheme depends essentially on the correctness of the ladder approximation (4.5) to the two-electron Green's function. In agreement with the argument of Kadanoff and Baym presented in the previous section, it is commonly admitted that assumption (4.5) is valid essentially in the low-density limit. This can be understood by the fact that in this case all diagrams containing fermionic loops give a negligible contribution, since they are at least proportional to the density n. Moreover the system should present an instability in the Cooper channel only (i.e. a superconducting instability) because the T-matrix scheme takes into account particle-particle scattering exclusively. Therefore this approximation is not suited for the half-filled case ($n = 1$) where a charge-density wave appears in addition to superconductivity. Another interesting argument has been proposed recently according to which the ladder approximation (4.5) represents in fact the leading contribution of a $1/M$ expansion for a generalized Hubbard model in which the electron have M additional internal degrees of freedom (M-colors model) [86].

An important property of the T-matrix approximation scheme is the fact that it is *conserving* [87]. This means that it is consistent with the microscopic conservations laws

[3] The local interaction of Eq.(2.2b) implies that $T(1,2|1',2') = T(1|1')\,\delta(1-2)\,\delta(1'-2')$, i.e. the internal structure of the pairs is not relevant, and the translational invariance yields $T(1|1') = T(1'-1)$, which can be Fourier transformed.

for particle number, energy and momentum. Formally this is equivalent to the existence of a functional Φ satisfying

$$\sigma = \frac{1}{2}\frac{\delta\Phi[G]}{\delta G}. \tag{4.15}$$

Using Eqs.(4.13a-4.13d), one can deduce the expression of Φ:

$$\Phi\left[G\right] = \frac{1}{\beta}\,\mathrm{Tr}\big(\log(T^{-1})\big) \tag{4.16}$$

where Tr means summation over wave vectors $\mathbf{k}$ and Matsubara frequencies z_α (or z_ν). For a conserving approximation, it has been shown that the thermodynamic grand potential $\Omega(T,V,\mu)$ can be expressed in terms of G, σ and Φ [88]. It reads

$$\Omega(T,V,\mu) = -\frac{2}{\beta}\,\mathrm{Tr}\big(\sigma G + \log(\sigma - G_0^{-1})\big) + \Phi\left[G\right]. \tag{4.17}$$

This relation is extremely useful for the present work whose goal is to study the thermodynamic properties of the combined system of electrons and pairing fluctuations. Eq.(4.17) completes in principle the presentation of the T-matrix approximation for the attractive Hubbard Hamiltonian (2.1). However its self-consistency, i.e. the fact that σ involves G and not G_0 as in a perturbative approach, makes its rigorous solution very difficult. Analytically an iterative approach becomes rapidly very heavy [85] and a numerical calculation requires much effort to give satisfactory results [51]. A "viable" alternative to the full self-consistency which has already produced several meaningful results is the following strategy. An important physical ingredient of the model, which is assumed to be present in the fully self-consistent solution of the problem, is put "by hand" into the T-matrix equations and its consequences are investigated by iterating only partially the self-consistency relations. For instance, in Ref.[89], an explicit expression of the T-matrix was used and its influence on the one-particle quantities were studied. In the following section a similar strategy is presented. It allows to circumvent the difficulty represented by the self-consistency while preserving the main physical properties contained in the T-matrix treatment of the Hamiltonian (2.1).

4.2.3 Assumptions and strategy for the calculation

Since they use the only approach giving reliable information about the fully self-consistent solution, numerical works on the T-matrix approximation constitute the basis of the strategy employed in this work. They provide several essential elements which are integrated into the approximation scheme so that a tractable analytical calculation allows to get satisfying answers to the questions raised in Section 4.1.
The first element borrowed from numerical works is the fact that, in the intermediate coupling regime (typically $U = 4t$), the imaginary part of $T(\mathbf{k}, z_\alpha \to \omega + i\eta)$ displays

a pronounced peak on the energy axis [51, 90]. [4] This reveals the existence of well-defined two-electron state corresponding to a pairing fluctuation mode, i.e. a resonant state of two electrons or a "virtual" Cooper pair. Then $T(\mathbf{k}, z_\alpha)$ can be viewed as the propagator of the latter which is thereby treated as a bosonic quasiparticle. In agreement with a recent study [52], the T-matrix can be approximated by its low-energy expansion:

$$T^{-1}(\mathbf{k}, z_\alpha) \approx a + ck^2 - dz_\alpha. \tag{4.18}$$

Using the definition (4.13a), the coefficients appearing in Eq.(4.18) are related to the Taylor expansion of the particle-particle bubble (4.13b) as [5]

$$a = \frac{1}{U} - \mathcal{G}(0,0) \tag{4.19a}$$

$$c = -\frac{1}{2}\frac{\partial^2}{\partial k^2}\mathcal{G}(\mathbf{k},0)|_{k=0} \tag{4.19b}$$

$$d = \frac{\partial}{\partial \omega}\mathcal{G}(0, z_\alpha = \omega + i\eta)|_{\eta\to 0, \omega=0}. \tag{4.19c}$$

Since $T(\mathbf{k}, z_\alpha)$ can be seen as the propagator of a bosonic quasiparticle, the quantities a, c and d acquire a simple interpretation in this context. The imaginary part of the complex-valued coefficient d gives the inverse lifetime of the two-electron state whereas c is related to its effective mass. The coefficient a is proportional to the chemical potential of the quasiparticle.[6] At this point it is useful to recall the Thouless criterion for superconductivity, which was already mentioned briefly in Section 4.2.1 [41]. It relates the occurrence of the superconducting phase transition to the T-matrix by stating that $T^{-1}(k = 0, z_\alpha = 0) = 0$ at $T = T_c$. Eq.(4.19a) shows that this is equivalent to the fact that the coefficient a (or the chemical potential of the bosonic quasiparticles) vanishes at $T = T_c$. This is a crucial property which will be used later when trying to interpret the phase transition as a Bose-Einstein condensation (BEC). However, the above considerations are valid for a "normal" phase transition in which there is a low-temperature broken symmetry state. Superconductivity in a strictly 2D system involves the BKT transition and does not belong to this category [30]. Indeed recent calculations show that the phase coherence is present even though the Thouless criterion is not fulfilled [32]. [7] In order to avoid the complications of the BKT-physics which are beyond a T-matrix approximation treatment [18], the following calculations will be performed first for a 2D plane. Then a weak interplane coupling in the perpendicular direction will be introduced in order to restore the validity of the Thouless criterion in characterizing the superconducting phase transition.

[4] This property is not observed in the weak coupling regime where $\mathrm{Im}(T)$ resembles rather to the spectral function of a phonon with two peaks of opposite energies.

[5] The particular form of the coefficient d is due to the fact that the low-energy expansion concerns real frequencies ω which are related by an analytical continuation to the Matsubara frequencies z_α [46].

[6] The latter being the combination $-a/\mathrm{Re}(d)$.

[7] An argument claiming that this could be a numerical artifact has been proposed as well [74].

The second ingredient borrowed from numerical T-matrix calculations is the presence of a pseudogap in the one-particle density of state above the critical temperature T_c. Although it has not been observed in fully self-consistent approaches due mainly to numerical difficulties [90], alternative approximately self-consistent calculations have clearly detected its presence [52, 91]. In particular, Ref.[89] uses a self-energy given by

$$\sigma_0(\mathbf{k}, z_\nu) = -\frac{1}{\beta N} \sum_{\mathbf{q}, z_\alpha} G_0(\mathbf{k}-\mathbf{q}, z_\alpha - z_\nu)\, T_0(\mathbf{q}, z_\alpha) \tag{4.20}$$

where the expression of the T-matrix T_0 corresponds exactly to Eq.(4.18) but with values for the coefficients a, c and d which are given by the strong coupling limit ($U \gg t$) of the T-matrix approximation given in Refs.[46, 90]. [8] The imaginary part of σ_0 in Eq.(4.20) is found to display a pronounced peak on the energy axis, exactly at $-\xi_{\mathbf{k}}$. Such a behavior can be obtained roughly by writing $T_0(\mathbf{k}, z_\alpha) = \Delta^2\, \delta(k)\, \delta(z_\alpha)$, which allows to evaluate easily expression (4.20). The result for both cases is a pseudogap located around the Fermi energy in the one-electron density of states. The latter becomes more and more developed as the coefficient a tends to zero, i.e. as $T \searrow T_c$. These features are also present in the one-electron spectral functions $A(\mathbf{k}, \omega)$ where the observed structure resembles strongly to a zero-temperature BCS case but with peaks of finite linewidth [91, 92]. This is explained more quantitatively in Section 4.3.1 where is a simple model is introduced to take these features into account.

The strategy used in the forthcoming calculation can be presented. Using the above-mentioned model for the spectral functions $A(\mathbf{k}, \omega)$ and Eqs.(4.19a-4.19c), the T-matrix is re-calculated so that the influence of the particular electronic structure on the pairing fluctuations described by $T(\mathbf{k}, z_\alpha)$ can be determined. This method yields a satisfactory self-consistency (see Section 4.4.3) and can be used together with Eq.(4.17) to study the thermodynamic properties of the coupled system of electrons and pairing fluctuations. This strategy is summarized in Figure 4.1 and its mathematical formulation is given in the next section.

4.3 Calculation

4.3.1 Model for the spectral functions $A(\mathbf{k}, \omega)$

In order to follow the approximate self-consistent scheme presented in Section 4.2.3, it is first necessary to introduce a simple model for the spectral functions $A(\mathbf{k}, \omega)$. It should capture the essential features of an electronic band structure displaying a

[8] This constitutes a reasonable starting point since the bosonic character of the T-matrix makes it closer to the strong coupling case.

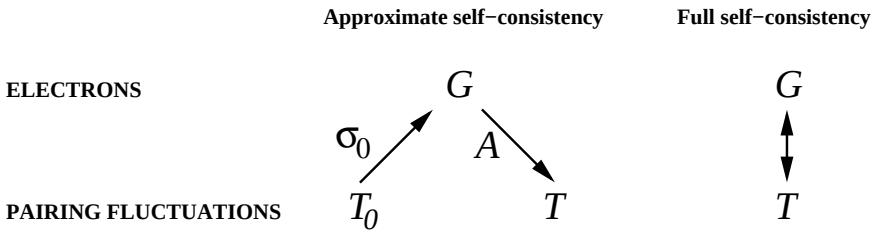

Figure 4.1: Principle of the approximate self-consistency. The first step ($T_0 \rightarrow G$ using σ_0) has already been performed by Capezzali and Beck in Ref.[89]. The second one ($G \rightarrow T$ using A) is the object of the present work and should give a result comparable to the fully self-consistent T-matrix scheme ($G \leftrightarrow T$).

pseudogap as obtained numerically.
The results of Refs.[91, 92] show that the corresponding spectral functions $A(\mathbf{k},\omega)$ have essentially a BCS form with two branches around the Fermi energy μ_0 whose relative weights swap when crossing the Fermi wave vector k_F. [9] Unlike the pure BCS theory, the peaks have a finite width which reaches a maximum value around k_F.
These features can be quantitatively taken into account as follows. Introducing first the quantity Δ corresponding to the half-width of the pseudogap [10] allows to define the BCS spectral functions as

$$A_{\mathrm{BCS}}(\mathbf{k},\omega) = 2\pi\big(u_{\mathbf{k}}^2\,\delta(E_{\mathbf{k}}-\omega) + v_{\mathbf{k}}^2\,\delta(E_{\mathbf{k}}+\omega)\big) \tag{4.21}$$

where

$$E_{\mathbf{k}} = \sqrt{\Delta^2+\xi_{\mathbf{k}}^2} \tag{4.22a}$$

$$u_{\mathbf{k}}^2 = \frac{1}{2}(1+\frac{\xi_{\mathbf{k}}}{E_{\mathbf{k}}}) \tag{4.22b}$$

$$v_{\mathbf{k}}^2 = \frac{1}{2}(1-\frac{\xi_{\mathbf{k}}}{E_{\mathbf{k}}}). \tag{4.22c}$$

The single-electron BCS density of states centered around the Fermi energy μ_0 is defined as

$$D_{\mathrm{BCS}}(\omega) = \frac{1}{N}\sum_{\mathbf{k}} A(\mathbf{k},\omega). \tag{4.23}$$

Evaluation of the wave vector sum yields the following expression

$$D_{\mathrm{BCS}}(\omega) = \begin{cases} D_0\big(\mu_0 + \mathrm{sign}(\omega)\,\sqrt{\omega^2-\Delta^2}\big)\,\dfrac{|\omega|}{\sqrt{\omega^2-\Delta^2}}, & |\omega| \geq \Delta \\ 0, & |\omega| < \Delta \end{cases} \tag{4.24}$$

[9] μ_0 must not be confounded with the chemical potential μ (see later Section 4.4.1).
[10] Δ is not to be confounded with the BCS gap (which is zero above T_c) although it plays formally the same role in the following.

where D_0 is the density of states for the 2D tight-binding Hamiltonian $\mathcal{H}_0$ from Eq.(2.4) and given explicitly in Appendix B.1. The quantity μ_0, referred to as the Fermi energy, will be discussed below. Eq.(4.21) describes correctly the electronic structure observed in Ref.[91], except for the finite linewidth of the peaks which is now taken into account by replacing the δ-functions by a normalized distribution function f_Γ with a finite (constant) width Γ. The spectral function for the pseudogap case reads therefore

$$A_{\rm PG}(\mathbf{k},\omega) = 2\pi\big(u_{\mathbf{k}}^2\, f_\Gamma(E_{\mathbf{k}}-\omega) + v_{\mathbf{k}}^2\, f_\Gamma(E_{\mathbf{k}}+\omega)\big) \tag{4.25}$$

and the corresponding density of states is

$$D_{\rm PG}(\omega) = \int dE\, D_{\rm BCS}(E)\, f_\Gamma(E-\omega). \tag{4.26}$$

This equation shows clearly how the BCS density of states is modified by the finite linewidth $\Gamma > 0$ which displaces a finite amount of spectral weight inside the gap region $[-\Delta,\Delta]$. The filling of the pseudogap for increasing temperatures above T_c is then simply achieved by increasing Γ. This mechanism is directly inspired by the numerical works [91, 92] and provides a satisfactory description of the one-particle spectral properties required for the following calculation. It will be illustrated later in Section 4.4.1.

The last point to be clarified is the determination of the quantity μ_0. As suggested by Eq.(4.24), it gives the position of the middle of the pseudogap inside the considered band. It plays then the role of a chemical potential by fixing the density n according to the relation

$$n = \int d\epsilon\, D_{\rm PG}(\epsilon-\mu_0)\, n_F(\epsilon-\mu_0) \tag{4.27}$$

where n_F is the Fermi-Dirac distribution function

$$n_F(\omega) = \frac{1}{e^{\beta\omega}+1}. \tag{4.28}$$

For sufficiently low temperatures ($\beta t \ll 1$), $n_F(\omega)$ is practically equal to the step function $\theta(-\omega)$. Moreover, for $\Gamma \lesssim \Delta$, $D_{\rm PG}$ can be replaced by $D_{\rm BCS}$ from Eq.(4.24). A simple variable substitution yields then

$$n = \int d\epsilon\, D_0(\epsilon)\, \theta(\mu_0-\epsilon) \tag{4.29}$$

which shows that μ_0 is nothing else than the chemical potential for the corresponding *noninteracting* problem. The relation between μ_0 and the "true" chemical potential μ is more subtle and will be discussed in Section 4.4.1. This concludes the presentation of the model for the spectral functions $A(\mathbf{k},\omega)$.

4.3.2 Calculation of the T-matrix

The next step toward the approximative solution of the T-matrix equations (4.13a-4.13d) is the evaluation of $T(\mathbf{k}, z_\alpha)$ itself. Following the strategy presented in Section 4.2.3, it allows to determine the consequences of the particular electronic structure contained in the spectral functions defined in the previous section on the propagator of the pairing fluctuations.
This amounts to calculating the coefficients a, c and d given by Eqs.(4.19a)-(4.19c) by re-expressing the Green's function $G(\mathbf{k}, z_\nu)$ contained in the particle-particle bubble $\mathcal{G}(\mathbf{k}, z_\alpha)$ by the model spectral functions (4.21) or (4.25). This done explicitly in Appendix B.1 for the BCS case. Then the coefficients a, c and d can be calculated and written as energy integrals over a weighted BCS density of states (4.24) times various combination of the Fermi function (4.28) and its derivatives. The results, presented exhaustively in Appendix B.2, are the following:

$$a = \frac{1}{U} - \int d\omega\, D_{a,1}(\omega)\, \frac{\tanh(\beta\omega/2)}{2\omega} \tag{4.30a}$$

$$\begin{aligned} c = & \int d\omega \Big(D_{c,11}(\omega)\, \frac{\tanh(\beta\omega/2)}{2\omega} \\ & + D_{c,31}(\omega) \big(\frac{\tanh(\beta\omega/2)}{4\omega^2} + \frac{n'_F(\omega)}{2\omega} \big) \\ & + D_{c,51}(\omega) \big(- \frac{\tanh(\beta\omega/2)}{4\omega^3} - \frac{n'_F(\omega)}{2\omega^2} + \frac{n_F{}''(\omega)}{2\omega} \big) \Big)\, 4\pi n t^2 \\ & + \int d\omega\, D_{c,32}(\omega) \big(\frac{\tanh(\beta\omega/2)}{4\omega^2} + \frac{n'_F(\omega)}{2\omega} \big)\, 2t \end{aligned} \tag{4.30b}$$

$$d = \mathcal{P} \int d\omega\, D_{a,1}(\omega)\, \frac{\tanh(\beta\omega/2)}{4\omega^2} + i\, \frac{\pi}{8}\, \beta\, D_{a,1}(\omega = 0) \tag{4.30c}$$

where $\mathcal{P}$ denotes the Cauchy principal part. These expressions are similar to the one obtained for the coefficients of the Ginzburg-Landau theory [93] and the latter can be straightforwardly obtained by taking the limit $\Delta \to 0$ in Eqs.(4.30a)-(4.30c). In this case a "Sommerfeld expansion" around $\omega = 0$ is often used to evaluate the integrals [45, 46]. This is unfortunately not possible in the case $\Delta > 0$, since the function to be expanded is proportional to $D_{\mathrm{BCS}}(\omega)$ which is not smooth enough around $\omega = 0$, unlike the weak coupling limit $\Delta = 0$ where it is simply $D_0(\mu_0 + \omega)$, the tight-binding density of states. Therefore the coefficients a, c and d will be evaluated numerically once the value of Δ is known. Moreover the integration range is limited here to the interval $[-W/2 - \mu_0, W/2 - \mu_0]$ due to the tight-binding dispersion $\varepsilon_{\mathbf{k}}$ from Eq.(2.5). This avoids the difficulties appearing in the continuum case where the upper bound is infinite and generates an ultraviolet divergence in the coefficient a, which has to be regularized [45, 46].
The finite linewidth Γ characterizing the spectral functions of the pseudogap regime can now be taken into account. Although the numerical calculations show that it is wave vector dependent with a global maximum at k_F [91], it is enough for the present

purpose to consider Γ as a constant.[11] For the same reason, it is simpler to take the distribution function f_Γ in $A_{\rm PG}(\mathbf{k},\omega)$ as a Gaussian, i.e.

$$f_\Gamma(\omega) = \frac{1}{\sqrt{2\pi}\Gamma}\,\exp\Big(-\frac{1}{2}\big(\frac{\omega}{\Gamma}\big)^2\Big), \tag{4.31}$$

instead of the usual Lorentzian. Then the coefficient a, c and d can be calculated with the spectral function (4.25), as shown in Appendix B.3. The results give expressions identical to Eqs.(4.30a-4.30c), except for all the density of states-like functions (B.10a-B.10g) that have to be modified in the same way as $D_{\rm PG}(\omega)$ in Eq.(4.26). For instance

$$D_{a,1}(\omega) \to \tilde{D}_{a1}(\omega) = \int dE\, D_{a,1}(E)\, f_\Gamma(E-\omega) \tag{4.32}$$

and so on.
As already mentioned, the coefficients a, c and d obtained in this section show strong similarities with the weak coupling ($\Delta = 0$) Ginzburg-Landau expressions (see for instance Refs. [46, 90]). As mentioned in Section 2.4, the latter would be the T-matrix coefficients in a non-self-consistent calculation, which would describe the pairing fluctuations as the Gaussian correction to the mean-field (BCS) solution. From this point of view, Eqs.(4.30-4.32) may describe a "renormalized"Gaussian fluctuation regime taking into account the fact that the underlying electronic structure displays a pseudogap. The study of the thermodynamics of such a regime constitutes the goal of the present chapter. It is therefore necessary to go back to Eq.(4.17) that gives the thermodynamic grand potential for the T-matrix approximation scheme.

4.3.3 Expansion of the thermodynamic potential

Having calculated the T-matrix (4.18) according to the approximate self-consistent scheme of Section 4.2.3, it is now necessary to consider the grand canonical potential $\Omega(T,V,\mu)$ in order to deduce the corresponding thermodynamic properties.
As observed in Section 4.2.1, the T-matrix can be interpreted as the propagator of the pairing fluctuations appearing in the system above the critical temperature T_c. Therefore the last term of Ω given by Eq.(4.16), which describes noninteracting bosonic quasiparticles, can be immediately seen as the contribution of these virtual Cooper pairs. The latter are characterized by the coefficients a, c and d calculated in Section 4.3.2 and discussed in details below in Section 4.4.2. The other terms of Ω can be given a more concrete meaning by iterating Dyson's equation (4.13c) for G and expanding $\log(1-G_0\sigma)$. To second order in the self-energy σ, Ω can be written as

$$\Omega \approx \Omega_f + \Omega_b + \Omega_i \tag{4.33}$$

[11] This can be justified by the fact that the temperature-dependent functions in Eqs.(4.30a-4.30c) are peaked around the Fermi energy $\omega = 0$ so that the details of the "tails" are not relevant.

where

$$\Omega_f = -\frac{2}{\beta}\sum_{\mathbf{k},z_\nu}\log\big(-G_0(\mathbf{k},z_\nu)^{-1}\big) \tag{4.34a}$$

$$\Omega_b = \frac{1}{\beta}\sum_{\mathbf{k},z_\alpha}\log\big(T(\mathbf{k},z_\alpha)^{-1}\big) \tag{4.34b}$$

$$\Omega_i = -\frac{1}{\beta}\sum_{\mathbf{k},z_\nu} G_0^2(\mathbf{k},z_\nu)\,\sigma^2(\mathbf{k},z_\nu). \tag{4.34c}$$

The interpretation of Ω_f is evident: it describes noninteracting electrons with the tight-binding spectrum from Eq.(2.5) but subject to the "true" chemical potential μ.[12] These electrons can thus be considered as "unpaired" in the sense that their contribution to the thermodynamics is not directly affected by the pairing fluctuations. Ω_b is the T-matrix contribution already discussed above and Ω_i represents an interaction between the pairing fluctuations. In Appendix C it is shown that it can be given a more transparent form

$$\Omega_i = -N\,b\left(\frac{1}{\beta N}\sum_{\mathbf{k},z_\alpha} T(\mathbf{k},z_\alpha)\right)^2 \tag{4.35}$$

involving a new coefficient b defined by

$$b = \frac{1}{\beta N}\sum_{\mathbf{k},z_\nu} G^2(\mathbf{k},-z_\nu)\,G_0^2(\mathbf{k},z_\nu). \tag{4.36}$$

Expression (4.35) corresponds exactly to the result which would be obtained by performing a variational calculation for the free energy of the time-dependent Ginzburg-Landau theory based on Bogoliubov's inequality [33]. Arguments are developed in Appendix C.1 that lead to the conclusion that Ω_i can be simply neglected in this calculation. This point is also discussed below when evaluating the coefficient b from Eq.(4.36). One arrives then to a very simple two-fluid picture for describing the thermodynamic properties of the system under consideration. They contain two distinct contributions, the first (Ω_f) from unpaired electrons and the second (Ω_b) from those contributing to the pairing fluctuations described by the T-matrix. The "equilibrium" repartition between the two parts is fixed by the chemical potential μ which enters the number equation (2.6), as it is usual in a grand canonical approach.
Eq.(2.6) can be expressed in terms of the thermodynamic potential Ω as

$$n = \frac{1}{N}\sum_i \langle n_{i\uparrow} + n_{i\downarrow}\rangle = -\frac{1}{N}\frac{\partial\Omega}{\partial\mu}. \tag{4.37}$$

[12] And not μ_0 since the latter appears only in the spectral functions used to calculate the T-matrix coefficients (4.19a-4.19c).

Starting from Eq.(4.17) giving Ω and using the T-matrix relations (4.13a-4.13d), it is easy to show that Eq.(4.37) reduces to

$$n = \frac{2}{N} \sum_{\mathbf{k},z_\nu} G(\mathbf{k}, z_\nu) \tag{4.38}$$

as expected. This relation is used in QMC to deduce the temperature dependence of the chemical potential for fixed density n and interaction strength U (see Section 5.3.2). In the present case the results of such a process are simply borrowed from other works using the same parameters [95] and Eq.(4.38) serves rather to develop further the two-fluid concept introduced above.[13] Introducing the decomposition (4.33) (without Ω_i) into Eq.(4.37) yields the simple result

$$n = n_u + n_p \tag{4.39}$$

which can be easily interpreted. The first term represents the unpaired electrons the number of which is given by the noninteracting expression

$$n_u = \frac{2}{N} \sum_{\mathbf{k}} n_F(\varepsilon_{\mathbf{k}} - \mu). \tag{4.40}$$

where the sum over Matsubara frequencies has been performed. The second term reads

$$n_p = \frac{1}{\beta N} \sum_{\mathbf{k},z_\alpha} T(\mathbf{k}, z_\alpha) \frac{\partial}{\partial \mu} T^{-1}(\mathbf{k}, z_\alpha) \tag{4.41}$$

and accounts for the density of electrons involved in the pairing fluctuations. Eq.(4.41) can be made more transparent by assuming that the coefficient d is real (see Section 4.4.2) and that the only relevant μ dependence is contained in the coefficient a. This yields

$$n_p \approx \frac{1}{N} \sum_{\mathbf{k}} n_B(\Omega_{\mathbf{k}}) \big(- \frac{\partial \Omega_{\mathbf{k}}}{\partial \mu} \big). \tag{4.42}$$

where n_B is the Bose-Einstein distribution

$$n_B(\omega) = \frac{1}{e^{\beta\omega} - 1}. \tag{4.43}$$

This expression describes bosonic quasiparticles with a dispersion $\Omega_{\mathbf{k}}$ given by

$$\Omega_{\mathbf{k}} = \frac{1}{\mathrm{Re}(d)} (a + ck^2). \tag{4.44}$$

[13] There is however a strong resemblance between Eq.(4.38) defining μ and Eq.(4.27) fixing μ_0. This will be explained in Section 4.4.1.

The weighting factor in Eq.(4.42) can be approximated by its value at $k = 0$ and taken out of the sum.[14] Then it satisfies

$$-\frac{\partial \Omega_{k=0}}{\partial \mu} = -\frac{1}{\mathrm{Re}(d)} \frac{\partial a}{\partial \mu} = 2 \tag{4.45}$$

as it can be easily seen by considering Eqs.(4.30a-4.30c). Thus, provided that both $\mathrm{Im}(d)$ and the interaction Ω_i can be neglected, it appears that a low-energy pairing fluctuation mode described by the T-matrix $T(\mathbf{k}, z_\alpha)$ involves exactly two electrons, in complete agreement with the picture of virtual Cooper pairs developed in Section 4.2.1.

The latter argument shows that the approach used above to treat the interplay between electrons and pairing fluctuations is able to describe correctly the thermodynamic properties of such a system. This analysis is continued in the following sections by giving concrete values to the theoretical parameters which allow to characterize more concretely the T-matrix.

4.4 Results for $D = 2$

The previous sections have shown how to calculate the T-matrix and how to use the latter in the study of the thermodynamic properties of the attractive Hubbard Hamiltonian in the pseudogap regime. The corresponding results for its 2D realization are presented hereafter. However they constitute only an intermediate stage since, due to the particularity of 2D superconductivity which cannot be treated by the method used here [18], a weak interlayer is introduced later in Section 4.5.1 to restore the "normal" case (see Section 4.2.3). Conditions are then determined under which the 2D results are (almost) not affected by the three-dimensionality so that, in this case, all the forthcoming considerations conserve their validity.

4.4.1 Choice of the parameters

In order to evaluate the T-matrix coefficients a, b, c and d, concrete values are needed for the parameters β, μ, Δ and Γ. The objective is to describe an intermediate coupling $U = 4t$ and a temperature region just above T_c where the pseudogap is well developed. This corresponds to a regime where the pairing fluctuations are important in both in the 2D and 3D anisotropic cases.[15]

An important constraint also comes from the considered method: as already mentioned in Section 4.2.1, the T-matrix approximation scheme is valid only at low electronic

[14] This step is allowed because of the presence of the Bose function n_B which retains only the low-energy contributions.

[15] For the 3D *isotropic* case, this question is studied in Section 5.3.4.

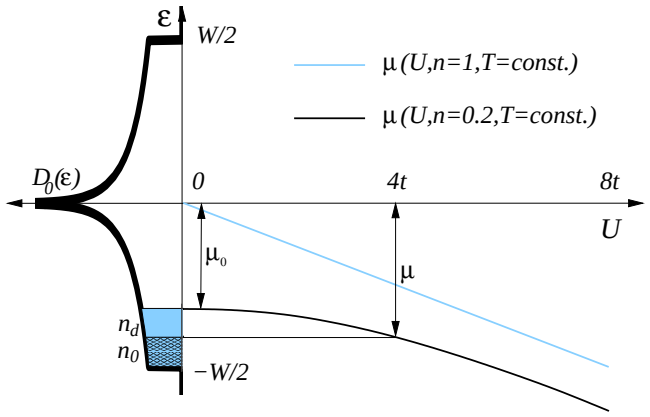

Figure 4.2: Schematic behavior of the chemical potential μ as a function of the coupling strength U. At half-filling ($n = 1$) it is equal to $-U/2$ whereas for small densities like $n = 0.2$ it reaches this value only asymptotically. At intermediate coupling ($U \sim 4t$), the difference between $\mu(U, n, T)$ and $\mu_0 = \mu(U = 0, n, T)$ allows to visualize the two contributions to the number equation (4.39).

densities n. A reasonable choice is

$$n = 0.2 \tag{4.46}$$

in a normalization where, in agreement with Eq.(4.38), $n = 1$ corresponds to half-filling. The other parameters are fixed as follows:

- The temperatures of interest lie in the interval commonly denoted $[T_c, T^*]$ where the pseudogap is first fully developed and then gradually fills up when T increases toward T^*. This behavior is well reproduced by the attractive Hubbard model for the intermediate coupling strength $U = 4t$.[16] For simplicity only temperatures close to the critical value T_c are considered. Typical values for the chosen density $n = 0.2$ are $T_c = 0.07t$ [32, 42] so that $\beta = 15t^{-1}$ corresponds to a regime with a well-developed pseudogap.

- For such low temperatures ($\beta t \gg 1$), the chemical potential μ can be considered as a constant. Its value is borrowed from QMC calculations [95] which solve the number equation (4.38). They give the result $\mu(\beta = 15t^{-1}, n = 0.2, U = 4t) = -3.5t$ in a convention where $\mu = 0$ corresponds to the middle of the noninteracting band (see Section 2.1). This has to be compared with the solution of Eq.(4.29) for the same temperature $\beta = 15t^{-1}$ which gives $\mu_0 = -2.9t$.

[16] The question whether the fully self-consistent T-matrix approximation succeeds in reproducing these features is still open [96], but it has been shown that approximatively self-consistent approaches did it [89, 52].

There is a difference

$$\mu - \mu_0 = -0.6t. \tag{4.47}$$

which has to be clarified. By its definition in Eq.(4.27) μ_0 gives the position of the middle of the pseudogap with respect to the center of the *interacting* band. However the *absolute* position of the latter, i.e. its position with respect to a fixed reference point such as the middle of the noninteracting band, is not specified in the band structure model defined in Section 4.3.1. This information is however contained in μ obtained from QMC calculations (see Section 5.3.2). Eq.(4.47) then means that the interacting band is shifted to lower energies with respect to the noninteracting one, as shown in Figure 4.2 and in agreement with the strong coupling asymptotic limit

$$\lim_{U/t\to\infty} \mu(\beta, n, U) = -\frac{U}{2} \tag{4.48}$$

which implies as well a negative band shift (see Section 2.2).

- The quantity 2Δ from Eq.(4.25) describes the width of the pseudogap. This has to be contrasted with the BCS theory where 2Δ represents the order parameter, which vanishes above T_c. Typical values are of the order of t and only weakly temperature dependent [95], so that the choice $\Delta = 0.5t$ is justified.

- Γ gives the width of the peaks of the spectral functions $A_{\mathrm{PG}}(\mathbf{k}, \omega)$. In the regime of interest (well-developed pseudogap), it is sufficient to take a constant value $\Gamma = 0.125t$ provided by numerical calculations [91] in order to reproduce the main characteristics of the density of states, as shown in Figure 4.3. However in the case of higher temperatures, it would be necessary to take into account the dependences of Γ on both the temperature and the wave vector in order to generate the "filling" of the pseudogap as $T \nearrow T^*$, as suggested by the numerical calculations [92]. This mechanism is illustrated in Figure 4.4.

The values of the parameters chosen above represent a single point in the U-μ phase diagram of the attractive Hubbard model. The pertinence of the present approach is however not restricted only to $(U = 4t, \mu = -3.5t)$ and a discussion of its domain of validity will be presented in Section 4.4.4 when the physical picture of the problem will have been more extensively analyzed.

4.4.2 T-matrix coefficients

Having fixed the values of the different parameters describing a regime with a well-developed pseudogap, the integrals giving the T-matrix coefficients a, b, c and d can be evaluated numerically. This allows to analyze more quantitatively the T-matrix and, thereby, the nature of the pairing fluctuations which produce the pseudogap. The results are summarized in Table 4.1 and commented hereafter.

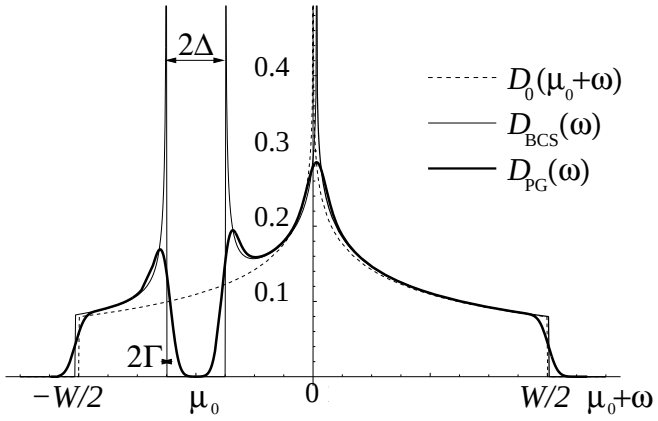

Figure 4.3: Comparison of the shapes of the density of states for various cases: $\Delta = \Gamma = 0$ (weak coupling), $\Delta > 0$, $\Gamma = 0$ (BCS) and $\Delta, \Gamma > 0$ (pseudogap regime)

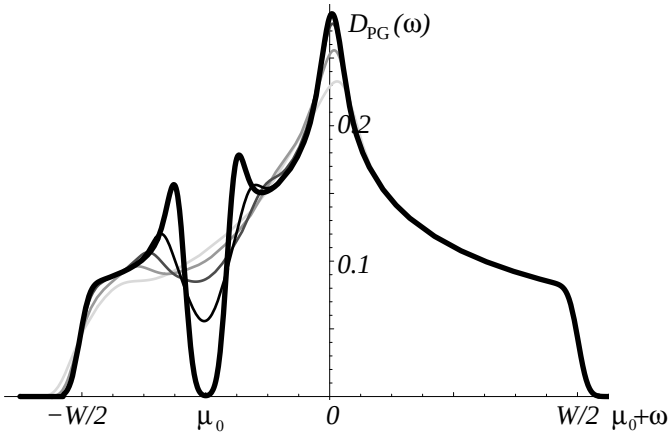

Figure 4.4: Filling of the pseudogap with increasing temperatures by varying the linewidth Γ. The thickest curve for $T = T_c$ is obtained with $\Gamma = 0.125t$ and the other thin ones correspond to higher T. They contain the additional k-dependent contribution to Γ which is peaked around $\omega = 0$, being as large as 8Γ over the interval $[-2\Delta, 2\Delta]$ for the largest temperature (lightest curve).

Table 4.1: T-matrix coefficients for various cases ($\beta = 15t^{-1}$ and $n = 0.2$)

Coefficient	Weak coupling $\Delta = \Gamma = 0$	BCS $\Delta = 0.5t,\ \Gamma = 0$	Pseudogap $\Delta = 0.5t,\ \Gamma = 0.125t$
$a\,[t^{-1}]$	0.158	0.019	0.021
$c\,[t^{-1}]$	2.828	0.182	0.199
$\mathrm{Re}(d)\,[t^{-2}]$	0.049	0.029	0.030
$\mathrm{Im}(d)\,[t^{-2}]$	0.547	0	0
$b\,[t^{-3}]$	2.246	0.184	0.217

Coefficient a

First, it is found that the coefficient a decreases with T when approaching the critical temperature from above. This dependence is weaker in the pseudogap regime than in the weak coupling case ($\Delta = \Gamma = 0$). Second, as suggested by Table 4.1, a shows clearly the tendency to become small (i.e. $a \ll 1/U$) at $T = T_c$. These results, represented schematically in Figure 4.5, are consistent with recent works [32] on the 2D attractive Hubbard model and confirm the validity of the present approximative approach. They show that the occurrence of (BKT) superconductivity in 2D does not satisfy the Thouless criterion $T^{-1}(0,0) = 0$ (see Section 4.3.2). This observation will be corrected in Section 4.5.1 where a weak interlayer coupling will restore the three-dimensionality. It is also clear that due to the limited accuracy of the model (4.25), the value of the coefficient a given in Table 4.1 is only indicative and a more accurate way of determining it will be given below in Section 4.4.3.

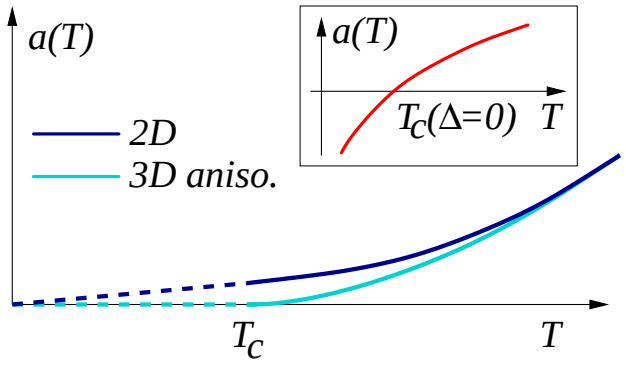

Figure 4.5: Influence of the dimensionality on the behavior of the coefficient a near the critical temperature T_c. The inset shows the weak coupling case ($\Delta = \Gamma = 0$).

Coefficient d

As announced the coefficient d is complex. The integral in Eq.(4.30c) gives the real part as $\mathrm{Re}(d) = 0.031t^{-2}$ whereas the imaginary part, corresponding to the inverse lifetime of the pairing fluctuations described by the T-matrix, is directly proportional to the quantity $\tilde{D}_{a,1}(\omega = 0)$. As $T \searrow T_c$ and the pseudogap gets fully developed, the latter vanishes so that the bosonic quasiparticles associated with $T(\mathbf{k}, z_\alpha)$ become long-lived and constitute well-defined two-electron states.

Coefficient c

Evaluation of expression (4.30b) gives $c = 0.19t^{-1}$. The form of the T-matrix in Eq.(4.18) suggests that c can be associated to the effective mass of the bosonic quasiparticles as

$$m_b = \frac{\mathrm{Re}(d)}{2c}. \tag{4.49}$$

This gives $m_b = 0.16m$, m being the effective mass of the tight-binding electrons obeying

$$m = \frac{1}{2t}. \tag{4.50}$$

Although the value of m_b seems unexpectedly small, a similar order of magnitude has been obtained by other authors in the intermediate coupling regime $U = 4t$ [47, 50]. A possible explanation would be based on the fact that the corresponding virtual Cooper pairs are only moderately bound to the lattice sites and thereby relatively mobile, in contrast to the strong coupling approach where the latter are truly "local" and have a large effective mass given by $m_b = (U/2t)m = 2m$ for $U = 4t$ (see Section 2.2). However a clear distinction must be made between the curvature near the origin $\mathbf{k} = (0, 0)$ of the quasiparticle band and the full width of this band.[17] The latter can be estimated by solving the equation $T^{-1}(\mathbf{k} = (\pi, \pi), z_\eta) = 0$ which defines the so-called η-peak [85]. Since $T^{-1}(\mathbf{k} = (0, 0), 0) \approx 0$ (taking $a \sim 0$), z_η gives directly the value of the bosonic bandwidth W_B. Inserting the noninteracting G_0 in Eq.(4.13b) allows to obtain an analytic expression for W_B:

$$W_B = -(1 - n)U - 2\mu \approx 3.8t. \tag{4.51}$$

Using a BCS-form for G [38] gives numerically a similar result which should not be altered by the further addition of a nonzero Γ. Therefore the bosonic band has a width W_B smaller than the electronic noninteracting value $W = 8t$ and is compatible with numerical T-matrix results [51, 90].

[17] Rigorously the bosonic band is defined by solving $T^{-1}(\mathbf{k}, \omega) = 0$ in the form $\omega = \Omega_{\mathbf{k}}$ for which Eq.(4.44) is then just the low-energy expression.

Coefficient b

The results from the evaluation of Eq.(4.36) for b using the method exposed in Section 4.3.2 are given in Appendix C.2. As explained in Section 4.3.3, the coefficient b represents an interaction between the bosonic quasiparticles described by the T-matrix. The numerical results displayed in Table 4.1 show that the presence of a pseudogap in the electronic band structure reduces strongly the value of b with respect to the weak coupling case where it is approximatively given by $7\zeta(3)\beta^2 D_0(\mu)/8\pi^2 \approx 2.24\, t^{-3}$. This behavior can be explained very roughly by the fact that b is proportional to the value of the density of states at $\omega = 0$, as suggested by its weak coupling expression. Therefore b becomes very small in the pseudogap regime so that the effects of interaction become negligible in this case.

Thus the evaluation of the T-matrix coefficients for the 2D case has shown that the T-matrix describes well-defined noninteracting bosonic quasiparticles whose chemical potential ($\propto a$) becomes very small close to the critical temperature.

4.4.3 Number equation and consistency checks

The parameter values given in Section 4.4.1 can be also used to evaluate explicitly the two contributions to the number equation (4.39). They allow then to perform several consistency checks showing that the results obtained up to this point (in Sections 4.4.1 and 4.4.2) make sense. Inserting the value $\mu = -3.5t$ into Eq.(4.40) yields

$$n_u = 2\int d\epsilon\, D_0(\epsilon)\, n_F(\epsilon - \mu) \simeq 0.1. \tag{4.52}$$

Therefore the unpaired electrons represent approximately half of the total density $n = 0.2$ and correspond essentially to the states situated at the bottom of the noninteracting band. The remaining occupied states contribute to the pairing fluctuations which form well-defined bosonic quasiparticles whose density follows from Eqs.(4.39)-(4.45) as

$$n_b = \frac{n - n_u}{2} = 0.05. \tag{4.53}$$

Thus in the present case of an intermediate coupling $U = 4t$, only half of the electrons participate in the pairing fluctuations above the critical temperature, in contrast to the strong coupling limit ($U \gg t$) where all the electrons are bound into pairs above T_c ($n_b = n/2$).
Knowing n_b from Eq.(4.53), it is now possible to re-calculate more accurately the value of the coefficient a just above the critical temperature. Performing the wave vector summation in Eq.(4.42) yields

$$n_b = -\frac{\mathrm{Re}(d)}{4\pi\beta c}\, \log\Big(1 - \exp\big(-\frac{\beta a}{\mathrm{Re}(d)}\big)\Big). \tag{4.54}$$

Solving the equation for a and using the values of β, c, d and n_b given above, leads to the results $a \sim 10^{-6}t^{-1}$. The distance between the latter and the origin is clearly too small to be found by the approach developed in Section 4.3. However it will not be of fundamental interest in the following since it concerns exclusively the strictly 2D case. In fact the above reasoning about a may also be seen as a first consistency check for the approach exposed in the previous sections. Indeed it shows that two ways of calculating the same coefficient a agree qualitatively on the result. Other cross-checks can be performed, in particular in order to test the numerical value of n_b given by Eq.(4.54) which constitutes a rather nontrivial issue.

- The first possibility bases itself on the "BCS" solution to the T-matrix equations mentioned in Section 4.2.3. Using Eq.(4.20) for the self-energy and replacing $T(\mathbf{k}, z_\alpha)$ by $\Delta^2\,\delta(k)\,\delta(z_\alpha)$ (i.e. all the weight of the T-matrix is concentrated at zero-energy) yields an electronic structure where 2Δ is effectively the width of the pseudogap. In this case the relation

$$\Delta^2 = \frac{1}{\beta N}\sum_{\mathbf{k},z_\alpha} T(\mathbf{k}, z_\alpha) \tag{4.55}$$

  has to be satisfied. Comparison with Eq.(4.41)-(4.45) gives

$$n_b = \mathrm{Re}(d)\,\Delta^2. \tag{4.56}$$

  Using $\mathrm{Re}(d) = 0.031t^{-2}$ and $\Delta = 0.5t$ provides the result $n_b = 0.008$ which is clearly too small. This discrepancy shows that the weak coupling approximation underlying Eq.(4.20) is not valid here.[18]

- The value of the quasiparticle effective mass discussed in Section 4.4.2 in connection with the coefficient c can also be used to calculate n_b. Indeed the above result $m_b = 0.16m$ corresponds to a precise value of a BCS-BEC crossover parameter used by other authors [47, 50], which, in turn, can be associated with a precise value of n_b. Both give the result $n_b = 0.033$, in the first case explicitly and in the second one indirectly by providing the chemical potential shift $\frac{\mu+W/2}{\mu_0+W/2} = n_u/n = 0.66$. This estimate shows a better agreement with Eq.(4.53).

- There exists a relation between n_b and the double occupancy n_2 defined by the expectation value of the operator $(1/N)\,\sum_i (c_{i,\uparrow}c_{i,\downarrow})^\dagger (c_{i,\uparrow}c_{i,\downarrow})$ which counts the average number of *local* pairs on each lattice site. It reads

$$n_2 = (\frac{n}{2})^2 + n_b \tag{4.57}$$

  and is easily obtained from QMC (it is just the potential energy divided by U, see Chapter 5). The results are $n_2 = 0.05$ for $n = 0.2$ and $\beta = 15t^{-1}$ so that $n_b = 0.04$, which is satisfactorily close to the value 0.05 coming from the number equation.

[18] In fact this approach suits better to the case where $\mu \simeq \mu_0$ which makes n_b very small.

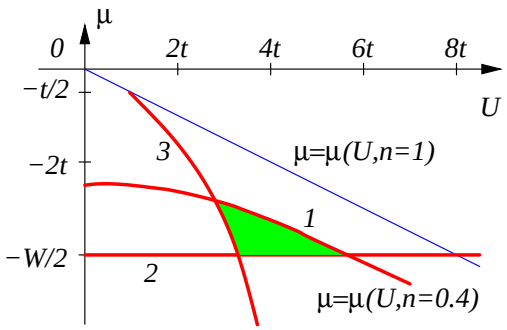

Figure 4.6: Domain of validity of the two-fluid picture, the curves 1, 2 and 3 corresponds the conditions (4.58), (4.59) and (4.60) respectively.

These considerations allow to establish a simple picture of the coupled system of electrons and pairing fluctuations in the intermediate coupling regime just above T_c. Whereas one part of the electrons behaves as uninteresting free fermions, the other part is equivalent to a set of long-living noninteracting bosons which are quantitatively characterized by the T-matrix coefficients. Their density n_b as given by the number equation (4.39) appears to be slightly overestimated, possibly due to the neglecting of the bosonic interaction ($\propto b$) and to the factorization in Eq.(4.45), which both might have lead to a *depletion* of n_b [90, 97].

4.4.4 Validity of the two-fluid picture

In the previous sections a two-fluid picture was developed to describe the coupled system of electrons and pairing fluctuations. Concrete values for the model parameters U and μ were introduced, [19] which allowed to determine quantitatively the properties of the system. The question may now arise to know what is the domain of validity of this picture in the U-μ parameter plane.
A qualitative answer is given in Figure 4.6 which shows that there are essentially *three* constraints defining a domain in the U-μ plane where the applicability of two-fluid approach used above is guaranteed.

1. First, the T-matrix approximation scheme must be valid. As already discussed above (Sections 4.2.1 and 4.2.2), this corresponds to low values of the electronic density n, say $n \lesssim 0.4$. Therefore the relation

$$\mu \lesssim \mu(U, n = 0.4) \tag{4.58}$$

has to be satisfied (the temperature dependence of $\mu(U, n)$ is neglected and T is taken as zero in this section).

[19] The other parameters like T_c, n, Δ or Γ are in principle unambiguously fixed by U and μ.

2. Second, the density n_b of the bosonic quasiparticles describing the pairing fluctuations should have an upper bound which is given by $n/2$, the value corresponding to the large-U limit of the attractive Hubbard model. As Figure 4.2 suggests, n_b depends essentially upon the difference between the quantities μ and μ_0 discussed in Section 4.4.1. It shows as well that the chemical potential μ must not exceed the noninteracting lower band limit $-W/2 = 4t$ in order to ensure that $n_b < n/2$. Thus the condition

$$\mu \gtrsim -\frac{W}{2} \tag{4.59}$$

   is necessary.

3. Finally, a lower bound is also required for n_b. This ensures that a nonnegligible part of the electrons are involved in the pairing fluctuations and avoids the case $n \simeq n_u$ encountered in the first consistency check presented in Section 4.4.3. The same reasoning as above based on Figure 4.2 leads to the conclusion that the following inequality has to be satisfied:

$$\mu < \mu_0\big(n(\mu)\big) - \frac{t}{2} \tag{4.60}$$

   where the shift $t/2$ typically guarantees that $n_u \sim n_p$.

A more quantitative answer to the above question, in particular concerning the behavior of the T-matrix coefficients when varying slightly U and μ, would become immediately quite delicate. Indeed opposite tendencies would appear, for instance for a lower U, Δ and Γ would decrease but $\beta = T_c^{-1}$ would increase, so that the results of the integrals (4.30a-4.30c) cannot be easily guessed. Such an analysis will not be undertaken here.

4.5 Results for $D > 2$

The fact that pairing fluctuations close to T_c can be represented by well-defined free bosonic quasiparticles suggests that the superconducting phase transition at T_c may be viewed as a Bose-Einstein condensation (BEC) of the latter. This point of view is however not valid in 2D, since free bosons do not condensate for $D \leq 2$.[20] To allow for such a possibility, which is in fact the main goal of this work as motivated in Section 4.1, it is necessary to include a nonvanishing hopping amplitude in the perpendicular direction. It has however to be small enough to preserve the properties of the T-matrix that justify the "bosonic interpretation" of the pairing fluctuations.

[20] There is also a more pragmatic reason for leaving the case $D = 2$ due to the fact that the T-matrix approximation is unable to describe the BKT physics.

4.5.1 Effect of a weak interlayer coupling

Before considering the thermodynamic properties from the point of view of a BEC, it is necessary to analyze precisely the influence of an interplane hopping which allows a nonzero BEC transition temperature.
A 3D anisotropic system is obtained by adding to the Hamiltonian $\mathcal{H}$ a term that contains the hopping between neighboring lattice planes, characterized by an amplitude $t_\perp$. The (electronic) anisotropy is defined by the ratio

$$\gamma^2 = \frac{t}{t_\perp}. \tag{4.61}$$

As a consequence, all the T-matrix equations (4.13a-4.13d) contain now a sum over a 3D Brillouin zone and the 2D tight-binding density of states $D_0(\epsilon)$ in Eq.(4.24) has to be replaced by the more complicated 3D anisotropic expression given by

$$D_{3\mathrm{D}}(\epsilon) = \int dE\, D_\perp(E)\, D_0(\epsilon - E) \tag{4.62}$$

where

$$D_\perp(\epsilon) = \int_{-\pi}^{\pi} dk\, \delta\big(\epsilon + 2t_\perp \cos(k)\big) = \frac{1}{2\pi t_\perp} \frac{1}{\sqrt{1 - \big(\frac{\epsilon}{2t_\perp}\big)^2}} \tag{4.63}$$

is the 1D tight-binding density of states. Eq.(4.62) shows clearly the consequence of an interlayer coupling $t_\perp$ on the density-of-states-like functions: similarly to the finite linewidth Γ of the spectral functions in Eq.(4.25), $t_\perp$ smears out the shape of the purely 2D results. Therefore, rather than going again through the whole calculations, it seems reasonable to introduce an additional linewidth

$$\Gamma_\perp \simeq 2t_\perp \tag{4.64}$$

that quantifies the energy scale over which the effects of the interplane hopping $t_\perp$ manifest themselves. Then it suffices to determine the conditions under which the results of Section 4.4.2 are preserved.
The first prerequisite is merely the existence of a pseudogap in the electronic density of states above T_c. As explained briefly in Section 4.2.3 and calculated in Ref.[91], it depends on the presence of specific peaks in the imaginary part of the self-energy. According to Ref.[91] the latter have a width near k_F which is similar to the one of the corresponding spectral functions $A(\mathbf{k}, \omega)$. Therefore one requires

$$\Gamma_\perp \ll \Gamma \tag{4.65}$$

in order to preserve a well-developed pseudogap. The second condition concerns the T-matrix coefficients given by Eqs.(4.30a-4.30c). Here $\Gamma_\perp$ affects the weighted

density-of-states functions (B.10a-B.10g) in a way analogous to Eq.(4.62). Therefore the values of the integrals are not altered as long as

$$\Gamma_\perp \ll \Delta. \tag{4.66}$$

Combining Eqs.(4.65) and (4.66) together with Eq.(4.61) and including the parameters values $\Gamma = 0.125t$ yields the following condition

$$\gamma^2 \gg 16 \tag{4.67}$$

to preserve the "bosonic interpretation" of the pairing fluctuations above T_c. In fact the inequality (4.65) is the strongest and shows that the pseudogap is a typical 2D phenomenon [98] and that it would hardly survive if the system became 3D isotropic (see Section 5.3.4).
There are however two nontrivial changes introduced by the interplane hopping that cannot be controlled by the condition (4.67) nor evaluated using the approximative T-matrix approach form above. This is essentially due to the fact that they are small and cannot be determined by the limited accuracy of the available method. Therefore it is necessary to borrow results from other works in order to fix the problem. These changes are:

Coefficient a. Dealing again with an "ordinary" superconducting phase transition in $D > 2$ (in contrast to the "particular" BKT transition for $D = 2$), the validity of the Thouless criterion is restored. Thus at $T = T_c$ the coefficient $a = T^{-1}(0, 0)$ is expected to vanish as shown in Figure 4.5. In term of the "bosonic interpretation", this implies that the chemical potential of the bosons given by $-a/\mathrm{Re}(d)$ vanishes as well. This feature is crucial for the discussion of the BEC in the next section.

Coefficient c. Virtual pairs may also hop from one plane to another and it makes sense to introduce a coefficient $c_\perp$ that multiplies k_z^2 in the T-matrix (4.18). It allows to define the bosonic anisotropy as

$$\gamma_b^2 = \frac{c}{c_\perp}. \tag{4.68}$$

Since it describes the correlated motion of two electrons along the z axis, it is expected to be proportional to the square of the single electron anisotropy γ^2. Quick and Sharapov derived the following expression in a similar context [99]:

$$\gamma_b^2 = 2\pi n \gamma^4 \tag{4.69}$$

where n is the electronic density.

In principle, provided that inequality (4.67) is satisfied, the considered system is constituted of free bosons in $D > 2$ whose the chemical potential vanishes at $T = T_c$. It is now possible to return to the question raised in the Section 4.1 about a possible BEC in short-coherence length superconductors.

4.5.2 Bose-Einstein condensation

First the calculation of the low-energy T-matrix made possible the interpretation of $T(\mathbf{k}, z_\alpha)$ as the propagator of well-defined bosonic quasiparticles. Then the extension to a 3D anisotropic system conditioned by Eq.(4.67) ensured the possibility of their condensation at a finite temperature $T_{c,\mathrm{BEC}}$. The final stage in characterizing the thermodynamic properties of the system under investigation is to establish whether the superconducting phase transition can be viewed as a BEC. If this is the case, then it should be possible to retrieve the critical temperature $T_c = 0.07t$ from an appropriate formula describing the condensation of the bosons associated with $T(\mathbf{k}, z_\alpha)$.
In this context the underlying electrons are apparently unimportant in determining the thermodynamic properties, which are then fixed by the bosonic degrees of freedom contained in the T-matrix only. Of course this is valid only when the pseudogap is well-developed because, if not, an interaction and a finite lifetime would dramatically alter this simple picture.
A reasonable choice of the bosonic anisotropy is $\gamma_b \sim 500 - 1000$ (see next section) so that the following inequality is expected to be satisfied

$$T_{c,\mathrm{BEC}} \gg \frac{c}{\gamma_b^2 \,\mathrm{Re}(d)} \sim \frac{6}{\gamma_b^2}. \tag{4.70}$$

This situation corresponds to the case of "strongly anisotropic" bosons which has been studied by Wen and Kan [100]. They derived an implicit equation for the critical temperature of a BEC under the conditions (4.67) and (4.70). It reads

$$T_{c,\mathrm{BEC}} = 4\pi n_b \frac{c}{\mathrm{Re}(d)} / \log\!\big(T_{c,\mathrm{BEC}} \frac{\gamma_b^2 \,\mathrm{Re}(d)}{c}\big). \tag{4.71}$$

All the parameters entering the above formula have been determined previously so that it can be used straightforwardly to see whether the considered system really consists in free bosons undergoing a BEC. The result is

$$T_{c,\mathrm{BEC}} = 0.4t. \tag{4.72}$$

This shows clearly that Eq.(4.71) gives a value which is substantially larger than the "true" critical temperature $T_c = 0.07t$. [21] It could be lowered to T_c by the choice of a higher anisotropy ($\gamma_b \sim 10^7$) but the latter would become so large that it would be meaningless to speak about a 3D system. Therefore this discrepancy is an intrinsic feature of the intermediate coupling range of the attractive Hubbard model. This is confirmed by applying the same procedure to the 3D isotropic case considered by

[21] Strictly speaking, the value $T_c = 0.07t$ obtained from numerical calculations applies for 2D systems only [32, 42]. However the corresponding value for the 3D isotropic case is $T_c = 0.13t$ (see Section 5.3.3), which shows that T_c evolves *smoothly* with the anisotropy. For $\gamma_b \sim 500 - 1000$ the 2D value is expected to be a good approximation, as confirmed by the Thouless criterion discussed previously.

Haussmann [50] where, after using the usual formula for $T_{c,\mathrm{BEC}}$, [94] a similar discrepancy between the true transition temperature and the BEC value is found as well.
Thus, in spite of favorable premises, the pure BEC physics, which works in the large-U limit, is not suited for the intermediate regime $U = 4t$. The observed inadequacy of the BEC critical temperature means that the "unpaired" electrons cannot be omitted. Although their contribution to the thermodynamic potential (4.34a) is uninteresting, they still play a role in inhibiting the bosonic states to arrange themselves to form the BE condensate as if they were real free bosons. [22] It is therefore normal that the true critical temperature lies below the one predicted by the BEC scenario. These will coincide once the effects of the "unpaired" electrons have disappeared, i.e. when $n_u = 0$, which corresponds to the strong coupling regime where *all* the electrons are forming the $n_b = n/2$ pairs.

4.5.3 Application to real materials

The theoretical considerations developed up to this point were concerned with the study of the thermodynamic properties of strongly anisotropic short-coherence length superconductors in the pseudogap regime just above the transition temperature T_c. As explained in the Introduction, these characteristics correspond precisely to underdoped high-temperature superconductors. It makes therefore sense to re-consider these materials in the framework of the above theoretical approach, bearing in mind however the limitations of the attractive Hubbard model in describing these materials.
The observation of thermodynamic properties suggesting a BEC was found to depend upon the strength of the electronic anisotropy γ, as stated in Eq.(4.67). Experimentally one rather determines the corresponding *bosonic* quantity γ_b, related to γ by Eq.(4.69). It is given by

$$\gamma_b = \lambda\, \gamma_m \tag{4.73}$$

where λ is the lattice anisotropy (out-of-plane lattice constant divided by in-plane lattice constant) and γ_m is the bosonic effective mass anisotropy (i.e. the anisotropy entering the corresponding GL theory [5]) which is extracted from penetration depth measurements. The data for underdoped $Bi_2Sr_2CaCu_2O_{8+x}$ (BSCCO) are given on Table 4.2. Taking $n \approx x = 0.1$, Eq.(4.73) gives $\gamma_b \sim 600$ and relation (4.69) yields $\gamma^2 \sim 750$. This value satisfies fully the condition (4.67) and may explain the observation of typical BEC features in the specific heat measurements of BSCCO [27]. On the other hand, the results for underdoped $YBa_2Cu_3O_{6+x}$ (YBCO) are $\gamma_b \sim 45$, $n \approx x \sim 0.5$ and $\gamma^2 \sim 15$. This values does not fulfill the above requirements and the BEC properties are "smeared out" by the interlayer coupling to give finally the XY-like behavior, as observed experimentally [27].
Another aspect worth to be mentioned is the following feature. Evaluating the BEC

[22] In fact all the electrons are involved in the evaluation of $T^{-1}(0,0)$ which gives the "true" critical temperature according to the Thouless criterion in $D > 2$.

Table 4.2: Material parameters for two underdoped high-temperature superconductors [5, 27]

Compound	in-plane lattice constant	out-of-plane lattice constant	anisotropy γ_m
BSCCO	5.4 Å	31.2 Å	200
YBCO	3.8 Å	11.7 Å	30

critical temperature formula (4.70) with the strong coupling parameter values ($c/\mathrm{Re}(d) \longrightarrow 2t^2/U = 0.5$ and $n_b \longrightarrow n/2 = 0.1$) and using the anisotropy of underdoped BSCCO $\gamma_b = 600$ gives $T_{c,\mathrm{BEC}} = 0.06t$. This value corresponds almost exactly to the transition temperature T_c of the system, as it has been chosen in Section 4.4.1.[23] Such a procedure was used in Ref.[27] and gave, together with the shapes of the specific heat curves, a strong experimental support for the interpretation of the superconducting transition in underdoped high-temperature superconductors like BSCCO as an authentic BEC [28]. In the light of the present work, the agreement between these two aspects seems to be the result of a coincidence rather than the manifestation of an authentic BEC of preformed pairs.

4.6 Discussion and conclusion

In this chapter the thermodynamic properties of short-coherence length superconductors in the pseudogap regime have been studied using on the self-consistent T-matrix approximation to the attractive Hubbard model. An analytic calculation using a simple model for the spectral functions allowed to evaluate both the T-matrix describing the pairing fluctuations and the thermodynamic grand potential. Although this approach was not fully self-consistent and required some inputs from other numerical works, several checks have established its reliability. For a sufficiently strong anisotropy along the third direction and a well-developed pseudogap, it has shown that the T-matrix describes long-lived noninteracting bosonic quasiparticles. In the considered intermediate coupling regime of the attractive Hubbard model not all the electrons contribute to the pairing fluctuations and a two-fluid picture with coexisting free electrons and bosonic pairing fluctuations is quite appropriate, the distribution between both parts being fixed by the (electronic) chemical potential. For $D > 2$, the Thouless criterion for the superconducting phase transition was reinterpreted as the vanishing of the bosonic chemical potential at $T = T_c$, showing strong similarities with a BEC of free bosons. Although the thermodynamic properties above T_c are determined by the bosonic degrees of freedom, it turned out that the unpaired electrons are still involved in fixing the value of the critical temperature, thereby moving the superconducting

[23] Although the latter concerns the strictly 2D case, it can be assumed to remain valid for a strongly anisotropic 3D case with $\gamma^2 = 750$.

transition a bit away from a pure BEC. However, provided that the anisotropy along the third direction is strong enough, BEC-like feature can still be present in the thermodynamic properties. This was illustrated for the case of underdoped high-temperature superconductors.

It is instructive to compare the above results with the other studies of the same problem already mentioned in Section 4.1. The approach by Tchernychyov [82] is the closest and leads to a similar conclusion about the existence of long-lived "noninteracting Cooper pairs inside the pseudogap". Although it is also based on a low-energy expansion of the (renormalized) particle-particle bubble, the T-matrix in Ref.[82] contains a double pole structure and is thus associated with sound-like fluctuation modes for which a bosonic interpretation is not possible. The boson-fermion (BF) model, introduced by Ranninger and Robin [80] and extended by Geshkenbein *et al.* [81] to the case of a d-wave superconductor, has been used successfully as a phenomenological model for short-coherence length superconductors like the underdoped high-T_c materials. It contains explicitly the two-fluid picture of coexisting free electrons and bosonic pairing fluctuations. The essential difference with the attractive Hubbard model considered here is the fact that the bosons constitute well-defined degrees of freedom over the whole temperature range $[T_c, T^*]$ whereas the present work has shown that this was justified for $T \gtrsim T_c$ only, the bosonic interaction and the finite lifetime destroying this picture for higher temperatures. Moreover the superconducting transition of the BF model is a BEC, which is not rigorously the case in the purely electronic model studied in this chapter.

The considerations developed above also raise some questions like for instance the origin of the discrepancy between the critical temperature T_c and the result of the BEC formula $T_{C,\mathrm{BEC}}$. Is it really an intrinsic property of the intermediate coupling regime (as also noted in Ref.[82]) or is it a consequence of an insufficiency of the method (like the neglect of the bosonic interaction which could have induced a depletion of the bosonic density and thereby of $T_{C,\mathrm{BEC}}$)? It is worth remarking that such a difference also appears when trying to apply carefully the BEC critical temperature formulas to underdoped high-temperature superconductors (see point (G) of Ref.[101]). An important conclusion of the above work is that a strong anisotropy is necessary to observe bosonic properties, from both theoretical and experimental point of view. But the specific heat curves of BSCCO presented in Ref.[27] suggest rather a 3D isotropic BEC for which c_V is somewhat different from the case of strongly anisotropic bosons [33]! Finally it would be interesting to perform a similar study for a model of a d-wave superconductor, using for instance the phenomenological approach called "nodal approximation" [102]. In this case the bosons (if they still exist) could be characterized by measurable quantities like the velocities v_F and v_Δ, allowing for deeper comparisons with the real materials.

Chapter 5

Quantum Monte Carlo study of the 3D attractive Hubbard model

In this chapter a study of the 3D attractive Hubbard model is performed using the Determinant Quantum Monte Carlo (DQMC) technique. This numerical method allows to determine the critical temperatures for both superconducting and charge-density wave (CDW) orders, as well as the temperature scale for pair formation. The latter process is related to precursor effects of superconductivity for which the role of dimensionality is investigated by comparing 2D and 3D systems for the same model parameters U and n.

5.1 Introduction

The DQMC method has been widely used to study the 2D attractive Hubbard Hamiltonian, mainly because it was able to give reliable results for the intermediate coupling regime, which may be relevant in understanding the pseudogap phase observed in underdoped high-temperature superconductors. This chapter is concerned with a study of its three-dimensional counterpart and thus provides additional elements for the analysis of precursor phenomena by considering specifically dimensionality effects.

In Section 1.3 it was stated that a pseudogap of superconducting origin was the consequence of an electronic pairing marked by a short coherence length and of the (quasi) two-dimensionality that characterize the underdoped high-temperature superconductors. This has lead to two a priori distinct interpretations in the literature, each of them privileging a different aspect.[1] The "strong coupling" version assumes that the coherence length is sufficiently small so that the Cooper pairs are still present above

[1] It is quite likely that both point of views coincide with another in the intermediate coupling regime, as illustrated in the previous chapter.

T_c but move around incoherently. The second interpretation insists on the role of the (quasi) two-dimensionality which enhances strongly the thermal fluctuations of the phase of the order parameter. The latter renormalizes the mean-field transition temperature $\sim T^*$ to a lower value T_c. However the second scenario does not apply for a 3D isotropic system [98]. Consequently the precursor effects which will be considered in connection with the 3D attractive Hubbard model in this chapter are due exclusively to a pairing characterized by a reduced coherence length. Thus the comparison between 2D and 3D allows to visualize the relative importance of the two effects in favoring the precursor manifestations of superconductivity.

It is important to stress that the study of the 3D attractive Hubbard model is already instructive by itself, since it is the first time that the latter is treated by DQMC for reasonable system sizes in 3D ($N = 6^3$, 8^3 and 10^3). One advantage of this method is the fact that it provides "exact" results, i.e. results without systematic errors coming from approximations in the calculation, except for the discretization of the imaginary time which however does not play an important role for the static properties considered in this chapter. The drawback is the finite size which introduces undesirable features into the results, both at low temperatures and around the phase transitions. But the fact that several sizes N are considered allows to identify these effects and eventually to suppress them by extrapolating to the thermodynamic limit $N \to \infty$. Another important feature of the 3D problem is the fact that superconductivity can be studied by considering a pair-pair correlation function since, in this case, it is associated with the breaking of the gauge symmetry U(1). Thus the exact critical temperature of the model can be deduced, an information which is still missing in the literature. Finally it is useful to recall that the application of the DQMC technique to the attractive Hubbard Hamiltonian does not generate the fermionic "minus-sign" problem and thus allows in principle to run simulations for any possible values of U and n.

Practically the Monte Carlo algorithm becomes inefficient as soon as one term of $\mathcal{H}$ (the kinetic or the interaction energy) dominates clearly the other one. In these cases, asymptotic analytical treatments for BCS and BEC regimes are available and a DQMC calculation makes no sense. Thus the parameter range in which the DQMC method works the best corresponds to the intermediate coupling regime where the kinetic and the potential energies have a similar magnitude. Concretely the DQMC study of the 3D attractive Hubbard model presented in this chapter consists in calculating two types of quantities: thermodynamic variables and two-point equal-time correlation functions. For a given interaction strength U and density n, they allow to determine the superconducting critical temperature T_c as well as the eventually different pair formation temperature scale T^* associated with the presence of precursor effects above T_c. At half-filling the critical temperature T_c^{CDW} for the onset of CDW ordering can be found as well.

Earlier works on DQMC studies of the attractive Hubbard model are almost all concerned with the 2D geometry. This is mainly due to the fact that this case may be relevant for the strongly anisotropic 3D high-temperature superconductors and, certainly, to the limitations in computational performances, which restrained the considered system sizes to a few hundred of lattice sites N. It is important to stress that the method used here to study superconductivity does not work in 2D. Indeed there is no breaking of the U(1) gauge symmetry at finite temperature in this case and the critical temperature suggested by the pair-pair correlation function is a finite-size effect and has to vanish in the thermodynamic limit, as required by the Mermin-Wagner theorem. It is however possible to access to the physics associated with the Berezinski-Kosterlitz-Thouless topological order, but more delicate phase-sensitive quantities have to be considered [103]. An earlier DQMC work on the 3D attractive Hubbard model exists nevertheless [104]. Unfortunately it is rather limited by the sizes ($N = 4^3$ mostly) and its conclusions represent only a tentative study of the present problem. More recently, a complete study of the 3D repulsive Hamiltonian at half-filling was performed in the same spirit as the present one, with a careful finite-size analysis and a quantitative determination of the (Néel) critical temperature [105]. As explained in Section 2.2, the repulsive and attractive version of the Hubbard model are equivalent for $n = 1$ so that this study also applies to the present problem and provides thus a useful reference point for the numerical calculations. Other methods like T-matrix [106] or DMFT [53] were also used recently to study the 3D attractive Hubbard Hamiltonian and their results will be compared to ones obtained by DQMC.

The remaining of this chapter is organized as follows. The DQMC method applied to the attractive Hubbard model is presented in Section 5.2. The results of the numerical calculations are given in Section 5.3. After some comments about technical aspects, the method for inverting the number equation (2.6) allowing to work at constant density n is first introduced, then the phase diagram $U-n-T$ of the Hamiltonian (2.1) is discussed, in particular regarding the BCS-BEC crossover when U is varied. The comparison of the temperature dependences of the spin susceptibility provides the necessary information to compare the precursor effects between 2D and 3D. This chapter ends with a conclusion where the perspectives opened by this work are also evoked.

5.2 Method: Determinant Quantum Monte Carlo

This section is devoted to the presentation of the Determinant Quantum Monte Carlo method. After having shown that the quantum problem in dimension D can be mapped into a classical one in dimension $D + 1$, the numerical method allowing to study the latter based on the Monte Carlo algorithm for the evaluation of configuration sums is introduced. The physical quantities that can be calculated using the DQMC scheme as

well as the information they provide about the interacting electronic system are also discussed.

5.2.1 Mapping of the quantum problem into a classical problem

In quantum statistical mechanics the expectation value of a time-independent operator $\mathcal{A}$ at a finite temperature $T = \beta^{-1}$ is given by the expression

$$\langle \mathcal{A} \rangle = Z^{-1} \, \mathrm{Tr} \exp(-\beta \mathcal{H}) \, \mathcal{A} \tag{5.1}$$

where $Z = \mathrm{Tr} \exp(-\beta \mathcal{H})$ is the partition function for the Hamiltonian $\mathcal{H}$ describing the electrons, in the present case given by Eq.(2.1). The fermionic trace Tr in expression (5.1) means that a basis of the many-particle Fock space diagonalizing $\mathcal{H}$ has to be found and then the expectation values of $\mathcal{A}$ for the elements of this basis calculated. For an interacting Hamiltonian this task is extremely difficult and the DQMC method offers an elegant way to circumvent this problem.
It requires first a recall from the path-integral formulation of quantum statistical mechanics where the finite temperature T is associated to an additional (imaginary) time variable $\tau \in [0, \beta]$. In the perspective of the numerical treatment, the latter interval is discretized in L equal segments $0 < \Delta\tau < 2\Delta\tau < ... < L\Delta\tau = \beta$. The exponential of $\mathcal{H}$ satisfies thus the identity

$$\exp(-\beta \mathcal{H}) = \exp(-\sum_{\ell=1}^{L} \Delta\tau \, \mathcal{H}) = \prod_{\ell=1}^{L} \exp(-\Delta\tau \, \mathcal{H}). \tag{5.2}$$

Recalling that $\mathcal{H}$ can be split into a one-body term $\mathcal{H}_0$ and an interaction term $\mathcal{H}_I$, each of the factor of Eq.(5.2) can be applied to the Trotter-Suzuki break up:

$$\exp(-\Delta\tau \, \mathcal{H}) = \exp\big(-\Delta\tau(\mathcal{H}_0 + \mathcal{H}_I)\big) = \exp(-\Delta\tau \, \mathcal{H}_0) \, \exp(-\Delta\tau \, \mathcal{H}_I) + \mathrm{O}(\Delta\tau^2) \tag{5.3}$$

where the proportionality coefficient of the error is essentially given by the commutator $[\mathcal{H}_0, \mathcal{H}_I]$. This step constitutes the only source of *systematic* error in the DQMC method but the latter can be minimized by choosing $\Delta\tau$ small enough, typically $\Delta\tau = 0.125 t^{-1}$. It also shows that this method is not well suited for very low temperatures because L becomes arbitrarily large in this case.[2] In Eq.(5.3) the first exponential factor can be easily diagonalized in reciprocal space (see Section 2.1) whereas the second one is still embarrassing. For the particular case of the Hubbard nonretarded local attraction, it can be further transformed using Hirsch's identity, a discrete version of the Hubbard-Stratonovich transformation based on the fact that on-site fermionic operator have a finite spectrum [107]. For site i in time-slice ℓ, it reads

$$\exp\left(\Delta\tau \, U \, (n_{i\uparrow} - \frac{1}{2})(n_{i\downarrow} - \frac{1}{2})\right) = c \sum_{x(i,\ell)=\pm 1} \exp\left(\alpha \, x(i,\ell) \, (n_{i\uparrow} + n_{i\downarrow} - 1)\right) \tag{5.4}$$

[2] In fact there exists QMC algorithms that allow to study specifically the case $T = 0$ [56, 55].

where

$$c = \frac{1}{2}\,\exp\big(\frac{\Delta\tau\,U}{4}\big) \tag{5.5a}$$

$$\alpha = \text{argtanh}\big(\sqrt{\tanh(\frac{\Delta\tau\,U}{4})}\big) \approx \frac{\sqrt{\Delta\tau\,U}}{4} \tag{5.5b}$$

In this way the quantum problem becomes trivial because only one-body operators are left in the exponential, but there is now a new space-time dependent (classical) variable $x(i,\ell)$ which couples to the electronic degrees of freedom. As a consequence of Eqs.(5.2-5.4), the partition function Z can be re-written as

$$Z = c^{LN} \sum_{\{x\}} \exp\big(-\alpha\,S[x]\big)\,\text{Tr}\prod_{\ell=1}^{L}\exp\big(-\Delta\tau\,\tilde{\mathcal{H}}^{\ell}[x]\big) \tag{5.6}$$

where

$$\sum_{\{x\}} = \sum_{\substack{x(i,\ell)=\pm 1\\ i=1,\ldots,N\\ \ell=1,\ldots,L}} \tag{5.7a}$$

$$S[x] = \sum_{\substack{i=1,\ldots,N\\ \ell=1,\ldots,L}} x(i,\ell) \tag{5.7b}$$

$$\tilde{\mathcal{H}}^{\ell}[x] = \sum_{\substack{i,j=1,\ldots,N\\ \sigma=\uparrow,\downarrow}} c^{\dagger}_{i\sigma}\tilde{H}^{\ell}_{ij}[x]c_{j\sigma} \tag{5.7c}$$

and the $N\times N$ matrix $\tilde{H}^{\ell}_{ij}[x]$ is given by

$$\tilde{H}^{\ell}_{ij}[x] = -t\,\delta_{\langle i,j\rangle} - \big(\mu - \frac{U}{2} + \frac{\alpha}{\Delta\tau}\,x(i,\ell)\big)\,\delta_{ij} \tag{5.8}$$

The fermionic degrees of freedom can be integrated out by performing the trace Tr in the grand canonical ensemble, leaving a classical partition function for an Ising-like spin field $x(i,\ell)$ in dimension $D+1$. Z can be thus written as

$$Z = \sum_{\{x\}} w[x] \tag{5.9}$$

where the weight of a configuration x is given by

$$w[x] = c^{LN}\,\exp\big(-\alpha\,S[x]\big)\,\det\big(\mathbb{I}_{N\times N} + \prod_{\ell=1}^{L} B^{\ell}[x]\big)^2 \tag{5.10a}$$

$$\big(B^{\ell}[x]\big)_{ij} = \exp\big(-\Delta\tau\,\tilde{H}^{\ell}_{ij}[x]\big) \tag{5.10b}$$

This final expression with the matrix determinant in Eq.(5.10a) gave the name to this method. The presence of the unity matrix $\mathbb{I}_{N\times N}$ is typical for the grand canonical

average since it generates all the occupations between 0 and N of the lattice sites. Moreover the square in Eq.(5.10a) is of fundamental importance since it makes $w[x]$ positive definite, avoiding thereby the well-known minus-sign problem appearing often in simulations of fermionic systems. This property is due to the fact that the auxiliary field x couples to both spin-up and spin-down electrons in the same way, as seen in Eq.(5.4).
Turning back to the expectation value of the operator $\mathcal{A}$, Eq.(5.1) becomes

$$\langle \mathcal{A} \rangle = Z^{-1} \sum_{x} w[x] A[x] \tag{5.11}$$

where $A[x]$ is given by exactly the same expression as Eq.(5.1) but with the substitution

$$\mathcal{H} \longrightarrow \tilde{\mathcal{H}}[x] = \sum_{\ell=1}^{N} \tilde{\mathcal{H}}^{\ell}[x], \tag{5.12}$$

the latter quantity $\tilde{\mathcal{H}}^{\ell}[x]$ being defined in Eq.(5.7c). In Section 5.2.3 the method for evaluating $A[x]$ is explained, based on Wick's theorem and on the equal-time Green's functions.

5.2.2 Monte Carlo algorithm to evaluate classical expectation values

As a consequence of the procedure of the previous section, the difficulty consists now no more in diagonalizing an operator but in evaluating huge sums running over the 2^{LN} configurations of the Ising-like spins $x(i,\ell) = \pm 1$ for $i = 1, ..., N$ and $\ell = 1, ..., L$, like in Eq.(5.11). The idea of *importance sampling* has been developed to deal with such cases. Since the distribution $w[x]$ is essentially a thermal average, only configurations lying in an appropriate narrow energy interval will contribute significantly to the sum at a given temperature T, like in a microcanonical approach. It is therefore of great interest to find a way to obtain satisfactory results by restricting the summation to a limited number of well-chosen configurations only.
The method used in DQMC to realize this idea is called "Metropolis Monte Carlo importance sampling" and is presented in the following. The set of configurations $\mathbb{X} = \{x_i, ..., x_M\}$ taken into account for the evaluation of $\langle \mathcal{A} \rangle$ and called the *sample* is viewed as a Markov chain, i.e. as a series in which each element x_k is generated from the previous one x_{k-1} only, the first one being chosen arbitrarily. The final goal is that, for M large enough, the elements of $\mathbb{X}$ are distributed according to the probability law

$$P[x] = \frac{w[x]}{Z}. \tag{5.13}$$

Then an evident estimator for the desired quantity $\langle \mathcal{A} \rangle$ is given by the sample average

$$\langle \mathcal{A} \rangle_{\mathbb{X}} = \frac{1}{M} \sum_{k=1}^{M} A[x_k]. \tag{5.14}$$

The above requirement is fulfilled by the following procedure called "Metropolis algorithm" which indicates how to generate the element x_{k+1} of the Markov chain using a stochastic process. It consists of four steps, starting with the configuration $x = x_k$. For each Ising-like spin $x(i,\ell)$, $1 \leq i \leq N$ and $1 \leq \ell \leq L$, an "update" is attempted:

1. define $x_{\text{trial}} = x$ except for $x_{\text{trial}}(i,\ell) = -x(i,\ell)$
2. calculate the ratio $R = \dfrac{w[x]}{w[x_{\text{trial}}]}$
3. pick up a random number $\rho \in [0,1]$
4. if $\begin{cases} \rho \geq R & : \text{accept the change } x = x_{\text{trial}} \\ \rho < R & : \text{keep } x \text{ unchanged} \end{cases}$

After this space-time "sweep" of LN attempts, x contains all the modified spins with respect to x_k and is simply taken as x_{k+1}. This procedure defines what is called "one Monte Carlo step". The proof that it indeed generates a sample $\{x_i, ..., x_M\}$ whose elements are distributed according to the law (5.13) can be found in Ref.[108]. A remarkable feature of the Metropolis algorithm is the fact that it works although Z is not directly available by considering relative probabilities only.
A crucial aspect of any MC scheme is the determination of the accuracy of the estimate (5.14) to $\langle \mathcal{A} \rangle$. In this context there exists a rigorous result analogous to the central limit theorem of statistics [109] which, when applied to the particular case of Markov chain sample, allows to write

$$|\langle \mathcal{A} \rangle - \langle \mathcal{A} \rangle_{\mathbb{X}}| \leq \epsilon_{\mathcal{A}}. \tag{5.15}$$

The error $\epsilon_{\mathcal{A}}$ satisfies [110]

$$\epsilon^2_{\mathcal{A}} = \frac{1}{M} \langle \Delta \mathcal{A}^2 \rangle \, (1 + 2\tau_{\mathcal{A}}) \tag{5.16}$$

where

$$\langle \Delta \mathcal{A}^2 \rangle = \langle \mathcal{A} \rangle^2 - \langle \mathcal{A}^2 \rangle \tag{5.17a}$$

$$\tau_{\mathcal{A}} = \sum_{k=1}^{M} \Phi_{\mathcal{A}}(k) \tag{5.17b}$$

$$\Phi_{\mathcal{A}}(k) = \frac{\dfrac{1}{M-k} \displaystyle\sum_{m=1}^{M-k} A[x_m] A[x_{m+k}] - \langle \mathcal{A}^2 \rangle}{\langle \Delta \mathcal{A}^2 \rangle} \tag{5.17c}$$

The quantity $\langle \Delta \mathcal{A}^2 \rangle$ is the variance of the operator $\mathcal{A}$ and can be estimated by

$$\langle \Delta \mathcal{A}^2 \rangle_{\mathbb{X}} = \frac{M}{M-1} \big(\langle \mathcal{A} \rangle^2_{\mathbb{X}} - \langle \mathcal{A}^2 \rangle_{\mathbb{X}} \big). \tag{5.18}$$

The quantity $\Phi_{\mathcal{A}}(k)$ is the autocorrelation function for the "measurements" of the operator $\mathcal{A}$ from which the autocorrelation time $\tau_{\mathcal{A}}$ can be extracted according to Eq.(5.17b). It takes into account the fact that successive measurements $A[x_k]$, $A[x_{x+1}]$, ..., $A[x_{k+\tau_{\mathcal{A}}}]$ generated by the Metropolis algorithm are correlated. If the $\{A[x_1], ..., A[x_M]\}$ were all independent, then $\tau_{\mathcal{A}} = 0$ and one retrieves the original statement of the central limit theorem [109].The error in the estimate $\langle\mathcal{A}\rangle_{\mathbb{X}}$ to $\langle\mathcal{A}\rangle$ is thus found to depend on the inverse square root of the total number of sweeps M. For $\tau_{\mathcal{A}} > 0$, the factor $1 + 2\tau_{\mathcal{A}}$ called *statistical inefficiency* increases $\epsilon_{\mathcal{A}}$ and is of crucial importance in determining when a MC calculation is imaginable or not. Two of its well-known manifestations are the "critical slowing-down" near a phase transition and the "stacking problem" when the energy barriers in the phase space become too high, in both cases $\tau_{\mathcal{A}}$ diverges and other methods have to be used.
Another problem raised by the autocorrelations is the fact that there exists no stable estimator for the quantity $\Phi_{\mathcal{A}}$ and thus for $\tau_{\mathcal{A}}$ [111]. In this work, it is overcome by using an approximate fitting procedure which is sufficient regarding the limited accuracy reachable with the DQMC method (see Section 5.3.1). For small k (i.e. $k \lesssim 4$), $\tau_{\mathcal{A}}$ should satisfy

$$\Phi_{\mathcal{A},\mathbb{X}}(k) = \frac{\dfrac{1}{M-k}\displaystyle\sum_{m=1}^{M-k} A[x_m]A[x_{m+k}] - \langle\mathcal{A}^2\rangle_{\mathbb{X}}}{\langle\Delta\mathcal{A}^2\rangle_{\mathbb{X}}} \approx \exp(-\frac{k}{\tau_{\mathcal{A}}}). \tag{5.19}$$

For larger k, $\Phi_{\mathcal{A},\mathbb{X}}$ becomes instable due to the noise. Another possibility would consist in "binning" a given number ($\sim \tau_{\mathcal{A}}$!) of successive measurements and considering their average as independent quantities [56]. However this method becomes inconvenient when more than one operator $\mathcal{A}$ is considered, since the autocorrelation time depends also strongly upon the latter.

5.2.3 Implementation of the Monte Carlo algorithm

The execution of a Monte Carlo simulation based on the scheme presented in the previous section requires essentially two types of calculations: the evaluation of the Metropolis ratio R and the "measurement" $A[x]$ of the operator $\mathcal{A}$ for a given configuration x of the LN Ising-like spins $x(i,\ell)$. For the case of the DQMC method, it turns out that both operations can be easily performed using one unique fundamental quantity: the (equal-time) Green's function. For both spins $\sigma =\uparrow, \downarrow$, it is defined as (compare with Eq.(2.13))

$$G_{ij}^{\ell}[x] = \langle c_{i\sigma}^{\ell}\, c_{j\sigma}^{\ell\,\dagger}\rangle_x. \tag{5.20}$$

In Eq.(5.20) the thermal average $\langle ...\rangle_x$ is defined analogously to Eq.(5.1) but with respect to the Hamiltonian $\tilde{\mathcal{H}}[x]$ from Eq.(5.12). Moreover the evolution in imaginary time $\tau = \ell\,\Delta\tau$ of the operators $c_{i,\sigma}^{\ell\,\dagger}$ and $c_{j,\sigma}^{\ell}$ is also given by a Heisenberg equation

with the Hamiltonian $\tilde{\mathcal{H}}[x]$, so that the latter are related in the following way to their time-independent counterparts appearing in the original Hubbard Hamiltonian [94]:

$$c^{\ell}_{i\sigma} = \exp(-\ell\,\Delta\tau\,\tilde{\mathcal{H}}[x])\,c_{i\sigma}\,\exp(\ell\,\Delta\tau\,\tilde{\mathcal{H}}[x]) \quad (5.21a)$$
$$c^{\ell\,\dagger}_{j\sigma} = \exp(\ell\,\Delta\tau\,\tilde{\mathcal{H}}[x])\,c^{\dagger}_{j\sigma}\,\exp(-\ell\,\Delta\tau\,\tilde{\mathcal{H}}[x]). \quad (5.21b)$$

In Ref.[56] it is shown that the $N \times N$ Green's function matrix at time $0 \leq \tau = \ell\,\Delta\tau \leq \beta$ is given by the expression

$$G^{\ell}[x] = \left(\mathbb{I}_{N\times N} + B^{\ell-1}[x]...B^{0}[x]\,B^{L}[x]...B^{\ell}[x]\right)^{-1} \quad (5.22)$$

where the matrices $B_{\ell}[x]$ are defined in Eq.(5.10b). Because of the terms proportional to $x(i,\ell) \neq 0$ in $\tilde{\mathcal{H}}^{\ell}[x]$, the matrices $B^{\ell}[x]$ do not commute with each other, so that the order in Eq.(5.22) is relevant. For the same reason, they are not invariant under the (space) lattice translations neither, which implies that they cannot be diagonalized in the usual reciprocal space basis as it is done for the noninteracting case in Eqs.(2.3-2.4). Therefore $G^{\ell}[x]$ has to be calculated as indicated in Eq.(5.22). Since its eigenvalues are expected to extend at least over the interval $[\exp(-\beta W/2), \exp(\beta W/2)]$, it turns out that the inversion in Eq.(5.22) becomes numerically unstable at low temperatures (large β). The reason is that, due to the limited precision of any computer, only the largest energy scales of $G^{\ell}[x]$ can be conserved with a finite number of digits. It is in fact very important to control all the energy scales present in $G^{\ell}[x]$ since the relevant physics in a fermionic system will always be situated around an intermediate "Fermi energy" ϵ_F, so that $\exp(-\beta\epsilon_F)$ must be correctly resolved by the numerics. An elegant solution to this problem has been developed by Loh and Gubernatis [56], consisting in a decomposition of the matrix products in Eq.(5.22) as

$$B^{\ell}[x]...B^{\ell+L_S}[x] = Q\,D\,R \quad (5.23)$$

where Q and R are unitary matrices (with eigenvalues in the interval $[-1,1]$) and D is diagonal and contains explicitly all the energies present in the problem. Using Eq.(5.23), the Green's function matrix $G^{\ell}[x]$ can be calculated reliably, preserving all the energy scales of the original Hamiltonian (2.1). The experience has shown that a singular value decomposition (SVD) is a good choice for Eq.(5.23)[59]. The parameter L_S will be determined later.
Once it is available, the Green's function $G^{\ell}_{ij}[x]$ can be used to execute the two tasks mentioned above.

1. Introduced in the previous section, the Metropolis ratio is defined as $R = w[x]/w[x_{\text{trial}}]$ where x and x_{trial} differ by one only spin at site (i,ℓ) which is flipped (i.e $x(i,\ell) = -x_{\text{trial}}(i,\ell)$). Instead of calculating the determinants appearing in the definition of w in Eq.(5.10a), is suffices to evaluate the quantity

$$R = \exp\big(-2\alpha\,x(i,\ell)\big)\,(1+\Delta^{\ell}_{ii}[x])^2\,(1-G^{\ell}_{ii}[x])^2 \quad (5.24)$$

where

$$\Delta^{\ell}_{ii}[x] = \exp\big(-2\alpha\, x(i,\ell)\big) - 1 \tag{5.25}$$

If the update is accepted, then $x(i,\ell) \to -x(i,\ell)$ and $G^{\ell}[x]$ has to be updated as well. This is done very easily according to

$$G^{\ell}[x] \to G^{\ell}[x] - \frac{1}{\sqrt{R}}\, G^{\ell}[x]\, \Delta^{\ell}[x]\, (\mathbb{I}_{N\times N} - G^{\ell}[x]) \tag{5.26}$$

where the $N \times N$ matrix $\Delta^{\ell}[x]$ contains only one nonzero element in position (i,i) and given by Eq.(5.25).

2. The second application of the Green's function is the calculation of the expectation value $A[x]$ of an operator $\mathcal{A}$ for the Hamiltonian $\tilde{\mathcal{H}}[x]$. In the second quantization formalism $\mathcal{A}$ can always be written in terms of products of creation and annihilation operators $c^{\dagger}_{i,\sigma}$ and $c_{i,\sigma}$. Since $\tilde{\mathcal{H}}[x]$ is a one-body operator (i.e. quadratic in the c's), Wick's theorem can be used to evaluate $A[x]$. For instance the potential energy (2.2b) at site i is given by

$$H_{I,i}[x] = \langle -U n_{i\uparrow} n_{i\downarrow}\rangle_x = -U\langle \overbrace{c^{\dagger}_{i\uparrow}}\, c_{i\uparrow}\, \overbrace{c^{\dagger}_{i\downarrow}}\, c_{i\downarrow}\rangle_x = -U(1 - G^{0}_{ii}[x])^2 \tag{5.27}$$

since $G^{\ell}_{ii}[x]$ does not depend upon the spin σ. More complicated expressions are calculated similarly (see next section).

Since the Green's function (5.22) has to be calculated for each imaginary time slice ℓ (because of the Metropolis updating procedure), it can also be used to provide further measurements of equal-time quantities, using the translational invariance in imaginary time of the original Hamiltonian. For instance the density can be calculated as

$$n = \frac{\langle \mathcal{N}\rangle_x}{N} = \frac{2}{LN} \sum_{\substack{i=1,\ldots,N \\ \ell=1,\ldots,L}} (1 - G^{\ell}_{ii}[x]). \tag{5.28}$$

Although the translational invariance in time is broken by the Ising-like spins $x(i,\ell) \neq 0$ (similarly to the translational invariance in space), the averaging over the whole space-time in Eq.(5.28) allows nevertheless to obtain a reliable result for n. This property is called *self-averaging* [110] and improves the quality of a measurement of an operator $\mathcal{A}$ by reducing the fluctuations (or the variance) and thereby the error (see Eq.(5.16)).
Since a calculation "from scratch" of the Green's function as given by Eq.(5.22) and including the stabilization from Eq.(5.23) is extremely CPU-time consuming, it is useful to use the "wrapping" relation

$$G^{\ell+1}[x] = B^{\ell+1}[x]\, G^{\ell}[x]\, B^{\ell+1}[x]^{-1} \tag{5.29}$$

when moving from one imaginary time slice ℓ to slice $\ell + 1$. However the use of Eq.(5.29) has to be restricted to a finite number L_W of time slices, since it contains no stabilization and will loose important physical information. In order to reduce the calculation time as well, the multiplications by the matrices $B^{\ell}[x]$ and their inverse appearing in Eqs. (5.22,5.29) can be lowered to order 2 operations (instead of 3) [3] by using the "checkerboard breakup". It consists in splitting the exponential of the nondiagonal kinetic energy term in Eq.(5.8) in separated contributions for each bond $\langle i, j\rangle$, the exponential of one bond matrix being extremely sparse (see Ref.[56]). This procedure is consistent with the error of order $\Delta\tau^2$ due to the Trotter-Suzuki breakup used in Eq.(5.3).

5.2.4 Principles and calculation of physical quantities

The DQMC method allows to calculate *directly* two types of physical quantities. The first ones are expectation values of bulk thermodynamic variables like the internal energy $\langle\mathcal{H}\rangle$ or the electron number $\langle\mathcal{N}\rangle$. The latter is particularly important in solving the number equation (2.6) in order to deduce the temperature dependence of the chemical potential $\mu = \mu(T, U, n)$ guaranteeing a constant density n (see Section 5.3.2). The second type of quantities are equal-time correlations of various types (spin, charge or pair) which correspond to the response of the electronic system to some external perturbation. They constitute the most convenient way to characterize theoretically a quantum many-body system and allow to make the connection with experimental studies [112]. If the external perturbation is sufficiently weak, the reaction of the electrons can be studied in the framework of the linear response theory, which allows to characterize the perturbed system in terms of its equilibrium properties only. The equal-time correlation functions considered below give in particular the necessary information to determine whether long-range order (LRO) of a given type is present in the system. More precisely they indicate when the corresponding correlation length ξ becomes larger than the linear size of the system $\sqrt[3]{N}$. To draw reliable conclusions about a possible LRO, several different values of the lattice size N have to be considered so that the behavior in an infinite system can be extrapolated.

[3] A matrix operation of order n means that it requires N^n single steps to be executed. For instance an ordinary matrix product is of order 3.

The equal-time correlation functions considered in this chapter are the following:

$$S_P(r) = \frac{1}{LN_r} \sum_{\substack{i,j=1,\dots,N \\ \ell=1,\dots,L}} \langle \Delta_i^\ell \Delta_j^{\ell\,\dagger} + \Delta_i^{\ell\,\dagger} \Delta_j^\ell \rangle \, \delta_{r,|\mathbf{r}_i - \mathbf{r}_j|} \tag{5.30a}$$

$$S_S(r) = \frac{1}{LN_r} \sum_{\substack{i,j=1,\dots,N \\ \ell=1,\dots,L}} \langle \mathbf{S}_i^\ell \cdot \mathbf{S}_j^\ell \rangle \, \delta_{r,|\mathbf{r}_i - \mathbf{r}_j|} \tag{5.30b}$$

$$S_C(r) = \frac{1}{LN_r} \sum_{\substack{i,j=1,\dots,N \\ \ell=1,\dots,L}} \langle n_i^\ell \, n_j^\ell \rangle \, \delta_{r,|\mathbf{r}_i - \mathbf{r}_j|} \tag{5.30c}$$

where $N_r = \sum_{i,j=1}^{N} \delta_{r,|\mathbf{r}_i - \mathbf{r}_j|}$ and the periodic boundary conditions (PBC) allow to average over the whole lattice. The relative distance r is restricted to discrete values 0, 1, $\sqrt{2}$, $\sqrt{3}$,..., $\sqrt{3}\sqrt[3]{N}/2 = r_{\max}$ and the quantities in the average brackets are the pair, spin and charge operators, respectively:

$$\Delta_i^\ell = c_{i\uparrow}^\ell c_{i\downarrow}^\ell \tag{5.31a}$$

$$\mathbf{S}_i^\ell = (c_{i\uparrow}^{\ell\,\dagger} \quad c_{i\downarrow}^{\ell\,\dagger}) \, \boldsymbol{\sigma} \begin{pmatrix} c_{i\uparrow}^\ell \\ c_{i\downarrow}^\ell \end{pmatrix} \tag{5.31b}$$

$$n_i^\ell = c_{i\uparrow}^{\ell\,\dagger} c_{i\uparrow}^\ell + c_{i\downarrow}^{\ell\,\dagger} c_{i\downarrow}^\ell \tag{5.31c}$$

where $\boldsymbol{\sigma}$ is the vector of Pauli matrices and the time dependence of the creation and annihilation operators is defined in Eq.(5.21). The expressions (5.30) can be calculated for the Hamiltonian $\tilde{\mathcal{H}}[x]$ from Eq.(5.7c) by applying the method of the previous section and using the definitions (5.31). In terms of the Green's function $G_{ij}^\ell[x]$, the average brackets read

$$\langle \Delta_i^\ell \Delta_j^{\ell\,\dagger} + \Delta_i^{\ell\,\dagger} \Delta_j^\ell \rangle_x = G_{ij}^\ell[x]^2 + (\delta_{ij} - G_{ji}^\ell[x])^2 \tag{5.32a}$$

$$\langle \mathbf{S}_i^\ell \cdot \mathbf{S}_j^\ell \rangle_x = 2\, G_{ij}^\ell[x] \big(\delta_{ij} - G_{ji}^\ell[x]\big) \tag{5.32b}$$

$$\langle n_i^\ell \, n_j^\ell \rangle_x = 4\big(1 - G_{ii}^\ell[x]\big)\big(1 - G_{jj}^\ell[x]\big) + \langle \mathbf{S}_i^\ell \cdot \mathbf{S}_j^\ell \rangle_x \tag{5.32c}$$

so that a measurement $S_{P,x}(r)$ of $S_P(r)$ is easily evaluated (for instance). It is also useful to define the corresponding Fourier transforms as

$$S_{P,x}(\mathbf{q}) = \frac{1}{LN} \sum_{\substack{i,j=1,\dots,N \\ \ell=1,\dots,L}} \exp\big(i\mathbf{q} \cdot (\mathbf{r}_i - \mathbf{r}_j)\big) \langle \Delta_i^\ell \Delta_j^{\ell\,\dagger} + \Delta_i^{\ell\,\dagger} \Delta_j^\ell \rangle_x. \tag{5.33}$$

In practice only the wave vectors $(0,0,0)$ and (π,π,π) will be used.
A few comment about these correlation functions are useful:

- In general a phase transition is studied by identifying an order parameter which becomes nonzero below the critical temperature. In the case of superconductivity

the latter is proportional to the anomalous Green's functions $\langle c_{i\uparrow}\, c_{i\downarrow}\rangle$ or $\langle c^{\dagger}_{i\uparrow}\, c^{\dagger}_{i\downarrow}\rangle$ [113]. Unfortunately the expectation values of these expressions are *always* zero for the two-body Hamiltonians $\tilde{\mathcal{H}}[x]$. Therefore the pair-pair correlation function $S_P(r)$ constitutes the simplest way to detect superconducting order.

- The presence of superconducting LRO can be established by evaluating $S_P(q = 0)$ from Eq.(5.33) and checking whether it is extensive quantity or not by using a finite-size analysis. In the thermodynamic limit $N \to \infty$ this property is equivalent to the fact that $S_P(r)$ tends to an nonzero value for large distances r, which is the main manifestation of an underlying LRO [114]. Then the "plateau" value of $S_P(r)$ can be used as a substitute for the (missing) order parameter [55].

- The correlation functions satisfy the identity

$$S_S(q = 0) = \beta\, \chi_P \tag{5.34}$$

  which gives thus access to the corresponding susceptibilities like the Pauli susceptibility χ_P in the case of spin-spin correlations.

- A "staggered" charge-charge correlation function $S^s_C(r)$ is defined by multiplying the density operators n^{ℓ}_k in Eq.(5.30c) by the factor $\exp(-i\mathbf{Q}\cdot\mathbf{r}_k)$ where $\mathbf{Q} = (\pi, \pi, \pi)$ and $k = i, j$. S^s_C is appropriate for the study of the charge-density wave order that appears for $n = 1$ (see Figure 2.2).

5.3 Results

5.3.1 Preliminary considerations

Before presenting the results of the study of the 3D attractive Hubbard model by the Determinant Quantum Monte Carlo technique exposed in the previous section, it is useful to mention several features associated with the concrete implementation of the latter method. One important aspect in this context is the numerical solution of the number equation (2.6) imposed by the grand canonical nature of the Hubbard Hamiltonian (2.1). This is discussed specifically in Section 5.3.2. The following is rather concerned with technical considerations which are relevant in determining the range of physical parameters $\{T, n, U, N\}$ which can be suitably treated by the DQMC scheme.

Tools

The algorithm of Section 5.2 has been transcribed into a Fortran 90 code, based on an original version written in Fortran 77 [115]. For standard operations like matrix

Table 5.1: Some technical data of the used computers.

Machine	Processor type	Frequency	Cache memory	RAM
PC	Athlon	700-1000 MHz	256-512 kB	256 MB
Eridan	MIPS R14000	500 MHz	8MB	500MB

multiplication or SVD decompositions, optimized subroutines from the BLAS and LAPACK libraries were used in order to reduce the calculation time. Parallel runs on multiprocessor servers required some basic commands from the MPI library.
The calculations were performed on essentially two types of computers. For "small" system sizes ($N = 4^3$ and $N = 6^3$) the PC's from the IRRMA cluster were sufficient whereas for "large" sizes ($N = 8^3$ and $N = 10^3$), the SGI Origin 3800 parallel server Eridan at EPFL was used. The technical data of these two types of machines are given in Table 5.1.

Limitations

In order to ensure a successful performance of the DQMC calculations, the choice of various physical parameters $\{T, n, U, N\}$ has to be subjected to several limitations. The most important ones are given in the following.

- The duration of the calculation has to be kept inside "reasonable"limits, taking into account on one side, the available CPU time and on the other side, the relevance of the results which may be obtained by the calculation. The structure of the DQMC algorithm exposed in Section 5.2 implies that the duration τ_s of a space-time lattice sweep satisfies

$$\tau_s \propto L^2\, N^3. \tag{5.35}$$

  As a consequence, only the sizes $N = 4^3$ and $N = 6^3$ were suitable for the PC's whereas the cases $N = 8^3$ and $N = 10^3$ required parallel runs on the Eridan server. Moreover exceeding the processor cache memory can slow down the calculation, as it has been observed on the PC's between $N = 6^3$ and $N = 8^3$ where τ_s increased by more than the expected factor of 13. This showed that the PC's are not suited for calculations with sizes of $N = 8^3$ and higher. Physically, the restriction to "small" systems generates various so-called "finite-size effects" which have to be suitably eliminated in order to get reliable informations about the thermodynamic limit $N \to \infty$. This is done by studying the size dependence of the observed properties and concrete examples are presented in Section 5.3.3.

- In principle the stabilization scheme for large L associated with Eq.(5.23) allows to consider arbitrarily small temperatures T. However, due to the finite size of

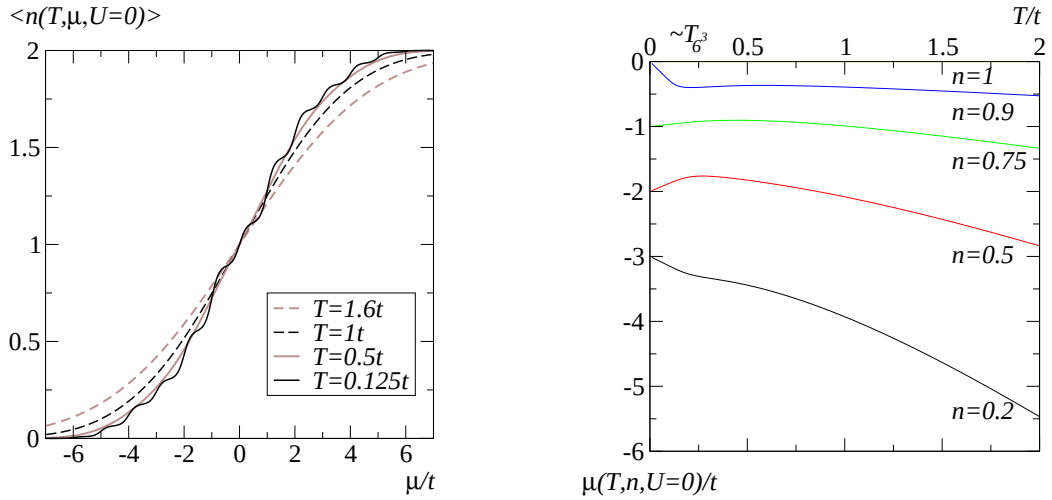

Figure 5.1: Effects of the discreteness of the energy levels due to a finite system size on the relations between n and μ for the noninteracting lattice electrons, $N = 6^3$.

the considered systems, a nonvanishing spacing $\Delta\epsilon_N$ appears between successive energy levels in the spectrum of the Hamiltonian (2.1). This affects particularly the low-temperature behavior of the chemical potential $\mu = \mu(T, n, U)$ and makes difficult to stabilize numerically the electronic density n, see Figure 5.1 for $U = 0$ and Section 5.3.2 for $U > 0$. The temperature below which these troubles appear can be estimated as

$$T_N \sim \Delta\epsilon_N \sim 3\,\frac{W}{N} \tag{5.36}$$

where $W = 12t$ is the 3D bandwith and the factor 3 takes into account (approximately) the degeneracies of the isotropic tight-binding Hamiltonian $\mathcal{H}_0$. For $N = 6^3$, T_N is of the order of $0.16t$ (see Figure 5.1). Preferably, T_N has therefore to be lower than the temperature scales of interest appearing in the problem. This is not satisfied for very low densities ($n \lesssim 0.1$) or weak coupling strengths ($U \lesssim 2t$). These effects become weaker when increasing U. Indeed the interaction smears the noninteracting degenerate levels and makes this problem less acute for $U \gtrsim 8t$.

- The accuracy of a Monte Carlo calculation is given by the statistical error introduced in Eq.(5.16). Situations have arisen where the autocorrelation time became very large. In such cases and for a finite number M of measurements, the *ergodicity* of the Monte Carlo sampling in phase space is no more guaranteed and the result can not be correct. This occurs for very low temperatures (typically $\beta > 15t^{-1}$) or strong couplings (typically $U > 12t$). Similarly to the simple case of the Ising model, this feature corresponds to the situation where the Markov chain is stuck around a given configuration in phase space, which is

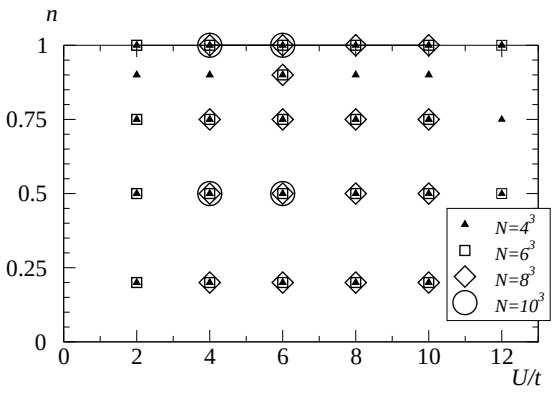

Figure 5.2: The parameters U and n used to "sweep" the phase diagram of the 3D attractive Hubbard model.

separated from other configurations of similar energies by barriers which are too high to be surmounted during the finite number M of sweeps of the simulation.

As a conclusion of the above, the choice of the parameters for the DQMC calculations is a heuristic procedure, balancing technical and physical constraints, in order extract the maximal information about the relevant properties of the attractive Hubbard model.

Choice of the parameters

An overview of the physical parameters used for a systematic study of the phase diagram $U - n$ of the 3D attractive Hubbard model is given on Figure 5.2. Following the discussion of the previous paragraph, the "large"-size calculations ($N = 8^3$ and $N = 10^3$), which require a considerable amount of CPU-time, are restricted to temperatures where the effects of a finite N are strongly enhanced. This corresponds to intervals containing the superconducting transition temperature T_c (see Section 5.3.3). The corresponding values of the chemical potential $\mu = \mu(T, n, U, N)$ guaranteeing a constant density n are discussed in Section 5.3.2.

Concerning the numerical parameters $\{\Delta\tau, M, L_S, L_W\}$, their choice is such that the statistical error (given by M and the physical quantities $\{T, n, U\}$), the systematic error (given by the imaginary time discretization $\Delta\tau$) and the numerical errors (given by L_S and L_W intervening during the calculation of the Green's function, see Eqs.(5.23) and (5.29)) have to be "consistent" with one another. This means that, having fixed $\Delta\tau = 0.125t^{-1}$ as is usual in the literature, an error is anyway present on the results and it makes no sense to try to reduce the statistical error to arbitrarily small values by overall increasing M. Thus typical values for M are 500-3000 sweeps, with 50-500 nonmeasured heating runs at the beginning to "equilibrate" the simulation. The above remark also applies when fixing the value of the parameters L_S and L_W which depend

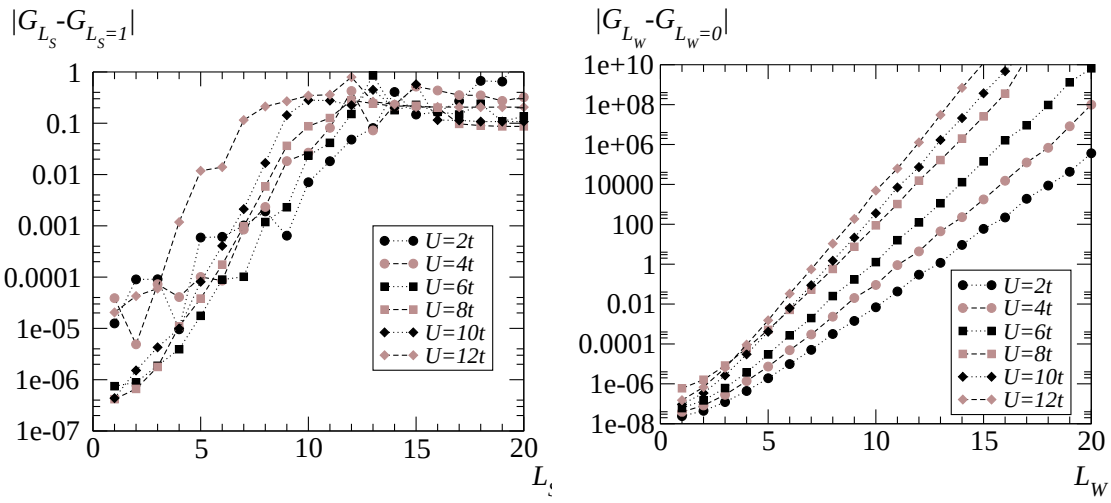

Figure 5.3: Determination of the numerical parameters L_S and L_W by comparing the "exact" Green's function $G_{L_S=1,\,L_W=0}$ to the results of a less precise but faster parameter choice: $G_{L_S>1,\,L_W=0}$ (left) and $G_{L_S=1,\,L_W>0}$ (right).

essentially upon U. As shown in Figure 5.3 where the error on the Green's function matrix $G_{L_S>1,\,L_W>0}$ with respect to the most accurate numerical result $G_{L_S=1,\,L_W=0}$ is shown, a reasonable accuracy of 1-2 decimals is reached by taking $L_S = L_W = 8$ for $U = 6t$, and eventually reducing these values for larger U. This choice is crucial in determining the duration of the simulation since the calculation of G "from scratch" using Eq.(5.22) takes more than 70 percents of the CPU-time of a DQMC sweep.

5.3.2 Grand canonical procedure

In order to study temperature dependent properties at constant electronic density n and coupling strength U, it is necessary to calculate the function $\mu = \mu(T, n, U)$ since a (grand canonical) DQMC simulation requires the physical parameters $\{T, \mu, U\}$ as input. As already mentioned in the previous section, this task may become quite delicate below the temperature T_N defined in Eq.(5.36) due the discreteness of the energy levels in a finite system.

Numerical solution of $n = \langle n(T, \mu, U)\rangle$

Because the DQMC calculations are long and of limited accuracy, standard numerical algorithms to solve equations like the bisection method are not suited here. However, taking advantage of the fact that the considered functions are relatively smooth (at least above T_N), polynomial interpolations between a finite number of DQMC points are expected to provide satisfactory results. The procedure which is used here to allow the study of temperature dependent quantities at constant n and U consists in two stages.

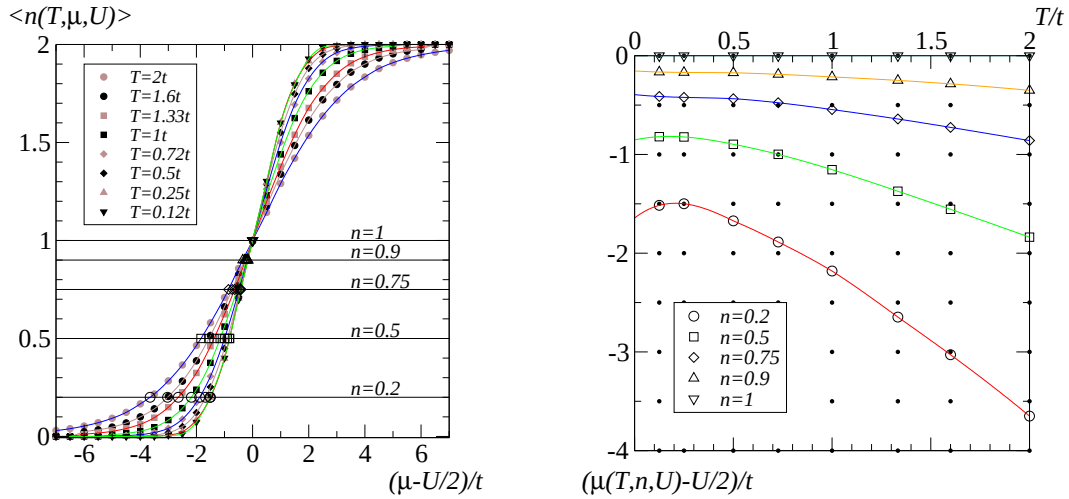

Figure 5.4: Inversion of the number equation $n = \langle n(T, \mu, U)\rangle$ as $\mu = \mu(T, n, U)$ for $U = 6t$, $N = 6^3$ and $\Delta\tau = 0.125t^{-1}$. The values (T_k, μ_l) for which the DQMC calculations of $\langle n_{kl}\rangle$ have been performed are indicated by the grid on the right-hand figure.

The first one provides an estimation of the function $\mu = \mu(T, n, U)$ based precisely on polynomial interpolation. It is illustrated on Figure 5.4 for the case $U = 6t$ and requires four steps:

1. the DQMC calculation of $\langle n_{kl}\rangle \equiv \langle n(T_k, \mu_l, U = 6t)\rangle$ for several T_k and μ_l (indicated by the grid in Figure 5.4);

2. the definition of the functions $n_k(\mu)$ interpolating between the points $\{(\mu_l, \langle n_{kl}\rangle)\}_l$ for each temperature T_k;

3. The numerical solution of $n_k(\mu) = n$ as $\mu = \mu_k(n)$ for $n \in [0, 1]$ for each temperature T_k;

4. The definition of the function $\mu = \mu(T, n, U = 6t)$ interpolating between the points $\{T_k, n_k(\mu)\}_k$.

Although a relatively large quantity of QMC runs is needed to calculate the density at each point $(T_k, \mu_l, U = 6t)$, the latter turn out to converge rapidly enough so that a few hundreds of sweeps only are necessary to get satisfactory results. The precise shape of $\mu = \mu(T, n, U = 6t)$ for $T < T_N$, which should display some similarities with the case $U = 0$ shown in Figure 5.1, is hard to reproduce, even by calculating additional points at low temperatures. The functions $\mu = \mu(T, n, U)$ obtained this way are nevertheless taken to generate the parameters $\{T_m, \mu(T_m, n, U), U\}$ used to run DQMC simulations with various temperature values T_m for fixed n and U. During the latter, $\langle n\big(T_m, \mu(T_m, n, U), U\big)\rangle$ is re-calculated in order to check whether the density is well stabilized. The corresponding results for $U = 6t$ are presented in Figure 5.5, showing

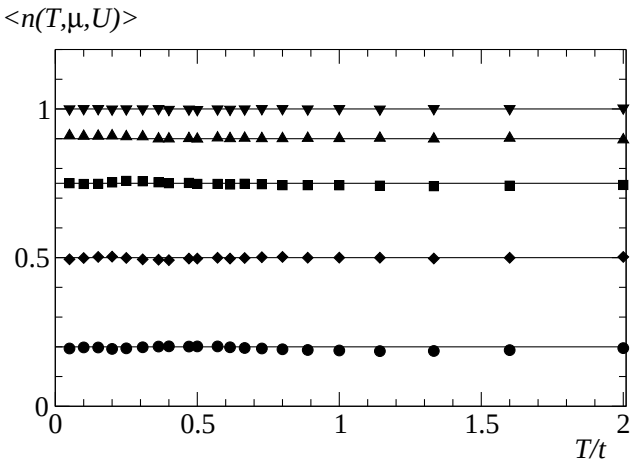

Figure 5.5: Results for $n = \langle n(T, \mu, U)\rangle$ for $U = 6t$, $N = 6^3$ and $\Delta\tau = 0.125t^{-1}$.

that some noise is always present in the expectation value of the density, even if μ is exact as it is the case at half-filling. These inaccuracies are due to the conjugation of both the statistical errors of the DQMC method and the approximative nature of the polynomial interpolations used to get the suitable chemical potential μ. Since important quantities like the internal energy $\langle\mathcal{H}\rangle$ are very sensitive to the value of the density $\langle n(T, \mu, U)\rangle$, an improvement of this procedure is necessary to stabilize n better.
The second step of the grand canonical procedure consists then simply in repeating the DQMC calculations with slightly different densities, i.e. with parameters $\{T_m, \mu(T_m, n + \Delta n, U), U\}$ where $\Delta n \simeq \pm 0.02$ typically. Then the value of any quantity A for the desired density n can be interpolated from the two (or eventually more) available values at $\mu_1 \equiv \mu(T_m, n - \Delta n, U)$ and $\mu_2 \equiv \mu(T_m, n + \Delta n, U)$ according to the formula:

$$A(n) = A(n_1) + \frac{A(n_2) - A(n_1)}{n_2 - n_1}\,(n - n_1) \tag{5.37}$$

where $n_1 \equiv \big\langle n\big(T_m, \mu_1, U\big)\big\rangle$ and $n_2 \equiv \big\langle n\big(T_m, \mu_2, U\big)\big\rangle$. Eq.(5.37) illustrates clearly the difficulties in stabilizing the density below $T = T_N$. In this case $n = \langle n(T, \mu, U)\rangle$ is almost a stair function and n_1 and n_2 become very close to another, which makes Eq.(5.37) numerically unstable because of the denominator $n_2 - n_1$.

Discussion

The results of the calculations of the relations $\mu = \mu(T, n, U)$ allow to make some important observations which are explained in the following.

- In order to preserve the particle-hole symmetry in the Hubbard Hamiltonian (2.1), one often uses the quantity $\mu - U/2$ as the chemical potential. This is

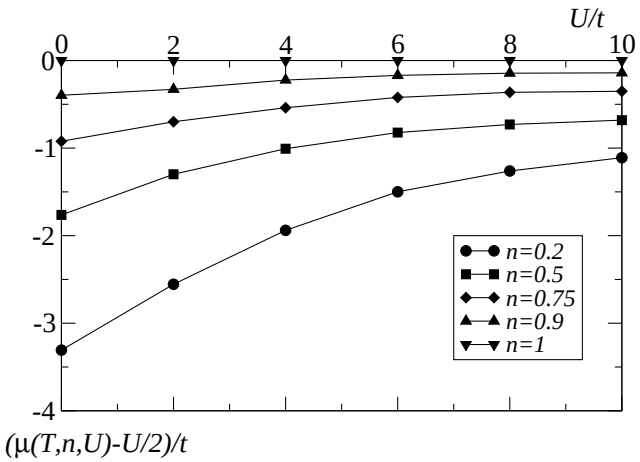

Figure 5.6: U dependence of the chemical potential $\mu = \mu(T, n, U)$ for $T = 0.25t$, $N = 6^3$ and $\Delta\tau = 0.125t^{-1}$.

also suggested by Hirsch's identity in Eqs.(5.4) and (5.8). Here the original definition of μ is conserved nevertheless, the shift $-U/2$ being mentioned explicitly when it is present.

- Comparison between Figures 5.1 and 5.4 shows that the temperature dependence of the chemical potential $\mu = \mu(T, n, U > 0)$ is qualitatively rather similar to the noninteracting case, even for $T < T_N$. The latter remark is however not valid for larger U values such as $U = 8t$ or $U = 10t$ where the low-temperature regime of $\mu(T, n, U)$ is smoother.

- The strong coupling limit of the attractive Hubbard model presented in Section 2.2 implies that $\mu(T, n, U)$ must be equal to $U/2$ for $U \to \infty$. The U dependence of the chemical potential is shown in Figure 5.6 and this tendency is clearly observed, in particular for low temperatures T where the effects of the discreteness of the energy levels are not yet too strong ($T > T_N$). It turns out that the largest coupling value shown in Figure 5.6 ($U = 10t$) is already quite close to the strong coupling limit. Indeed, in this case the bottom of the bosonic band is situated at a distance $W_B/2 = 6t_B = 1.2t$ below the chemical potential $U/2$. Figure 5.6 shows that, for $U = 10t$, this distance is a bit larger than $|\mu(T = 0.25t, n = 0.2, U = 10t) - U/2| = 1.2t$, which confirms clearly the proximity to the large-U asymptotic regime.

- The high-temperature behavior of the chemical potential $\mu(T, n, U)$ is also interesting. If T is much larger than both the kinetic and the potential energies, an expansion of the expectation value of the particle number operator $\langle \hat{\mathcal{N}} \rangle$ in β can be performed and the number equation (2.6) easily solved in this limit. The

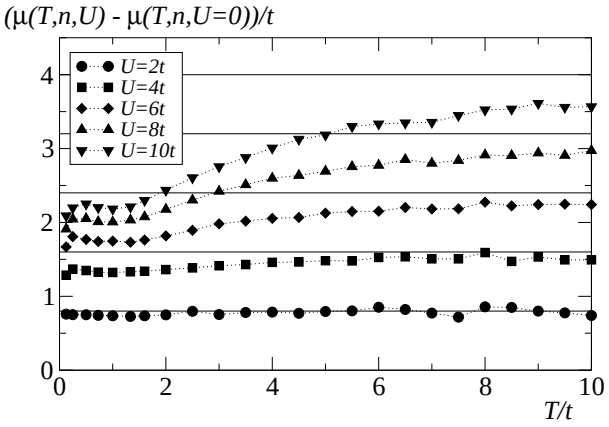

Figure 5.7: High-temperature behavior of the chemical potential $\mu = \mu(T, n, U)$ for $n = 0.2$, showing the proximity to the asymptotic regime described by Eq.(5.49), $N = 6^3$ and $\Delta\tau = 0.125t^{-1}$.

result reads [115]

$$\mu(T, n, U) \approx \mu(T, n, 0) + \frac{U}{2} + \frac{1-n}{2} U \tag{5.38}$$

where the approximation

$$\mu(T, n, 0) \approx 2\,(1-n)\,T \tag{5.39}$$

works only for densities n close to 1. This problem is eliminated by considering the quantity $\mu(T, n, U) - U/2 - \mu(T, n, 0)$ whose high-temperature behavior is a simple function of n and U. The results of the DQMC calculations are represented in Figure 5.7. They show that the asymptotic regime associated with Eq.(5.38) appears to higher and higher temperatures when increasing U. It is important to stress that the latter corresponds to the vanishing of the effects of the interaction U, which may be different from the vanishing of the precursor pairing (see Section 5.3.4).

5.3.3 Phase diagram $U - n - T$

This section is concerned with the quantitative determination of the $U - n - T$ phase diagram of the 3D attractive Hubbard model. It consists in calculating the functions $T_c(U, n)$, $T^*(U, n)$ and $T_c^{\mathrm{CDW}}(U, n = 1)$ separating the domains where the different regimes discussed in Section 2.2 are present. To fulfill this task, the study of the temperature dependence of the correlation functions (5.30) provides all the necessary information. Deeper investigations of the precursor regime between T_c and T^* will be presented in Section 5.3.4.

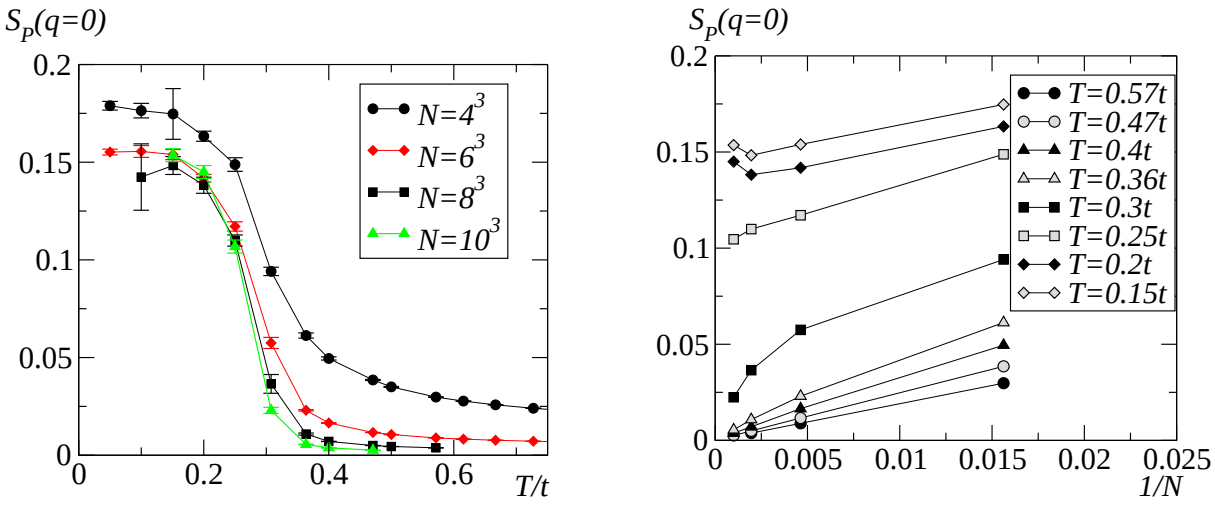

Figure 5.8: Finite-size studies of the pairing correlation function $S_P(q=0)$ around the superconducting phase transition, $U = 6t$, $n = 0.5$ and $\Delta\tau = 0.125t^{-1}$

Superconducting transition temperature T_c

For an infinite system the superconducting transition temperature T_c characterizes the onset of long-range superconducting order, i.e. the point where the correlation length ξ associated with the superconducting order parameter ψ becomes infinite. In a finite system, ξ is limited by the linear size $\sqrt[3]{N}$ (even for periodic boundary conditions) and the phase transition corresponds rather to the condition $\xi \sim \sqrt[3]{N}$. The properties of the latter and in particular the value of T_c are consequently modified: these are the well-known finite-size effects which are inherent in most numerical simulations. It is therefore important to analyze them carefully by considering several sizes ($N = 4^3, 6^3, 8^3$ and 10^3 in the present work) in order to deduce their behavior in the thermodynamic limit $N \to \infty$, which allows to discard this uninteresting dependence of the physical quantities.

As mentioned above, the important quantity to consider in determining the superconducting transition temperature T_c is the pair-pair correlation function S_P from Eq.(5.30a), more particularly the component at $q = 0$ of its Fourier transform (5.33). As shown by its definition, S_P "probes" the breaking of the U(1) gauge symmetry associated with the conservation of the particle number, which is the essence of superfluidity for dimension $D > 2$ [113]. Consequently $S_P(q=0)$ vanishes for $T \geq T_c$ in the thermodynamic limit, eventually with a discontinuous derivative. For a finite system, this behavior is smoothed off, but this effect becomes less and less pronounced with increasing sizes N. Therefore, by observing this quantity at a fixed temperature but for various N, a first estimate of the interval containing T_c can be easily deduced. This is shown in Figure 5.8 where the choice of the abscissa N^{-1} is a way commonly

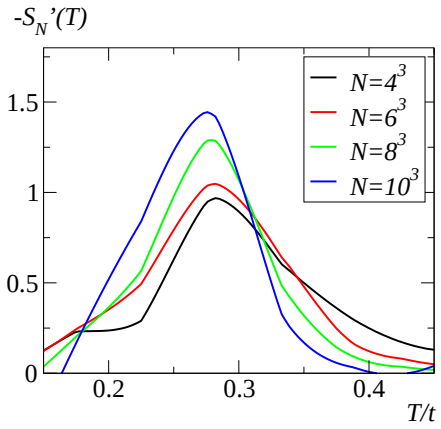

Figure 5.9: Temperature derivative $S'_N(T)$ of the pairing correlation function for various sizes, same parameters as in Figure 5.8.

used to suggest the behavior in the thermodynamic limit $N^{-1} \to 0$. Clearly, in this case ($U = 6t$ and $n = 0.5$), T_c is expected to lie in the interval $[0.25t, 0.36t]$, presumably close to $T = 0.3t$. Although it is not very accurate, this method to determine $T_c(U, n)$ is easily applicable, especially when the data are of bad quality and the larger sizes $N = 8^3$ or $N = 10^3$ cannot be calculated. This is the case for $U = 2t$ where $T_c < T_N$ (see Section 5.3.1).

A more satisfactory method consists in identifying a size-dependent critical temperature $T_c(N)$ with the inflexion point of the curve $S_P(q = 0)$ versus temperature T. Clearly it satisfies $T_c(N \to \infty) = T_c$ and thus provides a set of points $\{N^{-1}, T_c(N)\}$ from which T_c can be extrapolated, provided that the size-dependence of $T_c(N)$ is not pathological, which should not be the case here (unlike in the 2D attractive Hubbard model). In order to determine $T_c(N)$, the following procedure is followed.

1. A polynomial interpolation $S_N(T)$ of the data $\{T_m, S_P(q = 0)|_{T_m}\}_m$ is defined for each size N. Since it uses all the available temperatures $\{T_m\}$ (at least 10 points for $N = 4^3,\ 6^3$ and 8^3), it is satisfactorily stable for the next step.

2. The numerical derivative of $S_N(T)$ with respect to T is calculated according to the formula
$$\frac{dS_N(T)}{dT} \approx \frac{S_N(T + \Delta T/2) - S_N(T - \Delta T/2)}{\Delta T} \equiv S'_N(T) \tag{5.40}$$
with $\Delta T \simeq 0.05t$. This value corresponds to the distance between two successive temperature values T_m and T_{m+1}. Eventually, ΔT can be taken a bit larger to smooth off the noise that can be present in the QMC data $S_N(T_m)$.

3. The position of the minimum of the function $S'_N(T)$ is determined by a numerical algorithm and provides the desired value $T_c(N)$.

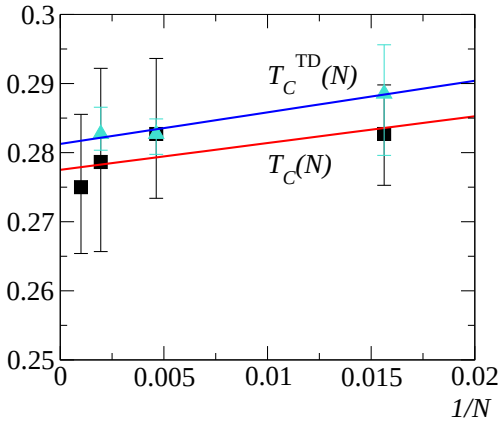

Figure 5.10: Finite-size behavior of the critical temperatures $T_c(N)$ and $T_c^{\mathrm{TD}}(N)$, same parameters than Figures 5.9 and 5.11

The application of this procedure for the case $U = 6t$ and $n = 0.5$ is shown in Figures 5.9 and 5.10. In the latter, the plot $T_c(N)$ versus N^{-1} allows to perform conveniently the extrapolation to the thermodynamic limit. For the considered case, it appears that $T_c(N)$ is rather insensitive to the finite size. This allows to approximate $T_c(N)$ by a straight line whose intersection with the axis $N^{-1} = 0$ gives the value

$$T_c(U = 6t, n = 0.5) = 0.277t \pm 0.01t. \tag{5.41}$$

The two methods presented above are applied to all the points (U, n) given in Figure 5.2 and allow to derive the desired function $T_c(U, n)$. But before discussing the results, it is instructive to consider still another method of characterizing the critical temperature T_c based on a *thermodynamic* quantity instead of a two-point correlation function: the specific heat c_V. The latter is expected to display a singular behavior at $T = T_c$ in the TD limit which manifests itself as a pronounced peak for a finite-size system. Thus, as for the case of $S_P(q = 0)$, a size dependent critical temperature $T_c^{\mathrm{TD}}(N)$ can be defined by finding an extremum of the derivative of a quantity calculated by QMC, namely the internal energy given by $\langle \mathcal{H} \rangle$, the expectation value of the Hamiltonian. Here, however, the calculation is more delicate because $\langle \mathcal{H} \rangle$ depends very sensitively upon the density. Thus the grand canonical procedure exposed in Section 5.3.2 and in particular the interpolation (5.37) are necessary to stabilize appropriately $\langle \mathcal{N} \rangle / N$ to the required value n. The same interpolation and optimalization procedures as explained for $S_P(q = 0)$ are used to give the results displayed in Figure 5.11. The extrapolation to the thermodynamic limit is shown in Figure 5.10 and shows a remarkable agreement with the results obtained with the pairing correlation function $S_P(q = 0)$ and the value given in Eq.(5.41). It it interesting to notice the shapes of the specific heat curves $c_V(T)$ in Figure 5.11. Apparently they are very different from the typical (asymmetric)

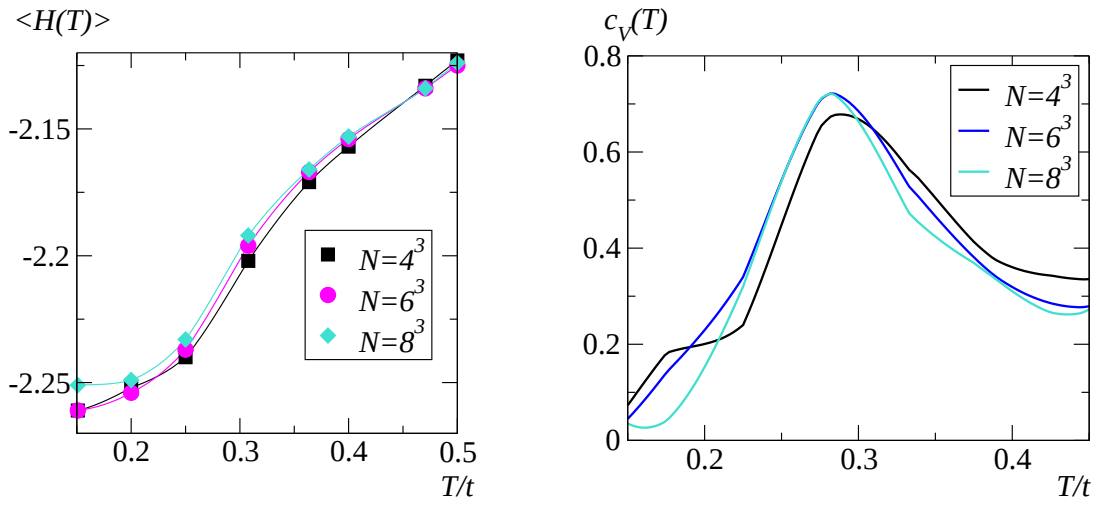

Figure 5.11: Temperature dependences of the internal energy $\langle \mathcal{H} \rangle$ and of the specific heat c_V for different system sizes, $U = 6t$, $n = 0.49$ (obtained by interpolation from $n_1 = 0.48$ and $n_2 = 0.5$) and $\Delta\tau = 0.125t^{-1}$.

BCS form and present already some resemblance with a BEC (symmetric) curve. But such an interpretation is delicate, given the finite size of the system and the limited accuracy of the numerical derivative in Eq.(5.40).

The critical temperature T_c having been calculated at each point of the U-n plane given in Figure 5.2, it is possible to deduce the function $T_c(U, n)$. Its U dependence is discussed in the following while the effect of the variation of the density n will be analyzed below, together with $T_c^{\mathrm{CDW}}(U, n)$. The asymptotics of $T_c(U, n)$ is well-known because it corresponds to two regimes which can be treated by relatively simple analytical approaches (see Section 2.2). In weak coupling the (lattice) BCS expression is

$$T_c(U,n) = \frac{2e^{\gamma}}{\pi}\sqrt{\left(\frac{W}{2}+\mu\right)\left(\frac{W}{2}-\mu\right)}\,\exp\left(\frac{-1}{D_0(\mu)U}\right) \tag{5.42}$$

where γ is Euler's constant, $W = 12t$ is the bandwidth and $\mu = \mu(T = 0, n, U = 0)$. Eq.(5.42) constitutes the low-temperature solution of the implicit Hartree-Fock (HF) gap equation

$$\frac{1}{U} = \frac{1}{N}\sum_{\mathbf{k}} \frac{\tanh\big(\beta_c(\epsilon_{\mathbf{k}}-\mu)/2\big)}{2(\epsilon_{\mathbf{k}}-\mu)}. \tag{5.43}$$

For strong coupling one neglects the residual bosonic interaction and uses the BEC expression [94] for bosons with hopping amplitude $2t^2/U$ and density $n/2$:

$$T_c(U,n) = 2\left(\frac{2\pi^2}{\Gamma(3/2)\zeta(3/2)}\right)^{2/3} n^{2/3}\,\frac{t^2}{U}. \tag{5.44}$$

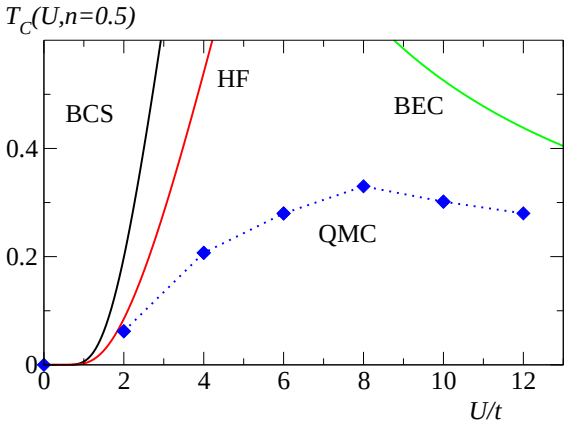

Figure 5.12: Superconducting critical temperature $T_c(U, n = 0.5)$ of the 3D attractive Hubbard model, comparing DQMC results with the asymptotic values given by Eqs.(5.42-5.44).

In the case of intermediate values of the interaction U, the critical temperature interpolates smoothly between these regimes. The DQMC results are shown in Figure 5.12 for the density $n = 0.5$ and correspond well to the expectations.
Other methods have been used to study this crossover regime and a comparison with the corresponding values for $T_c(U, n = \text{const.})$ constitutes a useful check for the results presented in this work. This is shown in Figure 5.13. Several observations are important. First, there is a good agreement between the QMC results, although the values by Staudt *et al.*[105] for the repulsive case are systematically a bit larger. This

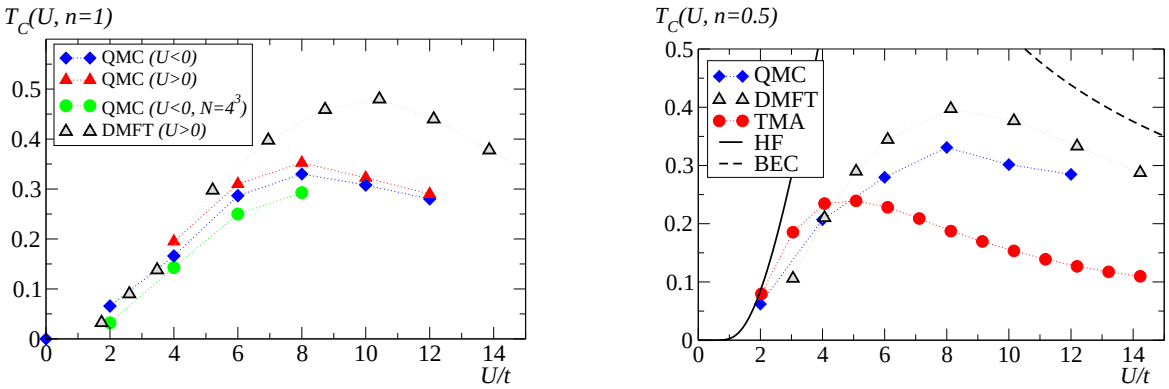

Figure 5.13: Comparison of the critical temperatures $T_c(U, n)$ obtained with various methods. *Half-filling* (left): the results from the present calculations (QMC $U < 0$) agree with Staudt *et al.* [105] (QMC $U > 0$). Refs.[104] (QMC $U < 0$, 4^3) and [117] (DMFT $U > 0$) are further apart. *Quarter-filling* (right, $U < 0$ only): the DMFT results proposed by Keller *et al.* [53] overestimate T_c in the intermediate and strong coupling regimes, whereas the corresponding values obtained by a (modified) T-matrix calculation (TMA) [106] are too low.

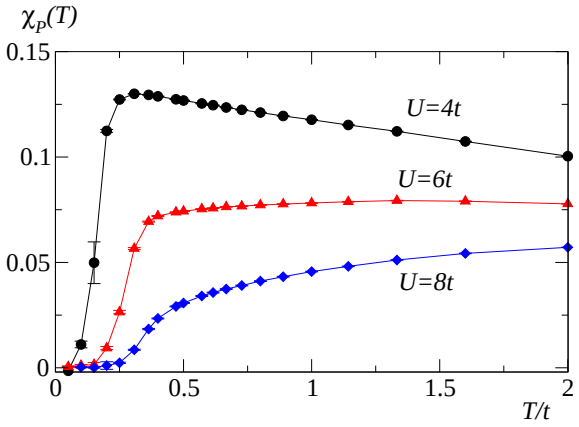

Figure 5.14: Temperature dependence of the Pauli susceptibility χ_P for various values of the coupling U. The position of its maximum gives the temperature T^*.

can be explained easily by the fact that the latter have been additionally extrapolated to the limit $\Delta\tau \to 0$, a step which has not been performed in this work. It increases slightly the values obtained for $\Delta\tau = 0.125t^{-1} > 0$ [116]. Second, it definitely turns out that the DMFT calculations by Georges *et al.* [117] at half-filling and by Keller *et al.* [53] at quarter-filling give values for T_c which are too large in both the intermediate and strong coupling regimes. [4] Finally the T-matrix calculations (**k**-independent by Keller *et al.* [106] and "usual" by Engelbrecht *et al.* [119]) provide satisfactory results as long as $U \lesssim 6t = W/2$, as already discussed in Chapter 4.
A last remark: the nice agreement between T_c deduced from the pair-pair correlation function and T_c^{TD} based on the specific heat seems obvious for $D = 3$, at least in 3D. However, for $D = 2$, the situation is different. As a consequence of the Mermin-Wagner theorem, T_c vanishes since it is associated with the breaking of the U(1) continuous symmetry. On the other hand T_c^{TD} becomes ill-defined because the specific heat of the BKT transition displays no singular behavior at the critical point. A study of the 2D-3D crossover in this context would be certainly very instructive.

Pair formation temperature scale T^*

In the context of the BCS-BEC crossover, T^* is associated with the temperature scale of electronic pair "formation", which is expected to become of the order of U in the strong coupling regime. In this work, the function $T^*(U, n)$ is extracted from the temperature dependence of the Pauli spin susceptibility χ_P, related by Eq.(5.34) to the spin-spin correlation function (5.30b). Indeed a simple relation exists between χ_P and the presence of pairs: since the two electrons forming the latter arrange themselves in

[4] In order to compare ∞-dimensional DMFT results with the present DQMC data, a rescaling of the values from Ref.[53] is necessary. The latter is determined by the condition $U_{\mathrm{QMC}}\, D_{3\mathrm{D}}(\mu_{3\mathrm{D}}(T, n)) = U_{\mathrm{DMFT}}\, D_0(\mu_0(T, n))$, which yields the relation $U_{\mathrm{QMC}} \approx 2\, U_{\mathrm{DMFT}}$ for $T \lesssim t$ and $n = 0.5$ [118].

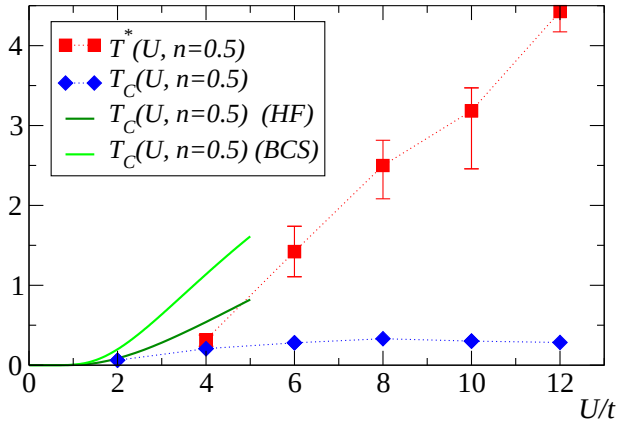

Figure 5.15: U dependence of the pair formation temperature scale $T^*(U, n = 0.5)$, compared to the weak-coupling "mean-field " critical temperatures given by Eqs. (5.42-5.43) and the "true" critical temperature $T_c(U, n = 0.5)$. The error bars give a an idea of the extension of the temperature interval related to T^*.

a spin singlet with total (intrinsic) angular momentum zero, the spin response to an external magnetic field described by χ_P becomes anomalously weak as soon as some pairing is present. One often refers to this behavior of χ_P as a "spin gap" [104], meaning thereby that the low-energy spin excitations require a finite energy to be activated. It is of great interest to relate these properties of the spin degrees of freedom to the spectral properties of the Hamiltonian $\mathcal{H}$ since the latter allows to discuss the presence of an eventual pseudogap in the density of states $D(\omega)$. This will be discussed in details in the next section. For the moment, the attention is devoted to the quantitative determination of the temperature scale T^*, related to the appearance of singlet s-wave electronic pairs.

Pragmatically T^* can be defined as the position of the maximum of the Pauli spin susceptibility, as suggested by Dos Santos [104]. In absence of interaction ($U = 0$), χ_P is a monotonically decreasing function of the temperature T. In the superconducting phase, the spin susceptibility vanishes at low temperatures $T \ll T_c$. Consequently χ_P must have a maximum and thus T^* is a well-defined quantity. It has moreover the important property of becoming equal to T_c in the BCS regime (see for instance Figure 1 of Ref.[95]). For large U, T^* represents a crossover regime spreading over a finite temperature interval rather than a single point on the T axis. Such a behavior can be deduced from the evolution of the sharpness of the maximum of χ_P with U. These properties of χ_P are illustrated in Figure 5.14.

Concerning the finite-size effects on T^*, they are mainly present for $U = 2t$ and $U = 4t$. In both cases, T^* is very close to T_c and a careful size analysis is necessary. This is shown in detail in the next section with the conclusion that both temperatures are almost equal in these two cases. For $U \gtrsim 6t$, T_c and T^* become clearly distinct and the finite system sizes have almost no influence on the position of the maximum of the

spin susceptibility. This can be understood by remarking that the (precursor) pairing becomes a *local* process for large U (since it is associated with very small coherence lengths ξ_0) and is not influenced by bulk properties like the (finite) size.
After having determined T^* at each point of the grid in Figure 5.2, it is possible to construct the function $T^*(U,n)$. Its U dependence is particularly interesting in the intermediate coupling regime where T^* starts to become different from T_c. The results are shown in Figure 5.15. The error bars around $T^*(U,n)$ give the temperatures where χ_P has lost one percent of its maximal value, in order to indicate the relative extension of the T^* region for different U. One observes that $T^*(U, n = \text{const.})$ first follows $T_c(U, n = \text{const.})$ up to approximately $U = 4t$. Then it enters (already) the "strong coupling" regime where it becomes approximately a straight line. The features appearing in Figure 5.15 are further discussed in Section 5.3.4 where a comparison with other works allows to study the influence of the dimensionality on the precursor manifestations of pairing.

CDW transition temperature T_c^{CDW}

As shown in Section 2.3, the charge-density wave (CDW) order is a property of the attractive Hubbard model at half-filling $n = 1$. It is studied by considering either the Fourier transform (5.34) at wave vector $\mathbf{q} = \mathbf{Q} \equiv (\pi, \pi, \pi)$ of the charge-charge correlation function (5.30c) or the "staggered" version of the same quantity (as discussed in the last remark of Section 5.2.4). The transition temperature T_c^{CDW} is determined by a finite-size analysis, as for the case of the superconducting T_c. However, unlike the latter case, the situation is a bit more delicate here. First, the free-electron version of $S_C(\mathbf{Q})$ diverges when $T \to 0$, due to terms proportional to $\beta\,\Delta\epsilon_N$ which appear in a system with a nonzero energy-level spacing $\Delta\epsilon_N$ due to a finite size N (see Figure 5.19 below for the same problem with C_S). This has to be contrasted with the well-behaved case of the the pair-pair correlation function $S_P(q = 0)$, whose free-electron counterpart is regular as $T \to 0$. Moreover, the CDW-related quantities turn out to converge particularly slowly during the Monte Carlo calculation and their fluctuations become very large below T_c^{CDW}. The reason for this fact is simple: the symmetry group SO(3) which is broken in the ordered phase is higher than the symmetry O(1) associated with particle-hole invariance characterizing the charge-charge correlation function S_C. In other words, this corresponds to trying to determine the magnetization correlations in the repulsive Hubbard model by considering exclusively the z component of the spin operators, instead of taking advantage of the full symmetry and using the full vector $\mathbf{S}$ as it is done in Eq.(5.30b). It is then clear that the convergence of the latter more "symmetric"quantity will be better during a Monte Carlo simulation.
The study of the temperature dependence of the CDW ordering can be performed nevertheless and gives the occasion to use an alternative method to treat the problem, briefly mentioned in Section 5.2.4. It is based on a general property of the correlation functions (5.30), which has already been used frequently to detect superconductivity [55]. It states that, in presence of (off-diagonal) long-range order like CDW or

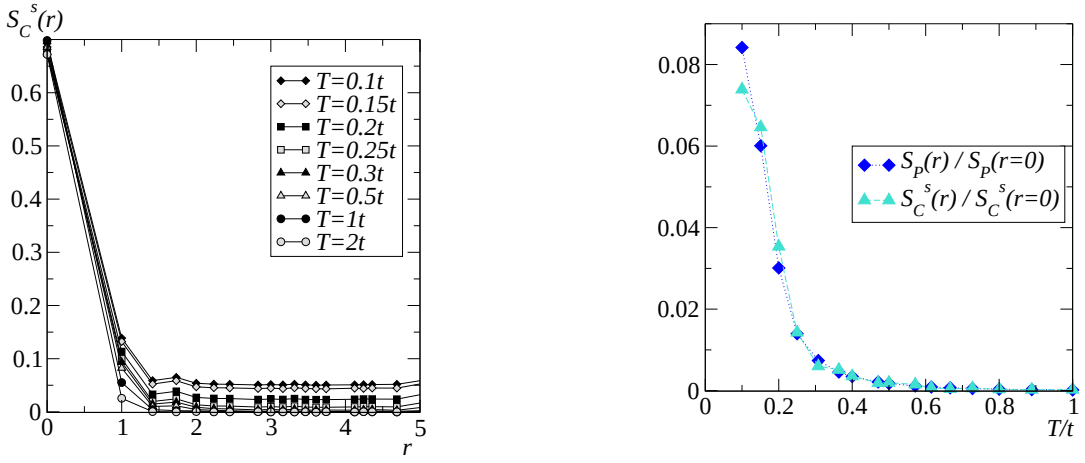

Figure 5.16: Detection of the presence of long-range CDW order by studying the large r behavior of the (staggered) charge-charge correlation function $S_C^s(r)$ (left) and illustration of the SO(3) symmetry at half-filling by the equivalence of CDW and superconducting orders (right), $U = 4t$, $N = 6^3$ and $\Delta\tau = 0.125t^{-1}$.

superconductivity, the latter quantities tend to a nonzero plateau value for large distances r. This behavior is illustrated in Figure 5.16, together with the temperature dependence of the plateau values (right-hand part). The latter resembles strongly to the results obtained by taking the Fourier transformation of the correlation function, a normal feature since both quantities coincide in the thermodynamic limit. Figure 5.16 also shows that, if they are both normalized by their value at $r = 0$, the superconducting and the CDW correlation functions are equivalent at half-filling. This is a manifestation of the SO(3)=U(1)$\otimes$O(1) symmetry present in this case, whereas only the gauge symmetry U(1) remains outside half-filling. As a consequence the relation $T_c(U, n = 1) = T_c^{\mathrm{CDW}}(U, n = 1)$ has to be satisfied and is correctly reproduced by the DQMC calculations, since the results for S_C^s and S_P turn out to be equivalent for $n = 1$.

One may ask what happens to the CDW order outside half-filling. The QMC results for the case $U = 6t$, $n = 0.9$ and the size $N = 8^3$ shown in Figure 5.17 allow to answer this question. They consist in a log-log plot of the normalized correlation functions $S_P(r)/S_P(r = 0)$ and $S_C^s(r)/S_C^s(r = 0)$, exactly the ones which coincided at half-filling in Figure 5.16. It appears clearly that both quantities display an algebraic decay at large r in absence of long-range order. Unlike the superconducting correlations which modify their asymptotics below $T_c(N)$ by "saturating" at a plateau value, the CDW correlations conserve the algebraic decay up to the lowest calculated temperature ($T = 0.1t$) and presumably up to $T = 0$. The numerical results are thus compatible with the following behavior for the staggered charge-charge correlation function at finite-temperature outside half-filling [114]:

$$S_C^s(r) \sim r^{-a\,|n-1|^b} \tag{5.45}$$

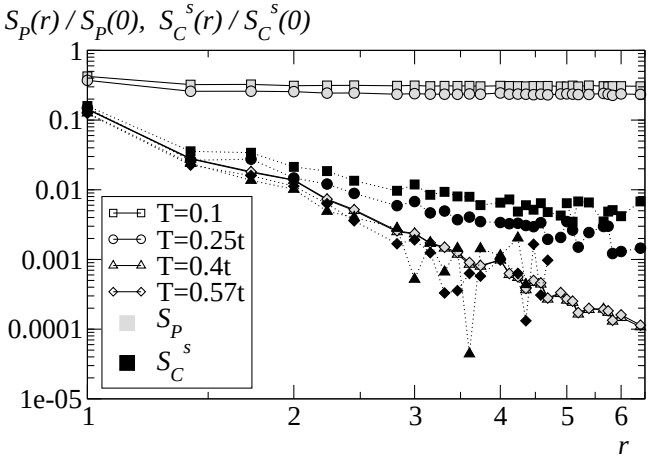

Figure 5.17: Comparison of the large r behavior of the pair-pair and charge-charge correlation functions $S_P(r)$ and $S_C^s(r)$ for a density $n = 0.9$ close to half-filling. The points for $r > 5$ of the high-temperature curves of $S_C^s(r)$ are very noisy and not shown for clarity reasons.

where a and b are positive nonuniversal constants, depending in particular of the interaction strength U. It is interesting to notice that these features are apparently not affected by the finite-size effects, except for the value of $T_c(N)$ for which this problem has already been discussed.

Although the CDW ordering is restricted to $n = 1$, it has a nonnegligible influence on the density dependence of the superconducting transition temperature for $n \neq 1$ as well. It is therefore instructive to discuss the function $T_c(U = \text{const.}, n)$ for $n \in [0, 2]$ in this context. The low-density regime $n \lesssim 0.2$ displays a crossover between dependences in $n^{1/3}$ and in $n^{2/3}$ for the BCS and BEC regimes, respectively. It is unfortunately hard to access by DQMC because $T_c(U, n \lesssim 0.2)$ is smaller than the finite-size temperature T_N under which artificial features alter the results. However a rapid decrease is observed at low densities, consistent with a dependence n^α, $\alpha < 1$, as shown in Figure 5.18. When coming closer to half-filling, the DQMC results suggest that $T_c(U = \text{const.}, n)$ has a maximum between 0.5 and 0.9 and then decreases slightly around $n = 1$. Such a behavior, observed for all the considered couplings U, is a clear reminiscence of the 2D case [120] where T_{BKT} even vanishes because of the different nature of the phase transition at half-filling (additional presence of CDW order). This feature is absent in the phase diagram of Micnas *et al.* [25] but has been already detected in the small-size ($N = 4^3$) DQMC calculations by Dos Santos [104]. Further simulations for intermediate densities are however necessary to be more quantitative on this interesting point.

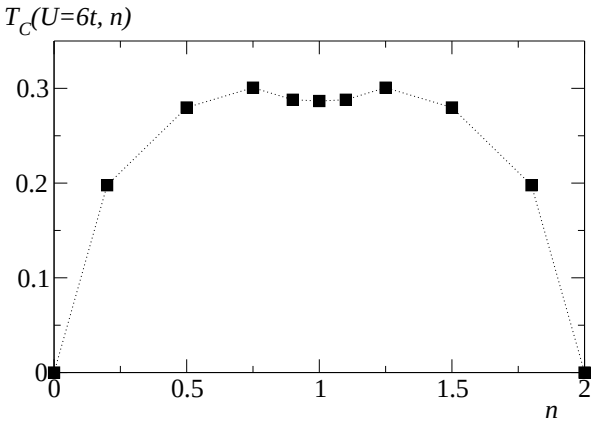

Figure 5.18: Density dependence of the superconducting critical temperature $T_c(U = 6t, n)$, showing a decrease occurring at half-filling due to the higher SO(3) symmetry associated with the phase transition, similarly to the case in two dimensions [120].

5.3.4 Pauli spin susceptibility and dimensionality effects

In this section, the spin susceptibility χ_P is used to study the influence of the dimensionality on the precursor pairing in the "normal" state above T_c. As explained in the introduction to this chapter (Section 5.1), the latter process is expected to present appreciable differences when going from 2D to 3D and is closely related to the pseudogap issue. It is therefore necessary to clarify first the relations between χ_P and $D(\omega)$ and to study the temperature dependence of the spin susceptibility.

Relations between the spin susceptibility and the spectral density

An explicit calculation of spectral quantities like the density of states $D(\omega)$ and the spectral function $A(\mathbf{k}, \omega)$ requires to use an additional numerical method called Maximum Entropy and based on imaginary *time-dependent* Green's functions [55, 59, 95, 92]. This has not been done in this work. However some information about $D(\omega = 0)$ can nevertheless be obtained from a time-independent quantity such as the Pauli spin susceptibility χ_P, as explained hereafter.
A close relation exists between χ_P and $D(\omega = 0)$, easily understood physically by recalling the mechanism leading to the Pauli paramagnetism. The response to an external magnetic field is the stronger the more states are available around the Fermi energy, allowing for the asymmetric rearrangement of the occupations between up and down spins. In the case of free electrons ($U = 0$), one can be even more quantitative by remarking that the spin susceptibility is given by the expression

$$\chi_{P,0}(T) = \frac{2}{T\,N} \sum_{\mathbf{k}} n_F(\epsilon_{\mathbf{k}} - \mu)\big(1 - n_F(\epsilon_{\mathbf{k}} - \mu)\big) \tag{5.46}$$

which has a low-temperature limit ($\beta t \gg 1$) reading

$$\chi_{P,0}(T) \approx 2\, D_0(\omega = 0) \tag{5.47}$$

in the normalization and units used in this chapter. A similar proportionality relation can be deduced for a BCS superconductor [94]. Moreover it has been shown by explicit QMC calculations in 2D that the temperature dependences of χ_P and $D(\omega = 0)$ are very similar of one another in the intermediate coupling regime ($U \sim 4t$) as well, even when a pseudogap appears in the density of states [121, 122]. This will be confirmed below in Figure 5.20.

For T above T_c (or T_{BKT} in 2D), the BCS approach valid for $U \ll t$ predicts that both quantities are given by the noninteracting version, i.e. $\chi_P = \chi_{P,0}$ and $D(\omega) = D_0(\omega)$. Thus the effect of the interaction $U > 0$ vanishes completely above the transition temperature. This is however no more the case for larger values of U and it is then necessary to reach the regime $\beta U \ll 1$ to restore the free electron behavior, as already noticed with the chemical potential $\mu(T, n, U)$ in Figure 5.7. In this limit χ_P becomes independent of U and reads [115]

$$\chi_P(T) \approx \frac{1}{T}\, n\, (1 - \frac{n}{2}). \tag{5.48}$$

For $T \gtrsim T_c$, the spin susceptibility reaches first a maximal value, corresponding to the temperature scale T^* defined in the previous section, and then starts to decrease monotonically. This regime, not yet corresponding to Eq.(5.48), is well captured by a RPA approximation [121] where χ_P is indeed a monotonically decreasing function of T situated below $\chi_{P,0}$ [5]. Thus T^* turns out to be associated with the temperature region where the RPA approach starts to become invalid. The different regimes present in the T dependence of the Pauli susceptibility are illustrated in Figure 5.19 for the case $U = 6t$ in 3D. It also shows, in the inset, the artificial divergence of $\chi_{P,0}$ for $T \to 0$ due to the finite-size effects, already mentioned in connection with the charge-charge correlation function S_C in the previous section.

As mentioned above, a temperature dependence similar to $\chi_P(T)$ is expected for $D(\omega = 0)_T$ with the exception however that the "RPA" regime above T^* already corresponds to the noninteracting density of states $D_0(\omega)$, as suggested by the Maximum Entropy studies of the spectral properties of the attractive Hubbard Hamiltonian [92]. Concrete examples for these temperature dependences are given in the following.

The case of intermediate coupling $U = 4t$

For the parameter choice $U = 4t$ and $n = 0.8$ the spin susceptibility $\chi_P(T)$ as well as the density of states at the Fermi energy $D(\omega = 0)$ are both available in 2D [95]. As shown by Figure 5.20, T^* is different from the transition temperature in this case

[5] Except eventually at very low temperatures where the effects of a nonconstant (bare) density of states $D_0(\omega)$ can modify this behavior.

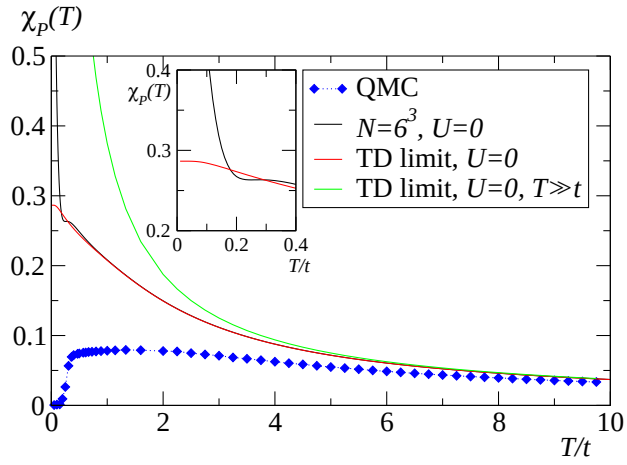

Figure 5.19: Typical temperature dependence of the spin susceptibility χ_P for $U = 6t$ and $n = 0.5$. It coincides with the free-electron expression (5.46) and the high-temperature expansion (5.48) for $T > U$ only. The interval between this asymptotic regime and the pair formation temperature scale T^* is referred to as "RPA" region. The inset show the singular behavior appearing below T_N due to finite-size effects.

and allows thus to compare the manifestations of precursor pairing in the temperature dependences of both χ_P and $D(\omega = 0)$. The curves in Figure 5.20 clearly indicate that the two quantities have common features, in particular an rapid increase just above the transition temperature. These similarities appear even better in the right-hand figure where the effects due to a nonconstant (bare) density of states are suppressed by divid-

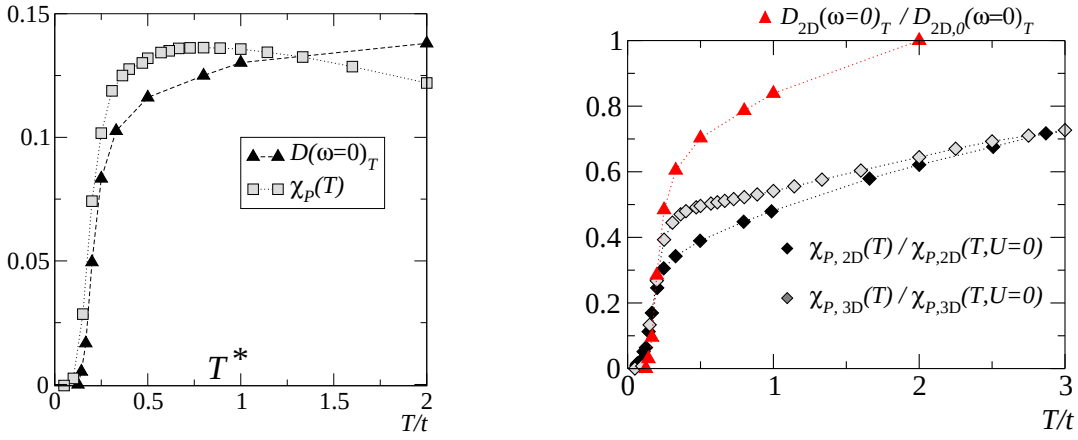

Figure 5.20: Temperature dependences of the density of states evaluated at the Fermi level $D(\omega = 0)$ and of the Pauli susceptibility χ_P. The density of states is the result of Maximum Entropy calculations for the parameters $U = 4t$, $n = 0.8$, $N = 8^2$ and $D = 2$, Figure 15 of Ref.[95]. The susceptibility data have been calculated for the same parameters.

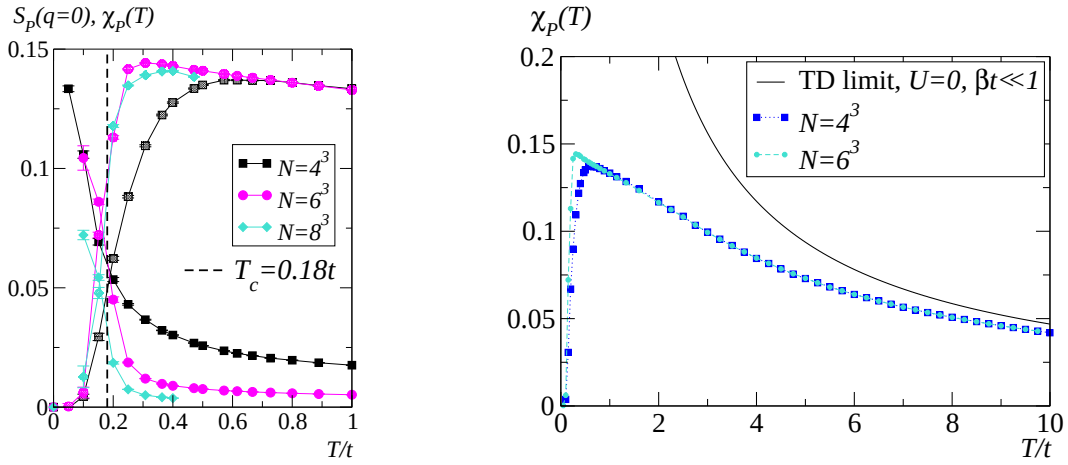

Figure 5.21: Temperature dependence of $\chi_P(T)$ for $U = 4t$, $n = 0.75$ and $D = 3$. Left: comparison between spin susceptibility and the pair-pair correlation function $S_P(q = 0)$ for T close to T_c and various sizes N. Right: high-temperature behavior of $\chi_P(T)$ compared with the asymptotic expression (5.48).

ing both quantities by their noninteracting counterparts. [6] As a consequence of these clear relations between the static spin response and the spectral properties, it is now possible to re-interpret T^*, previously defined as the temperature scale of electronic pair formation. It turns out that T^* gives the temperature where the lower values of the density of states $D(\omega = 0) < D_0(\omega = 0)$ becomes clearly perceptible in the response properties of the system. Figure 5.20 also confirms the remark made at the end of the previous section: the "RPA" regime above T^* of the spin susceptibility χ_P corresponds indeed to a density of state where the pseudogap effect is not yet perceptible, i.e. $D(\omega) \approx D_0(\omega)$.

Almost the same parameters ($U = 4t$ and $n = 0.75$) are used to obtain the results for the 3D case shown in Figure 5.21. A very clear difference appears in the temperature dependence of χ_P which is now much sharper around the superconducting phase transition. The "RPA" regime of a monotonic decrease of the spin susceptibility with the temperature extends down to the critical region and some care is required in determining T^* because of the finite-size effects present in this case. In fact the observed behavior resembles strongly to a BCS regime (see Figure 1 of Ref.[95]), where T_c and T^* have the same finite-size sensitivity and turn out to be finally (almost) equal to another. Therefore the spectral properties above the critical temperature are not expected to present any particularity like an anomalously low value of $D(\omega = 0)$.

As already mentioned, the case $D = 2$ and $U = 4t$ has been intensively studied because it displays a pseudogap in the density of states. It has been shown recently that the latter is due to superconducting fluctuations [42], an effect which is a direct consequence of the two-dimensionality. The fact that no sizeable precursor effects

[6] The noninteracting quantities are given by Eq.(5.46) for $\chi_{P,0}$ and by Eqs.(B.8) or (4.62) with $t_\perp = t$ for $D_0(\omega)$.

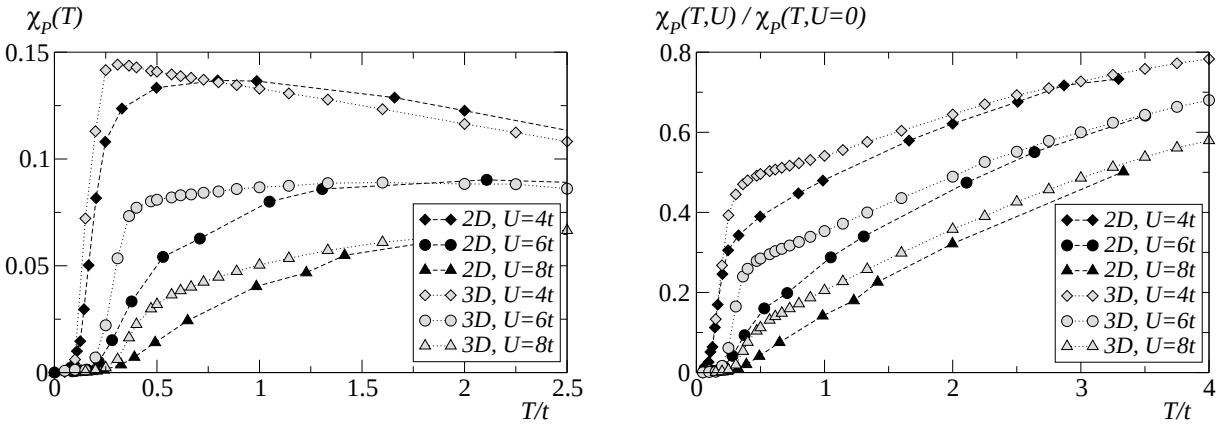

Figure 5.22: Comparison of the spin susceptibility in the intermediate coupling regime ($U = 4t,\ 6t$ and $8t$) between 2D and 3D. Left: "rough" data; right: the values of $\chi_P(T, n, U)$ are divided by $\chi_{P,0}(T, n)$ from Eq.(5.46) to isolate the consequences of a different dimensionality.

($T^* \approx T_c$) have been detected for the same parameters but in 3D confirms clearly this statement. This also agrees with the conclusion of Preosti *et al.* [98] who have studied the efficiency of the fluctuation scenario in producing a pseudogap in the context of the dimensional crossover between two and three dimensions. The right-hand part of Figure 5.20 illustrates clearly the above discussion. It shows that a difference in χ_P between 2D and 3D exists as long as the two-dimensional pseudogap is present.

Comparison between 2D and 3D

In order to study the influence of the dimensionality on the precursor pairing described by the attractive Hubbard model in the intermediate coupling regime, QMC results for the spin susceptibility χ_P provide useful informations, as it has been illustrated in the previous section for the case $U = 4t$. In Figure 5.22, the temperature dependence of χ_P is shown for the parameter values of interest ($U = 4t,\ 6t$ and $8t$). From the "rough" data of the left-hand graph, it appears that all curves display two distinct temperature scales T_c and T^* , except the one for $U = 4t$ and $D = 3$ already discussed previously. As a consequence, a regime characterized by a reduced density of states at the Fermi level $D(\omega = 0) < D_0(\omega = 0)$ above T_c is present in these cases. In the strong coupling limit $U \gg W$ this feature, present in both 2D and 3D, is called preferably a "correlation gap" [85, 96] and is characterized by the relations $T^* \sim U \gg T_c$. However, when decreasing the coupling strength U in 2D, it is expected to be transformed smoothly into the (fluctuation-induced) pseudogap for which T_c and T^* are close to another.
The comparison between $D = 2$ and $D = 3$ is made easier by dividing all the susceptibility data by the corresponding values for free electrons, i.e. by $\chi_{P,0}$ given by Eq.(5.46) at same T and n. The results are shown on the right-hand part of Figure

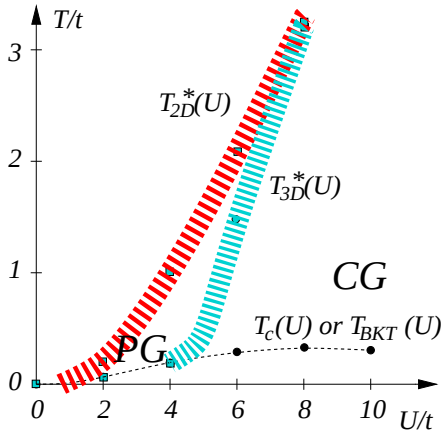

Figure 5.23: Schematic phase diagram of the intermediate coupling regime of the BCS-BEC crossover, as suggested by the analysis of the spin susceptibility χ_P. "PG" means a fluctuation-induced pseudogap whereas "CG" refers to the correlation gap of the strong coupling regime.

5.22. For the case $U = 4t$, the difference between 2D and 3D was explained by the absence of a fluctuation-induced pseudogap in 3D. For larger U a difference is still observed, becoming eventually weaker as the coupling increases.[7] For the latter cases it is more suitable to use the strong coupling language to explain the observations. Then the energy change resulting from the formation of a (local) Cooper pair can be roughly estimated as [115]

$$\Delta E \sim -U + 2\,(\mu(U=0) - 2Dt). \tag{5.49}$$

The first term is the gain in potential energy whereas the second is the loss in kinetic energy. Clearly a lower dimension D favors the pairing and this explains what appears in Figure 5.22 where the 2D curves of χ_P are always below the corresponding ones for $D = 3$. In the limit $U \gg t$, Eq.(5.49) further suggests that the difference between 2D and 3D vanishes, which seems to be compatible with the curves for $U = 6t$ and $U = 8t$.

The above findings suggest the schematic $U - T$ phase diagram presented in Figure 5.23 for the intermediate region of the BCS-BEC crossover. The absence of a fluctuation-induced pseudogap in 3D manifests itself in the lower part of the intermediate coupling regime ($U = 2t$ and $U = 4t$).[8] The fact that $T^*(U)$ becomes independent of the dimension for large U is consistent with the above energy argument based on Eq.(5.49).

[7] Unfortunately complete data in 2D for $U > 8t$ are not available in the literature.

[8] The existence of a fluctuation-induced pseudogap for $U = 2t$ is reported in Ref.[52].

5.4 Conclusion and perspectives

In the third part of this thesis the DQMC method was used to study some aspects of the 3D attractive Hubbard model. From the technical point of view, the first difficulty consisted in stabilizing the expectation value of the particle density operator $\mathcal{N}$, in order to work at constant density n when varying the temperature T. This problem, related to the solution of the number equation (2.6) like in any grand canonical approach, was solved in two stages using polynomial interpolations. The results were quite satisfactory because they allowed to calculate the specific heat by differentiating numerically the internal energy, a quantity which was found to be very sensitive to the density $\mathcal{N}$. Another important feature was the possibility to perform the calculations for four different system sizes (4^3, 6^3, 8^3 and 10^3) by using powerful computers. They allowed to do meaningful finite-size scalings in order to extrapolate the quantities of interest to the thermodynamic limit. The physical aspects were studied by means of time-independent correlation functions of various types (pair, spin and charge). They gave all the necessary information to construct the phase diagram $U-n-T$ of the 3D attractive Hubbard Hamiltonian (2.1). The dependences on U of the two temperature T_c and T^* interpolated well between the known limiting cases, BCS and BEC. The consequences of the presence of an additional CDW order at half-filling were considered as well. A comparison of the effects of precursor pairing between 2D and 3D confirmed the idea that the latter are stronger in 2D. This was especially clear in the weak-to-intermediate coupling regime ($U = 2t$ or $U = 4t$) where it takes the form of order parameter fluctuations, whereas nothing similar was observed in 3D.

The numerical results presented in this chapter are consistent with other QMC studies [104, 105]. They also show that the recent DMFT calculations by Keller *et al.* [53] overestimate the transition temperature for $U \gtrsim 6t = W/2$, in the same way as the earlier results by Georges *et al.* [117] did for the repulsive case at half-filling. The analysis of the dimensionality effects for the precursor pairing turned out to be in nice agreement recent works based on many-body treatments [42, 98]. It allowed to improve the understanding of the intermediate regime of the BCS-BEC crossover, a regime which is of great interest from both theoretical and experimental point of views.

Finally the results of this chapter show that the DQMC technique is able to provide key information about important issues, like the problem of precursor pairing considered in the last section. It can be further applied to investigate other questions that have been raised in this chapter. For instance a more systematic study of the specific heat curves can be undertaken by calculating new temperature values in order to improve the accuracy of the available results. Other examples concern the dimensional crossover between 2D and 3D by introducing anisotropic systems and the calculation of time-dependent quantities that give access to spectral and dynamic quantities via the Maximum Entropy method. In the latter case the computational effort is increased

since a space-time sweep scales then as $\tau_s \propto L^3 N^3$ (compare with Eq.(5.35)). However, by observing the observing the evolution of the systems treated by DQMC since 15 years, it makes no doubt that such studies will be possible soon.

Chapter 6

Conclusion

In this thesis several aspects of short-coherence length superconductors have been studied. BCS theory, which is the conventional microscopic approach to superconductivity, does not apply perfectly for this type of electronic pairing . The reason is that one of its main assumptions is not fulfilled. Indeed, the fact that the spatial extension of a Cooper pair is "short" (i.e. of the order of the lattice constant) does not correspond to a *mean-field* regime in which the pairs are so large that they overlap with many others. The new properties that result from this particular feature were called "anomalous" in the title of this thesis. This was motivated by the fact that they were quite different from those of a "normal" superconductor, which is satisfactorily described by BCS theory and its extensions. The maybe most spectacular manifestation of the short-coherence length pairing concerns the "normal" state above the transition temperature. It is characterized by the appearance of so-called *precursor* effects of superconductivity: in spite of the absence of long-range order, some quantities like the spin susceptibility and the density of states have a behavior displaying some similarities with the "true" superconducting state. This is the consequence of the existence of two distinct temperature scales in the problem: one for pair formation and one for pair condensation. Since the latter are equal in the BCS approach, the regime situated in-between was indeed expected to present novel physical properties.

The interest of the study of short-coherence length superconductors was twofold. First it can be integrated in the more general theoretical issue of the BCS-BEC crossover, where it represents an intermediate regime. Second it may help to understand some of the unusual properties that have been observed in underdoped high-temperature superconductors. The theoretical studies were based on the attractive Hubbard Hamiltonian, which constitutes a simple phenomenological model for short-coherence length pairing. They focused on three different aspects, which are briefly recalled hereafter.

- A new approach to the fluctuation-induced diamagnetism above the transition temperature has been developed. It allowed to analyze the influence of precursor

effects on the diamagnetic response.

- The thermodynamic properties of the pseudogap phase showed how the BEC properties survive in the intermediate regime. This revealed the importance of the dimensionality in this respect.

- The influence of the latter was also considered in the third part where the BCS-BEC crossover in 3D was studied. It turned out that the intermediate regime corresponding to the appearance of precursor pairing is less extended than in 2D.

All these considerations have contributed to clarify a non-conventional form of superconductivity, characterized by a short coherence length. During the last 15 years the extensions of the BCS theory and the searches for new pairing mechanisms have been mainly devoted to the understanding of the copper oxide high-temperature superconductors. The recent observations of high transition temperatures in other materials (MgB_2 and organic compounds) will certainly open new perspectives in this domain of condensed matter.

Appendix A

The singular terms of the correlation function $C(\mathbf{q})$

Here the value of the positional structure factor (3.15) at zero wave vector is shown to compensate the singular term of the current-current correlation function (3.14).
Starting from Eq.(3.15), it comes

$$\begin{aligned} S(\mathbf{q}=0) &= \sum_{n,s,n',s'} t(s,n)\, t(s',n') \\ &= \sum_{n,n'} (N_+ - N_-)^2 \end{aligned} \tag{A.1}$$

where N_+ (N_-) is the number of vortex line elements with $t(s,n) = +1$ $\big(t(s,n) = -1\big)$ in layer n. They correspond exactly to the 2D concepts of vortex and antivortex which are often interpreted as positive and negative charges of a 2D Coulomb gas.
The external flux generates N_F "charges" according to

$$N_F = \frac{L^2 B}{\Phi_0}. \tag{A.2}$$

Due to the incompressibility of the magnetic field ($\boldsymbol{\nabla}\cdot\mathbf{B} = 0$), this number is the same for all layers.
The neutrality condition requires that, in every layer n, the external flux is exactly compensated by the net charge $N_+ - N_-$ of the vortex-antivortex system:

$$N_F = N_+ - N_-, \ \forall n. \tag{A.3}$$

Therefore (A.1) can be written as

$$S(\mathbf{q}=0) = N^2 \big(\frac{L^2 B}{\Phi_0}\big)^2 \tag{A.4}$$

which is exactly the singular term of the current-current correlation function $C(\mathbf{q})$ in Eq.(3.14).

Appendix B

Calculation of the T-matrix coefficients

B.1 Method for calculating a, c and d using $A_{\mathrm{BCS}}(\mathbf{k},\omega)$

Expressions (4.19a-4.19c) for the coefficients a, c and d are based on the particle-particle bubble $\mathcal{G}(\mathbf{k},z_\alpha)$ from Eq.(4.13b). The latter is first re-expressed in terms of the spectral function $A(\mathbf{k},\omega)$ using the Lehmann representation for the Green's function $G(\mathbf{k},z_\nu)$ [94] :

$$G(\mathbf{k},z_\nu)=\frac{1}{2\pi}\int d\omega\,\frac{A(\mathbf{k},\omega)}{z_\nu-\omega}. \tag{B.1}$$

This gives:

$$\mathcal{G}(\mathbf{k},z_\alpha)=\frac{1}{\beta}\sum_{z_\nu}\int d\omega d\omega'\,\frac{1}{(z_\alpha-z_\nu)-\omega}\,\frac{1}{z_\nu-\omega'}\,\phi(\mathbf{k},\omega,\omega') \tag{B.2}$$

where

$$\phi(\mathbf{k},\omega,\omega')=\frac{1}{(2\pi)^2}\,\frac{1}{N}\sum_{\mathbf{q}}A(\mathbf{k}-\mathbf{q},\omega)\,A(\mathbf{q},\omega'). \tag{B.3}$$

Performing the frequency summation in Eq.(B.2) yields

$$\chi(\mathbf{k},z_\alpha)=-\int d\omega d\omega'\,\frac{1-n_F(\omega)-n_F(\omega')}{z_\alpha-(\omega+\omega')}\,\phi(\mathbf{k},\omega,\omega') \tag{B.4}$$

where n_F is the Fermi-Dirac distribution given in Eq.(4.28).
In order to evaluate the quantity $\phi(\mathbf{k},\omega,\omega')$, an explicit expression for $A(\mathbf{k},\omega)$ is necessary and the BCS form from Eq.(4.21) is taken in a first stage. The generalization to the pseudogap regime will be straightforward as shown later in Section B.3. For

simplicity the case $\mathbf{k} = 0$ which concerns the coefficients a and d is considered only. But this method applies as well to c once the two k derivations have been performed and the derivatives of the δ-functions have been removed by partial integrations over ω. Inserting expression (4.21) into Eq.(B.3) gives

$$\begin{aligned}\phi(0,\omega,\omega') &= \frac{1}{N}\sum_{\mathbf{q}}\Big(u_{\mathbf{q}}^4\,\delta(E_{\mathbf{q}}-\omega)\,\delta(E_{\mathbf{q}}-\omega') + v_{\mathbf{q}}^4\,\delta(E_{\mathbf{q}}+\omega)\,\delta(E_{\mathbf{q}}+\omega') \\ &\quad + u_{\mathbf{q}}^2 v_{\mathbf{q}}^2\left(\delta(E_{\mathbf{q}}-\omega)\,\delta(E_{\mathbf{q}}+\omega') + \delta(E_{\mathbf{q}}+\omega)\,\delta(E_{\mathbf{q}}-\omega')\right)\Big) \qquad \text{(B.5)}\end{aligned}$$

The property $\delta(x-a)\delta(x-b) = \delta(x-a)\delta(a-b)$ allows to write

$$\phi(0,\omega,\omega') = \delta(\omega-\omega')\,D_{a,1}(\frac{\omega+\omega'}{2}) + \delta(\frac{\omega+\omega'}{2})\,D_{a,2}(\omega-\omega') \qquad \text{(B.6)}$$

where

$$D_{a,1}(\omega) = \frac{1}{N}\sum_{\mathbf{q}}\left(u_{\mathbf{q}}^4\,\delta(E_{\mathbf{q}}-\omega) + v_{\mathbf{q}}^4\,\delta(E_{\mathbf{q}}+\omega)\right) \qquad \text{(B.7a)}$$

$$D_{a,2}(\omega) = \frac{1}{N}\sum_{\mathbf{q}} u_{\mathbf{q}}^2 v_{\mathbf{q}}^2\left(\delta(E_{\mathbf{q}}-\omega) + \delta(E_{\mathbf{q}}+\omega)\right). \qquad \text{(B.7b)}$$

Now the $\mathbf{q}$ integration can be performed by introducing the 2D tight-binding density of states

$$\begin{aligned}D_0(\epsilon) &= \frac{1}{N}\sum_{\mathbf{q}}\delta(\varepsilon_{\mathbf{q}}-\epsilon) \\ &= \frac{1}{2\pi}\,F\Big(\frac{\pi}{2},\sqrt{1-\big(\frac{\epsilon}{4t}\big)^2}\Big) \qquad \text{(B.8)}\end{aligned}$$

where F is the elliptic integral of the first kind. Integration over $\epsilon = \mu + \xi$ gives the final expressions for the "weighted" density of states $D_{a,1}$ and $D_{a,2}$ given below in Eqs. (B.10a-B.10g). The contribution (B.7) is often referred to as "Landau term" and describes interband effects.

The coefficients a, c and d are obtained from Eq.(B.4) which can be still simplified by making the variable transformation $(\omega,\omega') \rightarrow (\Omega = \frac{1}{2}(\omega+\omega'), \theta = \omega'-\omega)$, as suggested by Eq.(B.6). This allows to eliminate one of the integrals in Eq.(B.4) and to obtain finally the expressions given in the next section.

B.2 Results for a, c and d using $A_{\mathrm{BCS}}(\mathbf{k},\omega)$

The exact expressions for the coefficients a, c and d defined in Eqs.(4.19a-4.19c) are given in the following. They were calculated using the method of Appendix B.1 in-

volving the BCS spectral functions (4.21).

$$a = \frac{1}{U} - \int d\omega \left(D_{a,1}(\omega) \frac{\tanh(\beta\omega/2)}{2\omega} - D_{a,2}(\omega)\, n'_F(\omega) \right) \tag{B.9a}$$

$$\begin{aligned} c = \int d\omega \Bigg(& D_{c,11}(\omega) \frac{\tanh(\beta\omega/2)}{2\omega} \\ & + D_{c,31}(\omega) \left(\frac{\tanh(\beta\omega/2)}{4\omega^2} + \frac{n'_F(\omega)}{2\omega} \right) \\ & + D_{c,51}(\omega) \left(- \frac{\tanh(\beta\omega/2)}{4\omega^3} - \frac{n'_F(\omega)}{2\omega^2} + \frac{n_F{}''(\omega)}{2\omega} \right) \Bigg) \frac{1}{2} \left(\frac{d\xi_{\mathbf{k}}}{dk}\Big|_{k=k(\omega)} \right)^2 \\ + D_{c,12}(\omega) \frac{\tanh(\beta\omega/2)}{2\omega} + D_{c,32}(\omega) & \left(\frac{\tanh(\beta\omega/2)}{4\omega^2} + \frac{n'_F(\omega)}{2\omega} \right) \frac{d^2\xi_{\mathbf{k}}}{dk^2}\Big|_{k=k(\omega)} \end{aligned} \tag{B.9b}$$

$$d = \mathcal{P} \int d\omega\, D_{a,1}(\omega) \frac{\tanh(\beta\omega/2)}{4\omega^2} + i\,\frac{\pi}{8}\,\beta\, D_{a,1}(0). \tag{B.9c}$$

The "weighted" density of states are given by

$$D_{a,1}(\omega) = D_{\mathrm{BCS}}(\omega) \left(1 - \frac{\Delta^2}{2\omega^2}\right) \tag{B.10a}$$

$$D_{a,2}(\omega) = D_{\mathrm{BCS}}(\omega) \frac{\Delta^2}{2\omega^2} \tag{B.10b}$$

$$D_{c,11}(\omega) = D_{\mathrm{BCS}}(\omega) \frac{3\Delta^2}{4\omega^2} \left(-1 + \frac{\Delta^2}{\omega^2} \right) \tag{B.10c}$$

$$D_{c,12}(\omega) = D_{\mathrm{BCS}}(\omega) \frac{\Delta^2}{4\omega^4}\, \xi(\omega) \tag{B.10d}$$

$$D_{c,31}(\omega) = D_{\mathrm{BCS}}(\omega) \frac{\Delta^2}{\omega^3} \left(1 - \frac{3\Delta^2}{4\omega^2}\right) \tag{B.10e}$$

$$D_{c,32}(\omega) = D_{\mathrm{BCS}}(\omega) \frac{\xi(\omega)}{2\omega} \left(1 - \frac{\Delta^2}{2\omega^2}\right) \tag{B.10f}$$

$$D_{c,51}(\omega) = D_{\mathrm{BCS}}(\omega) \left(\frac{1}{2} - \frac{3\Delta^2}{4\omega^2} + \frac{\Delta^4}{4\omega^4}\right) \tag{B.10g}$$

and contain the original BCS expression D_{BCS} given in Eq.(4.24).
Eqs.(4.30a) and (4.30b) are a bit different from the above expressions (B.9a) and (B.9b) because negligible terms are omitted and the derivatives of the bare dispersion $\xi_{\mathbf{k}}$ are approximated by their value at $\omega = 0$ (i.e. at $k = k_F$) and factored out from the integrals.

B.3 Influence of a finite spectral linewidth $\Gamma > 0$

This section shows how to modify the method and the results presented above for the calculation of the T-matrix coefficients a, c and d when dealing with the spectral

functions of the pseudogap regime given by Eq.(4.25).
First the property of the δ-functions used to derive Eq.(B.6) is no longer true. It is however possible to obtain approximately a similar result by playing the following trick. Introducing the variable transformation $(\omega, \omega') \rightarrow (\Omega, \theta)$ defined after Eq.(B.8) in Section B.1 and taking the Gaussian form (4.31) for the distribution functions f_Γ, what is allowed as long as the spectral lineshapes are sufficiently small (i.e. $\Gamma \ll W$), it is then possible to write

$$f_\Gamma(E_{\mathbf{q}} - \omega)\, f_\Gamma(E_{\mathbf{q}} - \omega') = f_{\Gamma/\sqrt{2}}(E_{\mathbf{q}} - \Omega)\, f_{\sqrt{2}\Gamma}(\theta). \tag{B.11}$$

This identity yields an expression for $\phi(0, \omega, \omega')$ which is similar to Eq.(B.6). For simplicity the functions $f_{\Gamma/\sqrt{2}}$ and $f_{\sqrt{2}\Gamma}$ are taken to be equal to f_Γ. [1] The next step is the integration over the variable θ which can be achieved by expanding the fraction in Eq.(B.4) with respect to θ and keeping only the zeroth order term. The first corrections are of second order and can be safely neglected for the present purpose. This leads finally to expressions for the coefficients a, c and d which are very similar to those calculated for the BCS case. This is the main advantage of this method. The only difference lies in the "weighted" density of states functions (B.10a-B.10g) which have to be modified according to

$$D_{a,1}(\omega) \rightarrow \widetilde{D}_{a,1}(\omega) \equiv \int dE\, D_{a,1}(E)\, f_\Gamma(E - \omega) \tag{B.12}$$

for example. A tilde $\widetilde{D}$ will indicate the "broadened" version of a BCS function D from Eqs.(B.10a-B.10g).

[1] This will be justified *a posteriori* by noticing the weak influence of the finite width Γ on the values of the T-matrix coefficients a, c and d given in Table 4.1.

Appendix C

The bosonic interaction

C.1 The bosonic interaction term in the thermodynamic potential

The goal of this section is to show how to deal with the bosonic interaction term Ω_i from Eq.(4.34c) in order to justify its neglect in the number equation (4.39).
Replacing $\sigma(\mathbf{k}, z_\nu)$ by its explicit expression from Eq.(4.13d) allows to re-express Ω_i as

$$\Omega_i = -\frac{1}{\beta} \sum_{\mathbf{k}, z_\alpha} T(\mathbf{k}, z_\alpha)\, \sigma_b(\mathbf{k}, z_\alpha) \tag{C.1}$$

where σ_b represents a bosonic self-energy defined as

$$\sigma_b(\mathbf{k}, z_\alpha) = \frac{1}{\beta N} \sum_{\mathbf{q}, z_\beta} T(\mathbf{q}, z_\beta)\, R(\mathbf{k}, \mathbf{q}, z_\alpha, z_\beta) \tag{C.2a}$$

$$R(\mathbf{k}, \mathbf{q}, z_\alpha, z_\beta) = \frac{1}{\beta N} \sum_{\mathbf{p}, z_\nu} G(\mathbf{k}-\mathbf{p}, z_\alpha - z_\nu)\, G(\mathbf{q}-\mathbf{p}, z_\beta - z_\nu)\, G_0^2(\mathbf{p}, z_\nu). \tag{C.2b}$$

In agreement with Ref.[94], the above equations show that Ω_i is exactly the Hartree-Fock term of the grand potential of bosons interacting through the potential R. The "bare particles" are described by the T-matrix whereas the propagator of the "dressed bosons" is given by Dyson's equation

$$T_d^{-1}(\mathbf{k}, z_\alpha) = T^{-1}(\mathbf{k}, z_\alpha) - \sigma_b(\mathbf{k}, z_\alpha). \tag{C.3}$$

The corresponding expression of the bosonic part of the thermodynamic potential (4.33) is then

$$\Omega_b + \Omega_i = \Omega_d = \frac{1}{\beta} \sum_{\mathbf{k}, z_\alpha} \log\left(T_d(\mathbf{k}, z_\alpha)^{-1}\right). \tag{C.4}$$

In a first attempt to get some insight into the effects of the interaction R, the corresponding Hartree contribution to the grand potential $\Omega(T, V, \mu)$ can be calculated. It consists simply in inserting expression (C.2b) with zero arguments into Eq.(C.1) and gives the results displayed in Eqs. (4.35) and (4.36). It shows that the strength of the interaction is essentially determined by the coefficient b. The latter is calculated using the method of Appendix C.1 in the next section. The results of this calculation, which are discussed in Section 4.4.2, show essentially that b is becoming smaller and smaller when a pseudogap develops in the electronic structure. In that way, for $T \searrow T_c$, the effects of the bosonic interaction are expected to become weaker and weaker and should consist only in a weak renormalization of the T-matrix coefficients a, c and d. This can be in principle calculated by performing a low-energy expansion of $R(\mathbf{k}, \mathbf{q}, z_\alpha, z_\beta)$ similar to the one of $T^{-1}(\mathbf{k}, z_\alpha)$ in Eq.(4.18). However it is not sure that, in the framework of the present approximative approach, they would still lead to meaningful results.[1] Therefore the effect of the bosonic interaction contained in Ω_i are simply neglected in the following, so that

$$T_d(\mathbf{k}, z_\alpha) \approx T(\mathbf{k}, z_\alpha). \tag{C.5}$$

The validity of this assumption is tested in Section 4.4.3 where cross-checks are performed to confirm the numerical values obtained by this approach.

C.2 Calculation of the coefficient b

The result of the analytical calculation of the coefficient b is presented hereafter. The method explained in Section B.1 was used and a finite linewidth Γ characterizing the pseudogap regime was taken into account as well. The expression for b reads

$$b = \int d\omega \, D_{\text{BCS}}(\omega) \Big(u_\omega^4 \, \tilde{H}_{uu}(\omega) + v_\omega^4 \, \tilde{H}_{vv}(\omega) + 2u_\omega^2 v_\omega^2 \, \tilde{H}_{uv}(\omega) \Big). \tag{C.6}$$

Here the linewidth Γ of the spectral functions manifests itself as

$$\tilde{H}_{uu}(\omega) = \int d\Omega \, f_\Gamma(\Omega - \omega) H\big(\Omega, \xi(\omega)\big) \tag{C.7a}$$

$$\tilde{H}_{vv}(\omega) = \int d\Omega \, f_\Gamma(\Omega + \omega) H\big(\Omega, \xi(\omega)\big) \tag{C.7b}$$

$$\tilde{H}_{uv}(\omega) = \int d\theta \, f_\Gamma(\theta - \omega) \, \frac{1}{\theta} \Big(H_L\big(\theta, \xi(\omega)\big) - H_L\big(-\theta, \xi(\omega)\big) \Big) \tag{C.7c}$$

where the corresponding expressions for the BCS case are

$$H(\omega_1, \omega_2) = 2 \, \frac{1 - n_F(\omega_1) - n_F(\omega_2)}{(\omega_1 + \omega_2)^3} + \frac{n'_F(\omega_1) + n'_F(\omega_2)}{(\omega_1 + \omega_2)^2} \tag{C.8a}$$

$$H_L(\omega_1, \omega_2) = -\frac{1 - n_F(\omega_1) - n_F(\omega_2)}{(\omega_1 + \omega_2)^2} - \frac{n'_F(\omega_2)}{\omega_1 + \omega_2}. \tag{C.8b}$$

[1] Infrared divergences may appear and require sophisticated regularization schemes.

Bibliography

[1] J. Bardeen, L.N. Cooper, and J.R. Schrieffer, Theory of superconductivity, Phys. Rev. **108**, 1175 (1957).

[2] J.G. Bednorz and K.A. Müller, Possible high-T_c superconductivity in the Ba-La-Cu-O system, Z. Phys. B **64**, 189 (1986).

[3] C.E. Gough, M.S. Colclough, E.M. Forgan, R.G. Jordan, M. Keene, C.M. Muirhead, A.I.M. Rae, N. Thomas, J.S. Abell, and S. Sutton, Flux quantization in a high-T_c superconductor, Nature **326**, 855 (1987).

[4] M. Cyrot and D. Pavuna, Introduction to superconductivity and high-T_c materials, World Scientific, London (1992).

[5] T. Schneider and J.M. Singer, Phase transtion approach to high temperature superconcuctivity, Imperial College Press, London (2000).

[6] C.C. Tsuei and J.R. Kirtley, Pairing symmetry in cuprate superconductors, Rev. Mod. Phys. **72** 969 (2000).

[7] B. Batlogg and C. Varma, The underdoped phase of cuprate superconcuctors, Physics World **13**, 33 (2000).

[8] T. Timusk and B. Statt, The pseudogap in high temperature superconductors: an experimental survey, Rep. Prog. Phys. **62**, 61 (1999).

[9] M. Randeria, Precursor pairing correlations and pseudogaps, Proceedings of the International School of Physics “Enrico Fermi”, IOS Press, Amsterdam (1998).

[10] D. Pines, Understanding high-temperature superconductors: progress and prospects, Physica C **282**, 273 (1997).

[11] J.L. Tallon and J.W. Loram, The doping dependence of T^* - what is the real high-T_c phase diagram?, Physica C **349**, 53 (2001).

[12] P.A. Lee, Pseudogaps in underdoped cuprates, Physica C **318**, 194 (1999).

[13] T. Senthil, Electron fractionalization and cuprate superconductivity, preprint cond-mat/0105104.

[14] V.J. Emery, S.A. Kivelson, and O. Zachar, Spin-gap proximity effect mechanism of high-temperature superconductivity, Phys. Rev. B **56**, 6120 (1997).

[15] D. Manske, T. Dahm, and K.H. Bennemann, Phase diagram of hole-doped high-T_c superconductors: Effects of Cooper-pair phase fluctuations within fluctuation-exchange theory, Phys. Rev. B **64**, 144520 (2001).

[16] M.Randeria, Crossover from BCS theory to Bose-Einstein condensation, in "Bose-Einstein condensation", eds. A. Griffin, D. Snoke and S. Stringari, Cambridge University Press, London, (1994).

[17] V.J. Emery and S.A. Kivelson, Importance of phase fluctuations in superconductors with small superfluid density, Nature **374**, 434 (1995).

[18] V.M. Loktev, R.M. Quick, and S.G. Sharapov, Phase fluctuations and pseudogap phenomena, Phys. Rep. **349**, 1 (2001).

[19] M. Randeria and J.C. Campuzano, High T_c superconductors: new insights form angle-resolved photoemission, Proceedings of the International School of Physics "Enrico Fermi", IOS Press, Amsterdam (1998).

[20] Ch. Renner, B. Revaz, J.-Y. Genoud, K. Kadowaki, and Ø. Fischer, Pseudogap precursor of the superconducting gap in under- and overdoped $Bi_2Sr_2CaCu_2O_{8+\delta}$, Phys. Rev. Lett. **80**, 149 (1998).

[21] J. Corson, R. Mallozzi, J. Orenstein, J.N. Eckstein, and I. Bozovic, Vanishing of phase coherence in underdoped $Bi_2Sr_2CaCu_2O_{8+\delta}$, Nature **398**, 221 (1999).

[22] Z.A. Xu, N.P. Ong, Y. Wang, T. Kakeshita, and S. Uchida, Vortex-like excitations and the onset of superconducting phase fluctuation in underdoped $La_{2-x}Sr_xCuO_4$, Nature **406**, 486 (2000).

[23] I. Iguchi, T. Yamaguchi, and A. Sugimoto, Diamagnetic activity above T_c as a precursor to superconductivity in $La_{2-x}Sr_xCuO_4$ thin films, Nature **412**, 420 (2001).

[24] V.M. Krasnov, A. Yurgens, D. Winkler, P. Delsing, and T. Claeson, Evidence for coexistence of the superconducting gap and the pseudogap in Bi-2212 from intrinsic tunneling spectroscopy, Phys. Rev. Lett. **84**, 5860 (2000); M. Suzuki and T. Watanabe, Discriminating the superconducting gap from the pseudogap in $Bi_2Sr_2CaCu_2O_{8+\delta}$ by interlayer tunneling spectroscopy, Phys. Rev. Lett. **85**, 4787 (2000).

[25] R. Micnas, J. Ranninger, and S. Robaszkiewicz, Superconductivity in narrow-band systems with local nonretarded attractive interactions, Rev. Mod. Phys. **62**, 113 (1990).

[26] P. Carretta, A. Lascialfari, A. Rigamonti, A. Rosso, and A. Varlamov, Superconducting fluctuations and anomalous diamagnetism in underdoped $YBa_2Cu_3O_{6+x}$ from magnetization and ^{63}Cu NMR-NQR relaxation measurements, Phys. Rev. B **61**, 12420 (2000).

[27] A. Junod, A. Erb, and Ch. Renner, Specific heat of high-temperature superconductors in high fields at T_c: from BCS to the Bose-Einstein condensation, Physica C **318**, 333 (1999).

[28] A.S. Alexandrov, W.H. Beere, V.V. Kabanov, and W.Y. Liang, Contrasting effects of magnetic field on thermodynamic and resistive transitions in high-T_c cuprates, Phys. Rev. Lett. **79**, 1551 (1997); A.S. Alexandrov and V.V. Kabanov, Parameter-free expression for superconducting T_c in cuprates, Phys. Rev. B **59**, 13628 (1999).

[29] J. Hubbard, Electron correlations in narrow energy bands, Proc. R. Soc. London, Ser. A **276**, 238 (1963).

[30] V.L. Berezinskii, Violation of long range order in one-dimensional and two-dimensional systems with a continuous symmetry group. I. Classical systems, Sov. Phys. JETP **32**, 493 (1971); J.M. Kosterlitz and D.J. Thouless, Ordering, metastability and phase transitions in two-dimensional systems, J. Phys. C **6**, 1181 (1973).

[31] A. Moreo and D.J. Scalapino, Two-dimensional negative-U Hubbard model, Phys. Rev. Lett. **66**, 946 (1991).

[32] J.J. Deisz, D.W. Hess, J.W. Serene, Coupled electrons and pair fluctuations in two dimensions: a transition to superconductivity in a conserving approximation, Phys. Rev. Lett. **80**, 373 (1998).

[33] A. Sewer, X. Zotos, and H. Beck, unpublished.

[34] F. Pistolesi and G.C. Strinati, Evolution from BCS superconductivity to Bose condensation: Role of the parameter $k_F\xi$, Phys. Rev. B **49**, 6356 (1994).

[35] A.J. Legett in "Modern Trends in the Theory of Condensed Matter", eds. A. Pekalski and R. Przystawa, Springer Verlag, Berlin (1985).

[36] P. Nozière and S. Schmitt-Rink, Bose condensation in a attractive Bose gas: from weak to strong coupling superconductivity, J. Low Temp. Phys.**59**, 195 (1885).

[37] S.C. Zhang, A unified theory based on SO(5) symmetry of superconductivity and antiferromagnetism, Science **275**, 1089 (997).

[38] G.D. Mahan, Many-particle physics, Plenum Press, New York (1981).

[39] H. Frölich, Theory of the superconducting state. I. The ground state at the absolute zero of temperature, Phys. Rev. **79**, 845 (1950).

[40] L.N. Cooper, Bound electron pairs in a degenerate Fermi gas, Phys. Rev. **104**, 1189 (1956).

[41] D.J. Thouless, Perturbation theory in statistical mechanics and the theory of superconductivity, Ann. Phys. **10**, 553 (1960).

[42] B. Kyung, S. Allen, A.M.S. Tremblay, Pairing fluctuations and pseudogaps in the attractive Hubbard model, Phys. Rev. B **64**, 075116 (2001).

[43] T. Meintrup, T. Schneider, and H. Beck, Antiferromagnetism vs superconductivity in a tight-binding model with singlet nearest-neighbor pairing interaction, Europhys. Lett. **31**, 231 (1995); J.P. Wallington and J.F. Annett, BCS to Bose crossover in anisotropic superconductors, Phys. Rev. B **61**, 1433 (2000).

[44] M. R. Schafroth, Superconductivity of a charged ideal Bose gas, Phys. Rev. **100**, 463 (1955).

[45] M. Drechsler and W. Zwerger, Crossover from BCS-superconductivity to Bose-condensation, Ann. Phys. **1**, 15 (1992).

[46] C.A.R. Sá de Melo, M. Randeria, and J.R. Engelbrecht, Crossover from BCS to Bose superconductivity: transition temperature and time-dependent Ginzburg-Landau theory, Phys. Rev. Lett. **71**, 3202 (1993).

[47] S. Stintzing and W. Zwerger, Ginzburg-Landau theory of superconductors with short coherence length, Phys. Rev. B **56**, 9004 (1997).

[48] B. Chattopadhyay and S.R. Shenoy, Kosterlitz-Thouless signatures from 3D vortex loops in layered superconductors, Phys. Rev. Lett. **72**, 400 (1994).

[49] G. Blatter, M.V. Feigel'man, V.B. Geshkenbein, A.I. Larkin, and V.M. Vinokur, Vortices in high-temperature superconductors, Rev. Mod. Phys. **66**, 1125 (1994).

[50] R. Haussmann, Properties of a Fermi liquid at the superfluid transition in the crossover region between BCS superconductivity and Bose-Einstein condensation, Phys. Rev. B **49**, 12975 (1994).

[51] R. Micnas, M.H. Pedersen, S. Schafroth, T. Schneider, J.J. Rodrguez-Nez, and H. Beck, Excitation spectrum of the attractive Hubbard model, Phys. Rev. B **52**, 16223 (1995).

[52] D. Rohe and W. Metzner, Pair-fluctuation-induced pseudogap in the normal phase of the two-dimensional attractive Hubbard model at weak coupling, Phys. Rev. B **63**, 224509 (2001).

[53] M. Keller, W. Metzner, U. Schollwock, Dynamical mean-field theory for pairing and spin gap in the attractive Hubbard model, Phys. Rev. Lett. **86**, 4612 (2001).

[54] M. Capone, C. Castellani, M. Grilli, First-order pairing transition and single-particle spectral function in the attractive Hubbard model, preprint cond-mat/0109194.

[55] J.M. Singer, Monte Carlo Simulationen zu stark korrelierten Systemen, Dissertation, Universität Regensburg (1995).

[56] E.Y. Loh and J.E. Gubernatis, Stable numerical simulations of models of interacting electrons in condensed-matter physics, in "Electronic Phase Transitions", eds. W. Hanke and Yu.V. Kopaev, Elsevier Science Publishers (1992).

[57] P. Minnhagen, The two-dimensional Coulomb gas, vortex unbinding, and superfluid-superconducting films, Rev. Mod. Phys. **59**, 1001 (1987).

[58] F. Naef, Dynamical properties of quasi one-dimensional correlated electrons, Ph.D. Thesis, EPFL, Lausanne (2000).

[59] H.G. Mattutis, Determinanten Quanten Monte Carlo und analytische Fortsetzung für das Hubbard Modell, Dissertation, Universität Regensburg (1995).

[60] X. Zotos, in "L'intégrale fonctionelle et ses applications", Troisième cycle de la Physique en Suisse Romande (1993); N. Nagaosa, Quantum Field Theory in Condensed Matter Physics, Springer, Berlin (1999).

[61] A. Schmid, Diamagnetic susceptibility at the transition to the superconducting state, Phys. Rev. **180**, 527 (1969).

[62] J.P. Gollub, M.R. Beasley, R.S. Newbower, and M. Tinkham, Observation of enhanced diamagnetism above T_c in indium due to thermodynamic fluctuations, Phys. Rev. Lett. **22**, 1288 (1969).

[63] R. E. Prange, Diamagnetic susceptibility at the transition to the superconducting state, Phys. Rev. B **1**, 2349 (1970).

[64] M. Tinkham, Introduction to Superconductivity, McGraw-Hill, New York (1980).

[65] C. Baraduc, A. Buzdin, J.Y. Henry, J.P. Brison, and L. Puech, Fluctuations in quasi-2D superconductors under magnetic field - the case of $YBa_2Cu_3O_{7-\delta}$, Physica C **248**, 138 (1995).

[66] A. Sewer, H. Beck and X. Zotos, Orbital magnetic susceptibility of the attractive Hubbard model, Physica C **317-318**, 475 (1999).

[67] F. Pistolesi and G.C. Strinati, Evolution from BCS superconductivity to Bose condensation: calculation of the zero-temperature phase coherence length, Phys. Rev. B **53**, 15168 (1996).

[68] W.E. Lawrence and S. Doniach, Theory of layered superconductors, in "Proceedings of the Twelfth International Conference on Low Temperature Physics", ed. E. Kanda, Tokyo (1971).

[69] Z. Tešanović, Extreme type-II superconductors in a magnetic field: a theory of critical fluctuations, Phys. Rev. B **59**, 6449 (1999).

[70] B. Chattopadhyay, M.C. Mahato, and S.R. Shenoy, Vortex-loop crinkling in the three-dimensional XY model: numerical evidence in support of an ansatz, Phys. Rev. B **47**, 15159 (1993).

[71] B.I. Halperin and D.R. Nelson, Resistive transition in superconducting films, J. Low Temp. Phys. **36**, 599 (1979).

[72] N.H. March and M.P. Tosi, Atomic Dynamics of Liquids, Wiley, New York (1976).

[73] R. Côté and A. Griffin, Theory of the dynamic spin response function near the Kosterlitz-Thouless transition, Phys. Rev. B **34**, 6240 (1986).

[74] H. Beck, private communication.

[75] C. Meingast, V. Pasler, P. Nagel, A. Rykov, S. Tajima, and P. Olsson, Phase fluctuations and the pseudogap in $YBa_2Cu_3O_{6+x}$, Phys. Rev. Lett. **86**, 1606 (2001); V. Pasler, P. Schweiss, C. Meingast, B. Obst, H. Wühl, A.I. Rykov, and S. Tajima, 3D-XY critical fluctuations of the thermal expansivity in detwinned $YBa_2Cu_3O_{y-\delta}$-single crystals near optimal doping, Phys. Rev. Lett. **81**, 1094 (1998).

[76] S. Sengupta, P. Nielaba and K. Binder, Defect fugacity, spin-wave stiffness and T_c of the 2D planar rotor model, Europhys. Lett. **50**, 668 (2000).

[77] G. Kohring, R.E. Shrock, and P. Wills, Role of vortex strings in the three-dimensional O(2) model, Phys. Rev. Lett. **57**, 1358 (1986); J. Epiney, Diploma Thesis, ETH Zürich (1990); A. Schmidt and T. Schneider, Dimensional crossover in the layered XY-model, Z. Phys. B **87**, 265 (1992); A. Tanner, Ph.D. Thesis, University of Zürich (1994).

[78] A.K. Nguyen, A.Sudbø, and R.E. Hetzel, Vortex-loop unbinding and flux-line lattice melting in superconductors, Phys. Rev. Lett. **77**, 1592 (1996).

[79] W. Janke and T. Matsui, Crossover in the XY model from three to two dimensions, Phys. Rev. B **42**, 10673 (1990); G. Carneiro, R. Cavalcanti, and A. Gartner, Monte Carlo study of vortex-line-lattice melting, Phys. Rev. B **47**, 5263 (1993); X. Hu, S. Miyashita, and M. Tachiki, Monte Carlo simulation on the first-order melting transition of high-T_c superconductors in $\mathbf{B} \parallel \mathbf{c}$, Phys. Rev. B **58**, 3438 (1998).

[80] J. Ranninger, J.M. Robin, and M. Eschrig, Superfluid precursor effects in a model of hybridized bosons and fermions, Phys. Rev. Lett. **74**, 4027 (1995); J. Ranninger and J.M. Robin, Pseudogap in underdoped high-T_c superconductors in the framework of the boson-fermion model, Phys. Rev. B **56**, 8330 (1997); P. Devillard and J. Ranninger, Pseudogap phase in high-T_c superconductors, Phys. Rev. Lett. **84**, 5200 (2000).

[81] V.B. Geshkenbein, L.B. Ioffe, and A.I. Larkin, Superconductivity in a system with preformed pairs, Phys. Rev. B **55**, 3173 (1997).

[82] O. Tchernyshyov, Noninteracting Cooper pairs inside a pseudogap, Phys. Rev. B **56**, 3372 (1997).

[83] L.P. Kadanoff and G. Baym, Quantum Statistical Mechanics, W.A. Benjamin, New York (1962).

[84] E.E. Salpeter and H.A. Bethe, A relativistic equation for bound-state problems, Phys. Rev. **84**, 1232 (1951).

[85] M.Yu. Kagan, R. Frésard, M. Capezzali, and H. Beck, One-electron spectral functions of the attractive Hubbard model for intermediate coupling, Phys. Rev. B **57**, 5995 (1998);

[86] D. Foerster, Planar diagram approach to the correlation problem, Phys. Rev. B **61**, R5066 (2000).

[87] G. Baym, Self-consistent approximations in many-body systems, Phys. Rev. **127**, 1391 (1962).

[88] J.W. Serene and D.W. Hess, Quasiparticle properties of the two-dimensional Hubbard model in a propagator-renormalized fluctuation-exchange approximation, Phys. Rev. B **44**, 3391 (1991).

[89] M. Capezzali and H. Beck, Excitation spectrum of the two-dimensional attractive Hubbard model, Physica C **317-318**, 482 (1999)

[90] M.H. Pedersen, Crossover problem in the attractive Hubbard model, Ph.D. Thesis, Universität Zürich (1996).

[91] M. Capezzali, Superconductivity in two dimensions: spectral properties of the attractive Hubbard model and dynamics of vortices, Ph.D. Thesis, Université de Neuchâtel (1998).

[92] J.M. Singer, T. Schneider, and P.F. Meier, Spectral properties of the attractive Hubbard model, Eur. Phys. J. B **7**, 37 (1999).

[93] H.T.C. Stoof, Time-dependent Ginzburg-Landau theory for a weak-coupling superconductor, Phys. Rev. B **47**, 7979 (1993).

[94] A.L. Fetter and J.D. Walecka, Quantum Theory of many-particle Systems, McGraw-Hill, Boston (1971).

[95] J.M. Singer, M.H. Pedersen, T.Schneider, H. Beck, and H.G. Matuttis, From BCS-like superconductivity to condensation of local pairs: a numerical study of the attractive Hubbard model, Phys. Rev. B **54**, 1286 (1996).

[96] S. Moukouri, S. Allen, F. Lemay, B. Kyung, D. Poulin, Y.M. Vilk, and A.M.S. Tremblay, Many-body theory versus simulations for the pseudogap in the Hubbard model, Phys. Rev. B **61**, 7887 (2000).

[97] B.L. Gyorffy, J.B. Staunton, and G.M. Stocks, Pairing, condensation, and superconductivity described by a Hubbard model with an attractive interaction, Phys. Rev. B **44**, 5190 (1991).

[98] G. Preosti, Y.M. Vilk, and M.R. Norman, Evolution of the pairing pseudogap in the spectral function with interplane anisotropy, Phys. Rev. B **59**, 1474 (1999).

[99] R.M. Quick and S.G. Sharapov, Persistence of pseudogap formation in quasi-2D systems with arbitrary carrier density, Physica C **301**, 262 (1998).

[100] X.G. Wen and R. Kan , Charged boson condensation in high-T_c superconductors, Phys. Rev. B **37**, 595 (1988).

[101] Y.J. Uemura, Bose-Einstein to BCS crossover picture for high-T_c cuprates, cond-mat/9706151.

[102] A.C. Durst and P.A. Lee, Impurity-induced quasiparticle transport and universal-limit Wiedemann-Franz violation in d-wave superconductors, Phys. Rev. B **62**, 1270 (2000).

[103] F.F. Assaad, W. Hanke, and D.J. Scalapino, Temperature derivative of the superfluid density and flux quantization as criteria for superconductivity in two-dimensional Hubbard models, Phys. Rev. B **50**, 12835 (1994).

[104] R.R. dos Santos, Spin gap and superconductivity in the three-dimensional attractive Hubbard model, Phys. Rev. B **50**, 635 (1994).

[105] R. Staudt , M. Dzierzawa , and A. Muramatsu, Phase diagram of the three-dimensional Hubbard model at half-filling Eur. Phys. J. B **17**, 411 (2000).

[106] M. Keller, W. Metzner, and U. Schollwöck, Thermodynamics of a superconductor with strongly bound Cooper pairs, Phys. Rev. B **60**, 3499 (1999).

[107] J.E. Hirsch, Discrete Hubbard-Stratonovich transformation for fermion lattice models, Phys. Rev. B **28**, 4059 (1983).

[108] S.E. Koonin, Computational Physics, Benjamin/Cummings (1986).

[109] J.W. Negele and H. Orland, Quantum Many-Particle Systems, Addison-Wesley (1988).

[110] D.P. Landau and K. Binder, A Guide to Monte Carlo Simulations in Physics, Cambridge University Press (2000).

[111] A.D. Sokal, Monte Carlo Methods in Statistical Mechanics: Foundations and New Algorithms, Troisième cycle de la Physique en Suisse Romande (1989).

[112] D. Pines and P. Nozières, The Theory of Quantum Liquids: Normal Fermi Liquids, Addison-Wesley (1989).

[113] D. Forster, Hydrodynamic Flucutations, Broken Symmetry, and Correlation Functions, Addison-Wesley (1983).

[114] M. Guerrero, G. Ortiz, J.E. Gubernatis, Pairing correlations in the attractive Hubbard model on chains, ladders, and squares, Phys. Rev. B **62**, 600 (2000).

[115] X. Zotos, private communication.

[116] R. Staudt, Quanten-Monte-Carlo-Simulationen des dreidimensionalen Hubbard-Modells, Ph.D. Thesis, Universität Augsburg (1999).

[117] A. Georges and W. Krauth, Physical properties of the half-filled Hubbard model in infinite dimensions, Phys. Rev. B **48**, 7167 (1993).

[118] F. Gebhard, private communication.

[119] J.R. Engelbrecht and H. Zhao, Short-coherence length superconductivity in the Attractive Hubbard Model in three dimensions, preprint cond-mat/0110356.

[120] S. Allen, H. Touchette, S. Moukouri, Y.M. Vilk, and A.M.S. Tremblay, Role of symmetry and dimension in pseudogap phenomena, Phys. Rev. Lett. **83**, 4128 (1999).

[121] M. Randeria, N. Trivedi, A. Moreo, and R.T. Scalettar Pairing and spin gap in the normal state of short coherence length superconductors, Phys. Rev. Lett. **69**, 2001 (1992).

[122] N. Trivedi and M. Randeria, Deviations from Fermi-liquid behavior above T_c in 2D short coherence length superconductors, Phys. Rev. Lett. **75**, 312 (1995).

Remerciements

Je tiens à remercier tout ceux grâce à qui ce travail de thèse a été rendu possible.

En premier lieu les deux personnes qui m'ont supervisé et accordé leur confiance. Le Professeur Hans Beck, mon directeur de thèse, qui m'a attentivement guidé durant ces quatre années et permis de bénéficier de sa grande expérience de la Physique théorique. Le Docteur Xenophon Zotos qui, par sa disponibilité et sa patience, m'a non seulement aidé dans la résolution de nombreux problèmes mais également enseigné une attitude face aux difficultés de la Recherche.

Je remercie également les Professeurs Piero Martinoli et Florian Gebhard, qui ont accepté de faire partie du jury de cette thèse et contribué à la bonne atmosphère qui a régné lors de l'examen oral.

Un merci particulier au Docteur Sergei Sharapov qui a pris la peine de lire attentivement les premières versions de ce manuscrit, me permettant d'y apporter de précieuses améliorations.

Je suis également très reconnaissant envers mes collègues de l'IRRMA et de l'Université de Neuchâtel. Ils ont contribué, chacun à leur manière, au bon déroulement de mon passage dans ces deux endroits. Pour les anciens : Christophe, Vincent, Jérôme, Félix, Rainer, Raymond, Massimiliano (HCC) . . . et pour les nouveaux : Philippe, Paolo, Claudia, Angelo, Massimiliano, Macha, Stéphane, Laurent, John . . .

Finalement je voudrais remercier mes parents, ma soeur et mon amie Laure pour leur soutien et leur patience.